



**HAL**  
open science

## Development and rheological analysis of a surface polymer nanocomposite anti-friction

Ammar Al-Kawaz

► **To cite this version:**

Ammar Al-Kawaz. Development and rheological analysis of a surface polymer nanocomposite anti-friction. Physics [physics]. Université de Strasbourg, 2015. English. NNT : 2015STRAE025 . tel-01277405

**HAL Id: tel-01277405**

**<https://theses.hal.science/tel-01277405>**

Submitted on 22 Feb 2016

**HAL** is a multi-disciplinary open access archive for the deposit and dissemination of scientific research documents, whether they are published or not. The documents may come from teaching and research institutions in France or abroad, or from public or private research centers.

L'archive ouverte pluridisciplinaire **HAL**, est destinée au dépôt et à la diffusion de documents scientifiques de niveau recherche, publiés ou non, émanant des établissements d'enseignement et de recherche français ou étrangers, des laboratoires publics ou privés.

ÉCOLE DOCTORALE DE PHYSIQUE ET CHIMIE-PHYSIQUE  
INSTITUT CHARLES SADRON

**THÈSE** présentée par :

**Ammar AL-KAWAZ**

soutenue le : **10 Décembre 2015**

Pour obtenir le grade de : **Docteur de l'Université de Strasbourg**

Discipline/ Spécialité : Physique des Polymères

**Development and rheological analysis of a  
surface polymer nanocomposite anti-friction**

**THÈSE dirigée par :**

**M. GAUTHIER Christian** Professeur, Université de Strasbourg

**RAPPORTEURS :**

**M. KAPSA Philippe** Directeur de Recherche, ECL LTDS Lyon

**M. SERP Philippe** Professeur, Université de Toulouse

---

**AUTRES MEMBRES DU JURY :**

**M. CHEMTOB Abraham** Chargé de Recherche - HDR- Université de Haute Alsace

**Mme. JANOWSKA Izabela** Ingénieur de Recherches, Université de Strasbourg

**M. GERARD Pierre** Ingénieur ARKEMA - GRL



## **Acknowledgments**

I would like to express my deepest gratitude to the project director Pr. Christian Gauthier for his full support, precious advices and great contribution. In fact, I feel honoured to work under his supervision. His unsurpassed knowledge, piercing insight which develops my knowledge and understanding of the subject. I will remember extensively his perpetual encouragement and motivation on both an academic and a personal level without which this work would not be possible. A lot of thanks goes to Dr. Anne Rubin as Co - supervisor for her constant support and for her discussions and instruction on how to use the equipment and conduct the experiments. I wish her a promising future in the research administration.

I am extremely grateful to all of the jury members D.R. Philippe Kapsa, Pr. Philippe Serp, Dr. Pierre Gerard, Dr. Izabela Janowska and Dr. Abraham Chemtob for dedicating their valuable time and energies for this dissertation and taking interest in evaluating this work.

I owe my sincere thanks to Pr. Cuong Pham-Huu, Pr. Philippe Mesini and Dr. Nezha Badi for their generous help and fruitful suggestions during my thesis.

I would also like to express my gratitude to Dr. Marc Schmutz and Dr. Christian Blanck, and all others for sharing their knowledge and extending their assistance in completing this task.

I owe my sincere thanks to Mr. Damien and Dr. Leandro Jacomine to resolve the various problems faced during experimental work.

**Strasbourg, December 2015**



## General introduction

The area of tribology deals with the friction, wear and lubrication of interacting surfaces in relative motion. Polymer matrices are attractive due to their low weight and price nevertheless some of their physical properties are not favorable, and thus it is necessary to reinforce them by adding specific fillers. Recently, the use of polymer composite materials for tribological applications significantly increases. Many developments of new polymers composites have incorporated nano-fillers as reinforcing agents, resulting in the term “polymeric nanocomposites.” In fact, it has been demonstrated that these fillers of very small dimension (compared to the classical micrometer- size fibers or particles) can also result in marked improvements in the friction and wear properties of both bulk materials and coatings. In the domain of hard coatings, nanocomposite films are expected to be a solution to get strength and toughness at the same time. It is generally believed that the harder materials are favorable for achieving higher wear resistance [1]. The use of carbon nano-fillers in reinforcement of the transparent polymers coating, is an additional challenge, since any increase in the carbon content leads to making the composite coating more dark, so there are a need to, either use types of filler which do not affect the transparency of the composite or modify the surface of this filler to make them more effective at low concentration in the composites.

The present study was focused on the scratch resistance of nanocomposite polymer materials used in coating application. The material used in this work is poly (methyl methacrylate) PMMA reinforced with different types of nano carbon fillers (MWCNT, FLG and GO) and also with fatty acid amides namely Erucamide as a slipping agent. If it had been interesting to compare the impact of these types of fillers on the scratch behavior of the composite coating, it was decided to focus here on studying the effect of the technique used to prepare the composite on the mechanical and tribological performance.

The manuscript consists of three sections. The first section gives different aspects of nano carbon fillers, the main parameters that control the properties of the resulting composites and the techniques that are used for the fabrication of polymer nanocomposites coating. Then it gives a general idea about the mechanical and tribological properties of the polymer nanocomposites. It describes various scales and types of friction along with different factors affecting the friction coefficient for the coated systems.

The second section (material and methodology) presents more specifically the materials used, the various procedures developed for preparations the composites coating solutions, coating techniques, and the experimental devices. Using these tools, it is possible firstly, to characterize the composites and, secondly to characterize mechanical and tribological properties of coated samples.

The third section presents the experimental results that are obtained for chemical and structural characterization of the fillers and composites are discussed. In this section the experimental results of surface and mechanical properties for composites coatings are discussed. They are prepared by two different techniques, in situ polymerization and solution mixing technique and consist of: Few layer graphene filler (FLG-C18)/PMMA, Graphene oxide (GO)/PMMA, MWCNT grafted PMMA/PMMA and Erucamide/PMMA.



## Symbols

$t$	film thickness
$w$	angular velocity
$g$	the gap distance between the blade and the substrate in
$c$	the concentration of the solid material in the solvent
$\rho$	solution density
$E$	Young's modulus
$\delta_f$	failure stress of the fiber
$l_c$	critical fiber length
$\tau_c$	interfacial strength
$V_c$	percolation threshold
$H$	Hardness
$A$	the projected area
$Y$	the yield stress
$\nu$	Poisson's ratio
$\mu_{\text{appa.}}$	apparent friction coefficient
$\mu_{\text{adh.}}$	adhesive friction coefficient
$\mu_{\text{plough.}}$	ploughing friction coefficient
$\mu_{\text{loc}}$	Local friction coefficient
$p$	local pressure
$\tau$	local shear stress
$E'$	reduced modulus of elasticity
$F_n$	normal load
$F_t$	tangential force
$\omega$	Rear contact angle
$p_m$	Mean contact pressure
$a_f$	Frontal contact area
$a_r$	rear contact area
$\epsilon_e$	contact strains at the end of the elastic contact area
$\epsilon_p$	contact strains at the at the beginning of the plastic contact area
$E^*$	the normalized elastic modules
$\theta$	the apex angle of the conical scratching tip
$V_{\text{tip}}$	velocity of the moving tip
$L_g$	width of the groove
$R$	the radius of the tip
$\beta$	the angle between the tip and the surface
$\epsilon_r$	representative strain



$h_e$	groove depth elastic part
$h_p$	groove depth plastic part
$h_{ep}$	total groove depth
$\delta_b$	stress at tensile break
$\varepsilon_b$	strain at tensile break
Tg	Glass transition temperature
MWCNTs	Multiwall Carbon Nanotubes
FLG	Few layer graphene
ODA(C18)	Octadecylamin
FLG-C18	Few layer graphene functionalized Octadecylamin
GO	Graphene oxide

# Sum-up of the work in French

## 1. Résumé court

Les matériaux polymères ont une masse volumique faible comparés aux matériaux métalliques ou aux verres inorganiques. Ils sont donc intéressants pour nombre d'applications où l'on cherche à diminuer le poids. Leur principale limitation reste cependant leurs faibles propriétés mécaniques face aux agressions surfaciques. Une solution consiste à recouvrir les surfaces de polymères par des revêtements renforcés par des particules, telles que les nanoparticules carbonées.

Les objectifs principaux de cette étude sont :

- d'observer l'effet de nanoparticules carbonées sur la réponse en cisaillement de contact.
- de conserver la transparence du revêtement pour leur application en tant que vitrages.

La première partie du mémoire présente l'analyse bibliographie en deux parties : une première s'attache aux particules nano-carbonées, à leurs propriétés et aux techniques de fabrication d'un composite. Une seconde partie se concentre sur l'effet de ces nanoparticules sur les réponses mécaniques et tribologiques de composites.

La deuxième partie du mémoire présente les différentes nanoparticules utilisées, leurs préparations spécifiques ainsi que les fonctionnalisations nécessaires à une bonne dispersion dans la matrice polymère.

La troisième partie du mémoire présente les résultats mécaniques et tribologiques des différents revêtements réalisés.

## 2. Choix des particules renforts

### 2.1 Préparation des particules de renforts

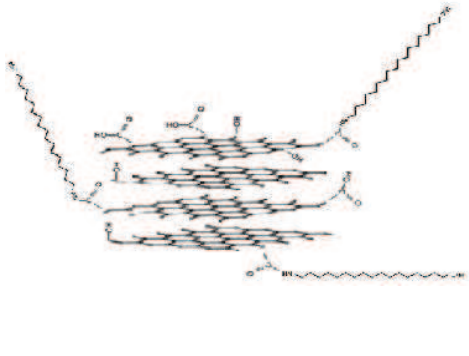
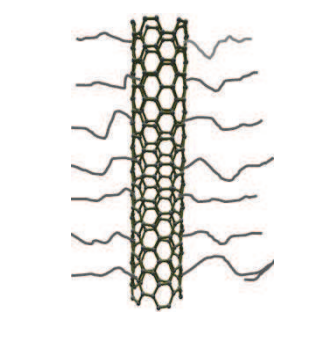
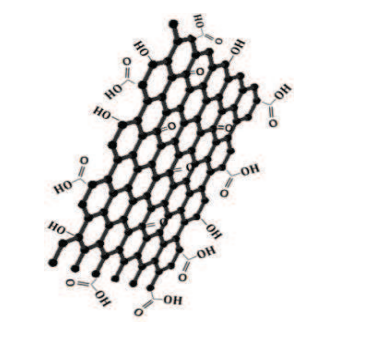
Une matrice acrylique a été renforcée avec des nanoparticules carbonées obtenues à l'ICPEES. Trois types de nanoparticules ont été testées afin de mettre en évidence un effet éventuel des facteurs de forme : du graphène multicouches (FLG - few layer graphene), de l'oxyde de graphène (GO - graphene oxide) et des nanotubes de carbones (MWCNT - multi wall carbon nanotubes).

- Pour assurer la meilleure dispersion possible de ces nanoparticules dans la matrice polymère il est nécessaire de réaliser des modifications chimiques de leur surface. L'objectif est double : limiter l'agrégation dues aux forces de van der Waals et augmenter la compatibilité avec la matrice. Après les étapes de purification des nanoparticules, les modifications chimiques de surfaces qui ont été retenues sont les suivantes : les FLG ont été fonctionnalisés avec de l'octadécylamine, longues chaînes

alkyles de 18 carbones. L'objectif est de favoriser la solubilité. Ces particules de renforts sont nommées FLG-C18.

- la surface des nanotubes de carbones a été modifiée par polymérisation radicalaire contrôlée. Le greffage de chaînes de poly(méthylméthacrylate) (PMMA) de différentes tailles a été obtenu. L'objectif est de favoriser l'insertion des nanoparticules par l'enchevêtrement des chaînes de PMMA dans la matrice. Ces particules de renforts sont nommées MWCNT-PMMA.
- l'oxyde de graphène a été utilisé en l'état. Ces particules de renforts sont nommées GO.

Le tableau suivant schématise les trois structures de nanoparticules avec lesquelles nous allons travailler.

FLG-C18	MWCNT-PMMA	GO
		

La fonctionnalisation chimique et son efficacité ont été caractérisées par infra-rouge, analyse thermogravimétrique et XPS pour chacun de ces types de nanoparticules.

## 2.2 Procédés de préparation des composites

Deux méthodes ont été retenues pour réaliser des matériaux composites dans une matrice acrylique, la polymérisation en masse et le mélange en solution. Par ailleurs, comme deux gammes d'épaisseur de revêtements composites ont été visées, trois stratégies de préparation ont été réalisées.

Les revêtements d'épaisseur de l'ordre de 150-200  $\mu\text{m}$  ont été obtenus par moulage direct entre deux lames de verre. Dans ce cas, on polymérise en masse : on mélange les particules de renforts fonctionnalisées, le monomère préalablement distillé (MMA) et l'amorceur (AIBN) sous atmosphère inerte à température contrôlée. Lorsque la viscosité de la solution augmente de façon significative le moulage est réalisé.

Les revêtements d'épaisseur compris entre 12-20  $\mu\text{m}$  ont été obtenus par étalement à épaisseur contrôlée d'une solution (technique Docteur Blade) obtenue à partir d'un mélange de PMMA et de composites nanoparticule/PMMA sous forme de poudre. Ces poudres ont été obtenues de deux façons différentes. La première est la méthode de polymérisation in situ. Elle consiste à polymériser le MMA dans une suspension de particules dans le DMF, puis à précipiter. La deuxième consiste à mélanger une solution de nanoparticules fonctionnalisées dans le THF et

une solution de PMMA dans le THF, puis à précipiter. Dans les deux cas les solides sont broyés à l'état de poudre. La figure suivante présente des exemples de poudres obtenues à partir des particules de MWCNT et de PMMA pur.

Pour l'ensemble des composites préparés :

- la chromatographie d'exclusion stérique a permis de mesurer les masses molaires moyennes ;
- la calorimétrie à balayage différentiel a permis de déterminer les températures de transition vitreuse des produits préparés.

Dans l'ensemble ces caractérisations ont montré peu de variations par rapport à la matrice de PMMA pure.

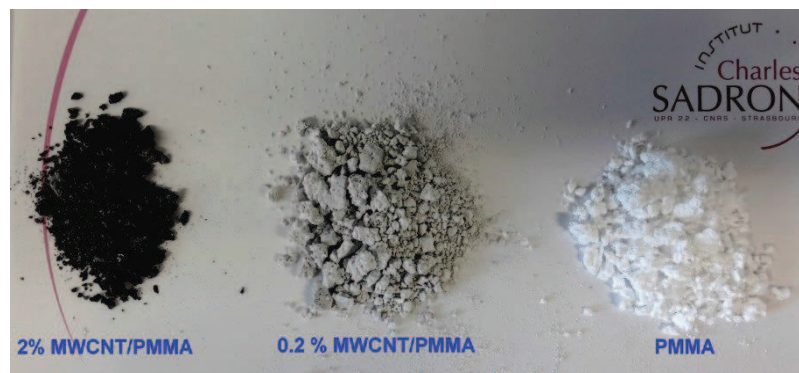


Figure 1 exemple de poudres réalisées

### 3. Caractérisations mécaniques des composites

L'objectif de l'étude est d'identifier des couplages nanoparticules / matrice de PMMA qui renforcent la rigidité de surface du PMMA tout en conservant le maximum de transparence. Deux méthodes de caractérisation ont été utilisées. La technique de nano-indentation a permis de déterminer le module d'Young et la dureté moyenne des composites. La technique de sclérométrie a permis de déterminer la réponse en cisaillement de contact des différents revêtements.

L'épaisseur des revêtements impose la gamme de profondeur analysée. En effet pour s'affranchir de l'influence du substrat, la profondeur d'analyse ne doit pas dépasser le dixième de l'épaisseur du revêtement. Le tableau suivant récapitule les trois types de dépôts réalisés :

Procédé de préparation	Technique de dépôt	Type de substrat	Epaisseur du revêtement	Technique de caractérisation
Mélange solution	Doctor Blade	Lame de verre	~ 12-15 $\mu\text{m}$	Indentation
Polymérisation in situ sans solvant	Moulage	PMMA	~ 150-200 $\mu\text{m}$	Sclérométrie
Mélange solution	Doctor Blade	PMMA	~ 20 $\mu\text{m}$	Sclérométrie

#### 3.1 Réponses mécaniques en volume

Les mesures de nano-indentation ont été analysées par la méthode d'Oliver et Pharr (avec un coefficient de Poisson fixé à 0.3). L'ensemble des résultats est proposé dans le tableau suivant :

<i>Revêtement testé</i>	<i>E (GPa)</i>	<i>H (MPa)</i>	<i>H/E</i>
Pure PMMA	3.7±0.06	176 ± 4	0.048
0.1% FLG/PMMA	3.9±0.1	200±2.5	0.062
0.5% FLG/PMMA	4.2±0.03	200±3.5	0.062
1% FLG/PMMA	4.5 ± 0.1	225 ±12	0.063
0.1% GO/PMMA	/	/	
0.5% GO/PMMA	3.8±0.05	190 ±7	0.05
1% GO/PMMA	4.7±0.05	197±4.5	0.042
0.1% MWCNT-grafted PMMA	4.1±0.13	201 ±12	0.049
0.5% MWCNT-grafted PMMA	3.8±0.12	194 ±8	0.051
1% MWCNT-grafted PMMA	4.4±0.03	217±11	0.049
2% MWCNT-grafted PMMA	4.6±0.6	212±12	0.046

Ces résultats mettent en avant deux points majeurs :

- l'ajout de nanoparticules de renfort dans la matrice de polymère PMMA augmente sensiblement le module d'Young (au vu des faibles pourcentages en masse incorporés dans la matrice). Cette augmentation est de l'ordre de 10 % à 30 % suivant le taux de nanoparticules ajouté.
- La présence d'un type de renfort dans la matrice de PMMA entraîne une modification de la déformation au seuil de plasticité (H/E).

### 3.2 Réponses mécaniques en surface

L'analyse en surface est réalisée sur un montage développé dans l'équipe dont la particularité est de pouvoir enregistrer l'aire réelle de contact tout au long de la mesure. Toutes les mesures sont réalisées à température ambiante dans une atmosphère contrôlée à faible humidité relative (RH < 4%). La vitesse de glissement de la pointe est fixée à 30  $\mu\text{m/s}$ .

Les paramètres qui sont analysés sont :

- le coefficient de frottement apparent  $\mu_{\text{app}}$ , rapport entre la force tangentielle mesurée lors du glissement de la pointe et la force normale appliquée sur la pointe.
- le coefficient de frottement local  $\mu_{\text{loc}}$  qui s'obtient en enlevant la part géométrique du matériau déplacé en avant de pointe au coefficient de frottement apparent. Ce coefficient caractérise le frottement vrai à l'interface pointe/substrat. Il est déduit de  $\mu_{\text{app}}$  et de la géométrie du contact à partir d'un modèle développé dans l'équipe.
- la pression moyenne de contact  $p_{\text{mean}}$ , rapport entre la force normale appliquée sur la pointe et l'aire visualisée du contact.
- l'angle de retour  $\omega$  de la matière derrière la pointe. Cet angle caractérise la part visco-élastique du matériau relativement au temps de contact.

La déformation dans le contact est proportionnelle au rapport du contact  $a$  sur le rayon de la pointe  $R$  (dans le régime élastique elle est égale à  $4/(3\pi).a/R$  et dans le régime plastique,

égale à  $0.2 a/R$ ). Pour faciliter la lecture les paramètres définis ci-dessus sont donc tracés en fonction de  $a/R$ .

Les trois régimes classiques observés sont schématisés dans la figure suivante. Dans le cas d'un régime élastique l'aire de contact est symétrique ( $\omega = \pi/2$ ). Dès qu'une dissymétrie apparaît dans l'aire de contact, on entre dans une transition entre le régime élastique et plastique et  $\omega$  diminue. Lorsque le régime plastique est atteint, le contact est dissymétrique avec des bourrelets de plasticité devant la pointe et sur les bords du sillon de rayure. L'angle  $\omega$  atteint alors un plateau qui est typiquement de 0.35 radians.

Le tableau suivant résume les pourcentages en masse des renforts testés. Les renforts MWCNT-PMMA ont été testés avec 3 longueurs moyennes de chaînes de PMMA greffés sur les nanoparticules (déterminées par microscopie à transmission électronique).

Epaisseur du revêtement déposé sur PMMA	Renfort FLG-C18	Renfort GO	Renfort MWCNT-PMMA (longueur 1)	Renfort MWCNT-PMMA (longueurs 1, 2 et 3)
~ 150-200 $\mu\text{m}$	0.05	0.05	0.05	-
	0.1	0.1	0.1	
	0.2	0.5	0.2	
~ 12-20 $\mu\text{m}$	0.1	0.1	0.5	2
	0.5	0.5	1	2
	1	1	2	2

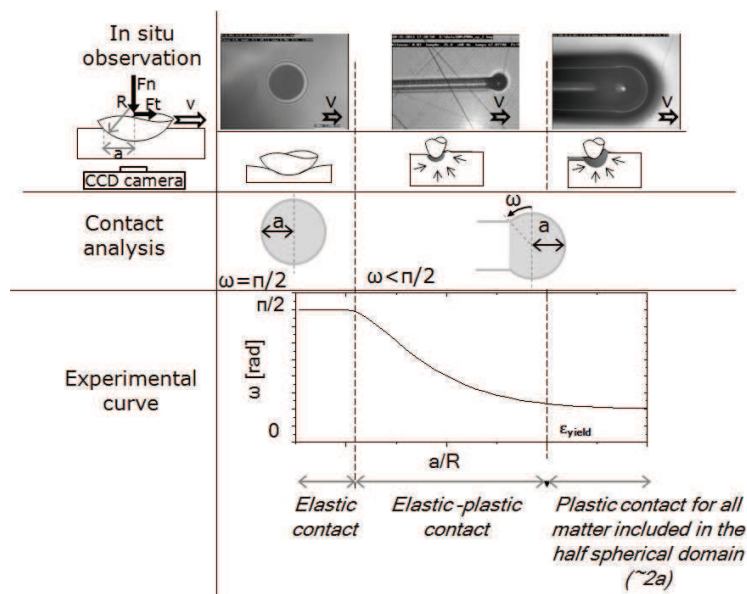


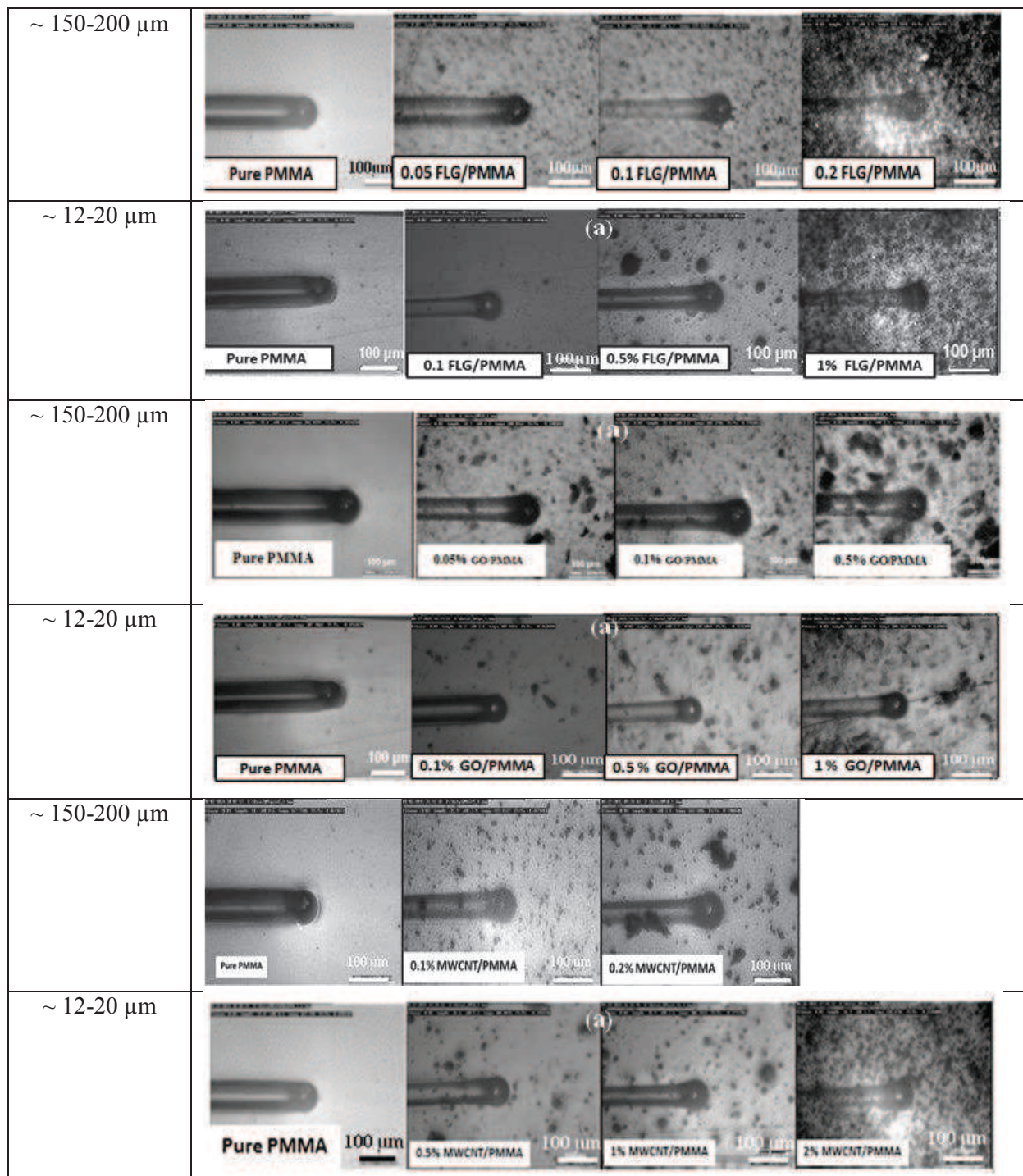
Figure 2 schéma de principe de l'analyse de sclérométrie.

Il est à noter que pour des épaisseurs de l'ordre de la centaine de micromètres la transparence n'est plus conservée dès que le taux de renfort dépasse 0.2 % alors que pour des épaisseurs de l'ordre de la dizaine de microns, la transparence persiste jusqu'à 2 % de renfort.

Par ailleurs, la connaissance de l'épaisseur du revêtement analysé permet de déterminer le rayon de contact critique (correspondant à un enfoncement de pointe au dixième de l'épaisseur) au-delà duquel l'effet du substrat n'est plus négligeable.

Le tableau suivant montre, pour les trois types de renforts utilisés et pour un rapport  $a/R$  égal à environ 0.35 :

- l'aspect général de la dispersion ;
- la modification progressive de l'allure du contact d'un régime purement plastique (pour un revêtement de PMMA pur) vers un régime élastique/plastique. Ce qui est confirmé par l'ensemble des courbes représentant l'évolution de l'angle  $\omega$  en fonction de  $a/R$ .



### ➤ Effet de la dispersion des particules sur la réponse en frottement

Le choix d'un procédé de préparation des nanocomposites (polymérisation en masse ou mélange de solutions) peut favoriser la dispersion. Par exemple pour le cas de l'oxyde de graphène, la figure 3 montre qu'une préparation avec mélange de solution favorise la dispersion.

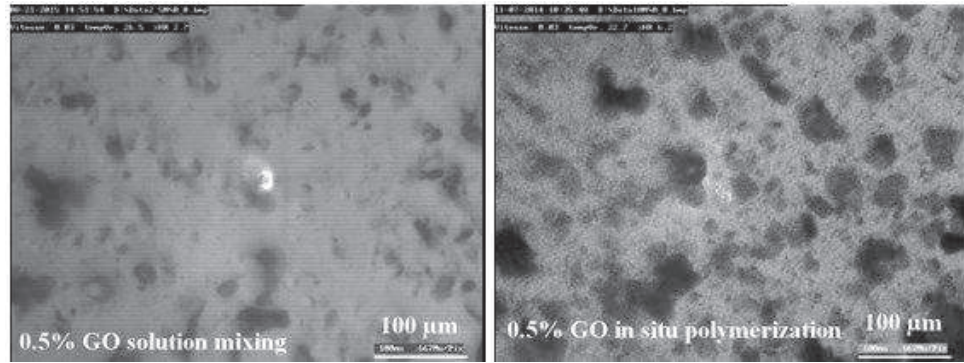


Figure 3 revêtements de 0.5% GO/PMMA obtenus par 2 procédés différents

La figure 4 présente le coefficient de frottement local en fonction du rapport  $a/R$  pour deux pourcentages d'incorporation de renforts d'oxyde de graphène. Pour ce renfort, la technique de polymérisation in situ diminue drastiquement le coefficient de frottement local comparé à la technique de mélange de solutions.

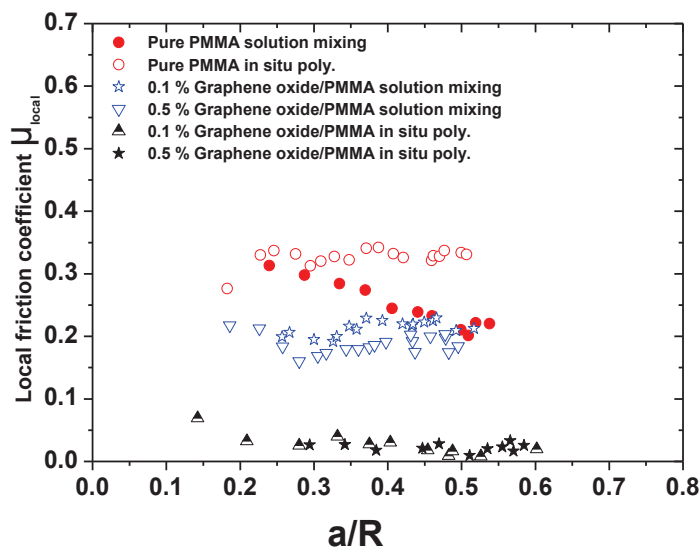


Figure 4 coefficient de frottement local en fonction du rapport  $a/R$ .

### ➤ Cas GO : effet de l'épaisseur du revêtement

Puisque les deux épaisseurs de revêtements testées ont un rapport d'environ 10, la question qui se pose est de savoir si les propriétés mécaniques de surface sont similaires avec un taux



de renforts similaires par unité de surface. Les propriétés de surfaces ont été comparées pour les 3 types de renforts. Pour le FLG-C18 et le GO les résultats sont quasiment identiques. Le MWCNT-PMMA présente par contre des propriétés différentes comme le montrent les courbes suivantes. Deux films sont comparés : un film d'épaisseur  $\sim 150 \mu\text{m}$  contenant 0.1% de renfort et un film d'épaisseur  $\sim 20 \mu\text{m}$  contenant 1% de renfort. L'évolution de la pression moyenne de contact en fonction du rapport  $a/R$  suit une allure similaire alors que le coefficient de frottement local du revêtement fin est quatre fois plus faible que celui du revêtement épais.

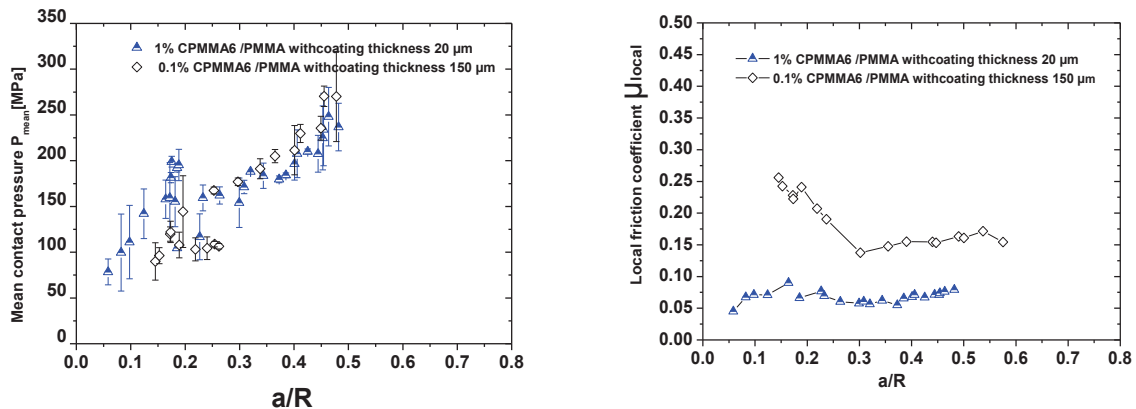


Figure 5 pression moyenne de contact et coefficient de frottement local en fonction du rapport  $a/R$

### ➤ Cas MWCNT : effet de la longueur moyenne de brins de PMMA greffés

La préparation des MWCNT greffés par des chaînes de PMMA a pu être réalisée avec des longueurs moyennes de PMMA différentes. Cela a été caractérisé par analyse thermogravimétrique et microscope électronique à transmission. La question est donc de savoir si l'épaisseur de PMMA fonctionnalisée sur le MWCNT a une influence sur la réponse mécanique du nanocomposite.

Trois épaisseurs croissantes de fonctionnalisation ont été comparées (cf fig. 6, nommées CPMMMA4, CPMMMA6 et CPMMMA8 respectivement) dans le cas d'un pourcentage de renfort constant (2%). La figure 6 (gauche) montre l'évolution de l'angle  $\omega$  en fonction du rapport  $a/R$ . Le comportement diffère nettement entre le revêtement de PMMA pur et les trois composites considérés : pour ces derniers le domaine de plasticité apparaît beaucoup plus tardivement ( $a/R = 0.35$  pour le PMMA et  $a/R = 0.45$  et  $0.5$  pour les composites). Quand le PMMA greffée sur les MWCNT a l'épaisseur la plus faible, le domaine de plasticité apparaît le plus tôt. L'évolution des pressions moyennes de contact est la même pour tous les composites.

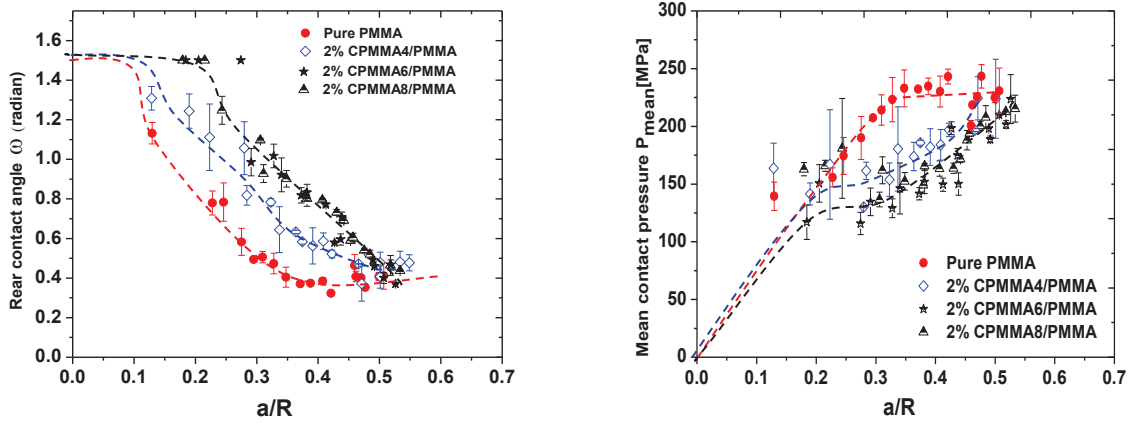


Figure 6 angle  $\omega$  et pression moyenne de contact en fonction du rapport  $a/R$ .

### ➤ Comparaison entre un revêtement renforcé et un revêtement sans renfort avec un plastifiant

Les nanoparticules carbonées avaient été choisies dans le but d'augmenter la raideur dans le contact. L'objectif initial était d'ajouter également une couche de l'ordre du micron d'un plastifiant afin de réduire la contrainte de cisaillement. L'ensemble des deux contributions ayant pour but d'obtenir un revêtement anti-friction (le coefficient de frottement étant le rapport entre la contrainte de cisaillement et la pression moyenne de contact). Or il est apparu assez rapidement que le caractère lubrifiant des nanoparticules carbonées diminuaient de façon significative le frottement. La question est donc de savoir si, à épaisseur de couche équivalente le pouvoir lubrifiant de ces couches carbonées est comparable à celui de petites chaînes.

La comparaison porte sur deux revêtements (*i*-renfort par des nanoparticules ; *ii*-plastifiant) d'épaisseur identique dont le coefficient de frottement est similaire (Fig. 7-gauche). Le plastifiant utilisé est de l'erucamide. La représentation du diamètre de contact ( $2a$ ) en fonction de la force normale appliquée  $F_n$  (Fig. 7-droite) montre que le revêtement renforcé a bien une raideur de contact plus élevée

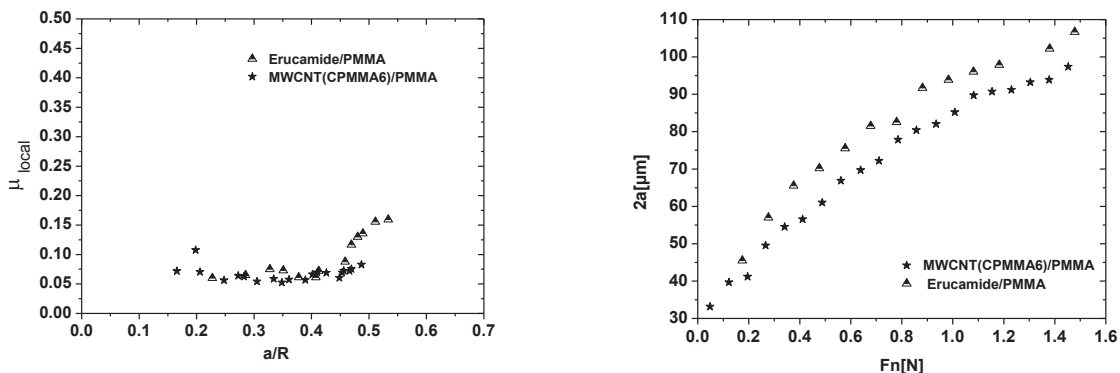


Figure 7 coefficient de frottement local en fonction du rapport  $a/R$  et diamètre de contact ( $2a$ ) en fonction de la force normale appliquée  $F_n$ .

## ➤ Conclusions et perspectives

L'objectif de cette thèse est l'identification de couplages (nanoparticules / matrice de PMMA) qui renforcent la rigidité de surface du PMMA tout en conservant le maximum de transparence. Le choix s'est porté sur trois types de nanoparticules carbonées : du graphène multicouches (FLG), de l'oxyde de graphène (GO) et des nanotubes de carbones (MWCNT).

L'ensemble de ces travaux ont permis d'aborder plusieurs aspects :

- l'aspect chimie avec la fonctionnalisation des nanoparticules, la synthèse des revêtements composites et les caractérisations par diverses techniques à chaque étape,
- l'aspect mécanique avec la caractérisation mécanique, en volume et en surface, des revêtements réalisés.

Les résultats majeurs montrent que

- les nano-composites réalisés retardent l'apparition de la plasticité comparé à un PMMA pur, même à faible pourcentage, et permettent ainsi de limiter les effets de rayures de surfaces,
- le faible pourcentage de renfort permet de conserver la transparence et plus l'épaisseur diminue plus on peut augmenter ce taux de renfort sans dégrader les propriétés mécaniques du revêtement,
- les nanoparticules choisies comme agents de renfort de la matrice polymère s'avèrent être également de très bons candidats pour la diminution du frottement,

Pour la suite il serait peut-être intéressant d'utiliser les couches carbonées comme agent lubrifiant et d'ajouter un très faible pourcentage de plastifiant classique (type Erucamide) pour l'utiliser à l'inverse comme antiplastifiant.

# Contents

<b>Symbols.....</b>	<b>v</b>
<b>Sum-up of the work in French .....</b>	<b>vii</b>
<b>Section one: Significant issues covering the subject .....</b>	<b>1</b>
<b>1 Context .....</b>	<b>3</b>
<b>1.1 Introduction .....</b>	<b>3</b>
<b>1.2 Multiwall Carbon Nanotubes (MWCNTs).....</b>	<b>3</b>
<b>1.3 Graphene and graphene oxide .....</b>	<b>4</b>
<b>1.4 Slip additives .....</b>	<b>5</b>
<b>1.5 Surface coating.....</b>	<b>7</b>
<b>1.6 Nano-carbon dispersion's issue in thermoplastic.....</b>	<b>8</b>
<b>1.7 Modification of nanocarbon surface .....</b>	<b>8</b>
<b>1.8 Fabrication of polymer nanocomposites .....</b>	<b>10</b>
1.8.1 Melt mixing process .....	10
1.8.2 Solution mixing process .....	10
1.8.3 In-situ polymerization .....	11
<b>1.9 Fabrication of surface coating .....</b>	<b>11</b>
1.9.1 Introduction .....	11
1.9.2 Surface coating methods .....	12
<b>1.10 Conclusions .....</b>	<b>13</b>
<b>2 Mechanical and tribological properties of polymer nano-composites ....</b>	<b>15</b>
<b>2.1 Mechanical properties .....</b>	<b>15</b>
2.1.1 Elastic properties .....	15
2.1.2 Hardness .....	17
<b>2.2 Tribology of polymer nanocomposite.....</b>	<b>19</b>
2.2.1 Definitions .....	19
2.2.2 Influence of nanofillers on nanocomposites tribological properties .....	21
2.2.3 Tribological analysis and relevant scales .....	23
2.2.4 Tribological measurement: direct observation of the contact during scratching.....	25
2.2.5 Tribological properties of coatings.....	30
<b>2.3 Conclusions .....</b>	<b>33</b>

<b>Section two Experimental works .....</b>	<b>35</b>
<b>3 Experimental work.....</b>	<b>37</b>
<b>3.1 Material and methodology .....</b>	<b>37</b>
3.1.1 Materials.....	37
3.1.2 Few layers graphene (FLG).....	37
3.1.3 Graphene oxide (GO) .....	37
3.1.4 Multiwall carbon nanotubes (MWCNTs).....	38
3.1.5 Erucamide.....	38
3.1.6 Surface modification of nanofiller.....	39
<b>3.2 Fabrication of polymer nanocomposite samples .....</b>	<b>41</b>
3.2.1 In-situ polymerization without solvent (Dispersion- reaction).....	41
3.2.2 In- situ polymerization in solvent (Dispersion-reaction-precipitate) .....	42
3.2.3 Solution mixing (Dispersion – dispersion – precipitates) .....	42
<b>3.3 Characterization techniques of the nanofillers and composite samples .....</b>	<b>44</b>
<b>3.4 Sample preparation for surface mechanical measurements.....</b>	<b>44</b>
3.4.1 Cast coating by in situ polymerization .....	45
3.4.2 Doctor Blade technique .....	46
<b>3.5 Techniques and equipments to characterize mechanical properties of the coated samples .....</b>	<b>49</b>
3.5.1 The conditions for analysis the contact mechanics in the coating.....	49
3.5.2 Nano-indentation tests .....	50
3.5.3 Scratch tests .....	52
3.5.4 Intron Uniaxial tensile testing machine .....	54
<b>Section three: Results and discussion.....</b>	<b>55</b>
<b>4 Few layer graphene (FLG).....</b>	<b>57</b>
<b>4.1 Chemical and structure characterization .....</b>	<b>57</b>
<b>4.2 Characterization of PMMA/FLG composites .....</b>	<b>60</b>
4.2.1 Surface mechanical properties of in situ-polymerization coats.....	61
4.2.2 Surface mechanical properties of solution mixing coatings .....	65
<b>4.3 Comparative study of the effect of different techniques of coating .....</b>	<b>69</b>
<b>4.4 Comparative study of the effect of coating thickness on the surface mechanical properties.....</b>	<b>71</b>
<b>4.5 Conclusions .....</b>	<b>72</b>
<b>5 Graphene oxide (GO).....</b>	<b>74</b>
<b>5.1 Chemical and structure characterization .....</b>	<b>74</b>
<b>5.2 Characterization of PMMA/GO composites.....</b>	<b>76</b>

5.3	Surface mechanical properties of in situ polymerization coatings .....	77
5.4	Surface mechanical properties of solution mixing coatings .....	80
5.5	Comparative study of the effect of different techniques of the coating .....	84
5.6	Conclusions .....	86
<b>6</b>	<b>Multi walled carbon nanotube (MWCNT) grafted PMMA.....</b>	<b>87</b>
6.1	Chemical composition and structure characterization .....	87
6.2	Characterization of PMMA/MWCNT-g-PMMA composites .....	91
6.2.1	Surface mechanical properties of in situ polymerization coatings .....	92
6.2.2	Surface mechanical properties of solution mixing coatings .....	95
6.3	Comparative study of the effect of different techniques of coating .....	99
6.4	PMMA reinforced MWCNT grafted with different thickness layer of PMMA .....	101
6.4.1	Surface mechanical properties.....	101
6.5	Comparative study of the effect of coating thickness on the surface mechanical properties.....	106
6.6	Conclusions .....	107
<b>7</b>	<b>Erucamide.....</b>	<b>109</b>
7.1	Surface mechanical properties of coating.....	109
7.2	Comparative study of the different roles between soft layer and hard layer in decreasing the coefficient of friction .....	112
7.3	Conclusions .....	114
	<b>General conclusions.....</b>	<b>115</b>
	<b>Perspective and future work .....</b>	<b>119</b>
	<b>Annex A.....</b>	<b>121</b>
	<b>References .....</b>	<b>125</b>



# **Section one: Significant issues covering the subject**





# 1 Context

## 1.1 Introduction

The word “composite” is used when at least one filler has been added to the polymer matrix with the aim to significantly change mechanical and tribological properties. Nano-composite is a composite in which one filler material has at least one of its dimension less than 100 nanometers (nm). The use of nano-sized particles or fibers coupled with enhancement of the chemical interactions between the filler and the matrix seems to produce better tribological performance [1]. A better and far more restrictive definition would require a true nano-composite to be a fundamentally new material (hybrid), in which the nanometer scale component or structure give rise to intrinsically new properties, which are not present in the respective macroscopic composites or pure component [2]. Carbon nanotubes (CNTs) and other nanocarbon particles have generated a great deal of interest due to their unique physical properties and they are considered to be ideal candidates for mechanical reinforcement of polymers [3].

The properties of a composite material depend not only upon the individual component phases (matrix, filler) but also upon their interaction interface. The incorporation of CNTs to polymer matrices has demonstrated the improvement of mechanical, electrical, thermal and morphological properties of the produced nano-composites. Carbon nanotubes form very long bundles due to the high surface energy and the stabilization by numerous  $\pi$ - $\pi$  electron interactions among the tubes. The full utilization of CNTs has been severely limited due to difficulties associated with dispersion of CNTs during a processing, and their poor interfacial interaction with the polymer matrix [4].

Tribological applications of polymers include gears, bearing materials, artificial human joints.... It includes for instance coatings, floorings and various types of surfaces for optimum tactile properties. For such tribological applications, there is no polymer used in its pristine form. The reason is that no polymer can provide a reasonable low working wear rate with optimum coefficient of friction required. Hence, there is a need to modify most polymers by suitable filler that can reduce the wear rate and depending upon the design requirement, either increases or decreases the coefficient of friction. The main advantage of nano-composites over traditional composites is in its ability to improve both strength and toughness properties simultaneously and isotropically [1].

Carbon nanofiller can have many structures, differing in length, thickness and number of layers. In our research, we used three types of carbon nanofillers (Multi Wall Carbon Nanotube, Few Layer Graphene and Graphene Oxide) to prepare PMMA/carbon based nano-composites as anti-friction coatings.

## 1.2 Multiwall Carbon Nanotubes (MWCNTs)

Carbon nanotubes (CNTs) were discovered by Iijima in 1991 [5]. These particles are tube-shaped material with excellent properties such as high tensile and flexural strengths, high

elastic modulus and a high aspect ratio, that make them appropriate for tribological applications. Their discovery opens new routes to configure new nanostructured surfaces in tribology. In these composites, it was noted that the friction and wear rates were reduced through the addition of nanotubes. Multiwall Carbon Nanotubes (MWCNTs) shape can be a coaxial assembly of CNTs or a sheet rolled like a scroll. Due to this shape, MWCNTs can be used to manufacture composites with superior tribological properties.

In addition, based on the hypothesis of an inherent self-lubricity of nanotubes, these materials are good candidates at tribological interfaces [6] [7]. For instance Schönhense and Elmers [8] prepared MWCNTs/UHMWPE composites films containing 1wt% and 5wt% MWCNTs by gel extrusion process. These films exhibited not only high wear resistance but also a low friction coefficient compared to the pure UHMWPE films. However dispersion of the particles can be a serious issue. To solve this problem Kim and Cho [9] grafted PMMA onto the surfaces of amino-functionalized MWCNTs to produce a new composite with lower coefficient of friction compared to pristine PMMA. The lowest coefficient of friction was obtained for the nanocomposite coating reinforced with 3 wt.% MWCNT grafted PMMA. They concluded that the uniform distribution of MWCNTs in the matrix is a prerequisite for lowering friction, and the amount of MWCNTs used for coating should not be excessive in order to avoid creating brittle coatings.

Bin et al. [7] also studied the tribological properties of PMMA/MWCNT composites prepared by in situ polymerization method with different concentrations of MWCNTs (0.05, 0.1, 0.25, 0.75, 1, 1.5 and 2.5 wt.%). They found that MWCNTs significantly decreased the friction coefficient and the wear rate. They also revealed that PMMA/MWCNT composites with 1.0 wt. % MWCNT content showed both the smallest wear rate and the lower friction coefficient. The significant improvements on the tribological properties of PMMA/MWCNT composites are attributed to excellent mechanical properties and unmatched topological tubular structure of MWCNTs.

### **1.3 Graphene and graphene oxide**

Graphene, first obtained by Novoselov et al. in 2004 [10], is a new type of two-dimensional carbon material. It has a two-dimensional honeycomb structure composed by a single layer of carbon atoms and its basic structural unit is benzene six-membered ring which is the most stable in organic material. Significant applications are predicted in fields such as energy, materials, biology, medicine, electronics, due to its superior electrical, mechanical, and thermal properties [11].

Das et al. [12] studied the impact of reinforced PMMA with functionalized few layer graphene (FLG) by nano-indentation. The elastic modulus and hardness significantly increase with FLG content. As they showed by DSC, the crystallinity increases significantly with small additions of graphene (0.6 wt%) and they concluded, that few-layer graphene is also a good candidate for reinforcement of polymers.

Berman and Sumant [13] demonstrated a series of experiments, which compare the effect of graphene on friction and wear behavior of 440C steel in dry nitrogen environment. The results

indicate that small amounts of graphene on the sliding surface are able to afford reasonable low friction.

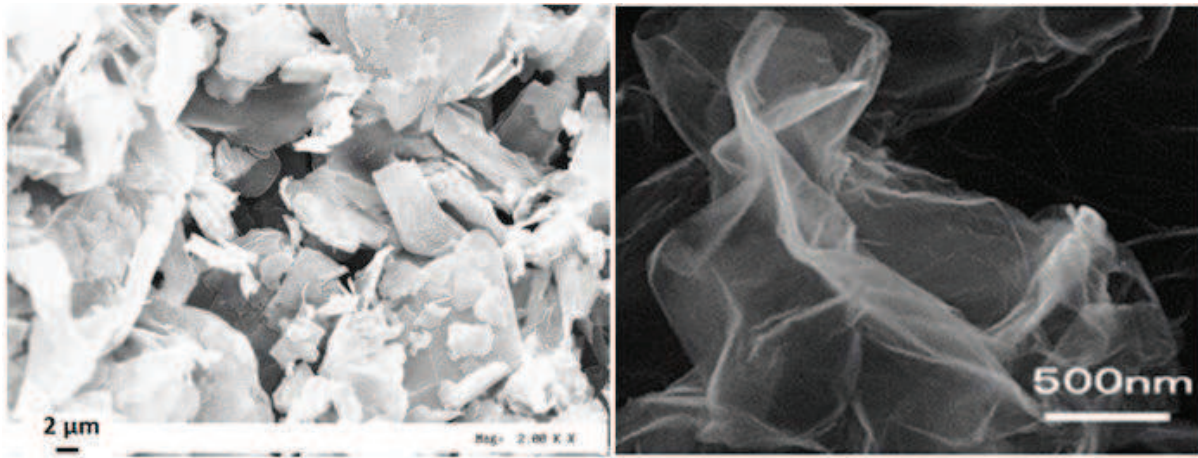


Figure 1-1 graphite (on the left) graphene oxide (on the right) [14]

Graphene oxide sheets (GOs) are basically prepared from graphite, obtained by harsh oxidative treatment thus they are decorated oxygenated mostly hydroxyl and epoxide functional groups on its basic planes, also carbonyl and carboxyl groups located at the sheet's edges. The presence of these functional groups makes graphene oxide sheets strongly hydrophilic, which allows GOs to readily swell and disperse in water. Moreover, these functional groups can be helpful to form a stronger interfacial interaction with the polymeric matrix, which improve the performance of the composite. Due to the reinforcement effect of graphene oxide, PMMA nanocomposites with excellent tribological properties can be obtained. On the other hand, these functional groups make GO non-conductive and prevent GO from being used in electronic devices directly [15].

Pan et al [16] synthesized GO/nylon nano-composites by an anionic ring-opening polymerization. The mechanical and tribological results showed that very low content of GO had a clear effect on the nylon matrix: it greatly decreased wear rates and slightly reduced friction coefficient. Song et al. showed that a GO/poly (methyl methacrylate) (PMMA) nanocomposites prepared by in-situ polymerization can decrease the average friction coefficient of the nanocomposites from 0.6 for pure matrix to 0.42 for composite with increasing the graphene oxide content [11]. In addition, the bulk properties of a GO/PMMA composite prepared in the work of Potts [17] showed an increase of strength and dynamic modulus and a shift in Tg over 15°C compared to neat PMMA. These examples and the preparation process may be a parameter to consider.

## 1.4 Slip additives

Slip and anti-block additives regulate the surface of polymer film and sheet to enhance performance in the fabrication equipment, downstream packaging equipment, or end-use. Slip agents are added during the mixing and extrusion step, it works by migrating from bulk polymer to the surface (the additives migrate to the surface over time and modify the surface

properties). The slip agents should be incompatible with the bulk polymer in other words they are not bonded into the bulk but are free to migrate. The ease and velocity of migration for slip agent through bulk polymer depends on the size of the molecule. Thus the migration rate of slip agents can be controlled by increasing the molecule chain length. It also increases the compatibility with the host polymer. It is notable, that there is no control over which film surface the slip agents appear on. They will migrate to both surfaces as sketched in Figure 1-2 [18], [19].

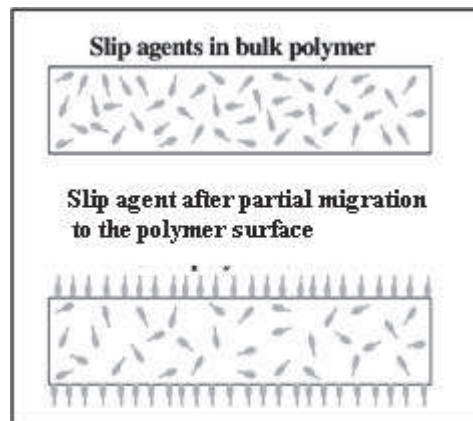


Figure 1-2 A sketch of the mechanism effect of slip agents [19].

Stearamide, Erucamide and Oleamide (Figure 1-3) are types of slip agents which can be produced by the amidisation of long chain fatty acids and are also called fatty amides. Fatty amides are described with two structural elements: amide group and hydrocarbon chain. Erucamide has longer chain, higher thermal stability and higher oxidation resistivity comparing with Oleamide and Stearamide. Erucamide is considered as an effective slip agent because it reduces a film's sliding friction [20].

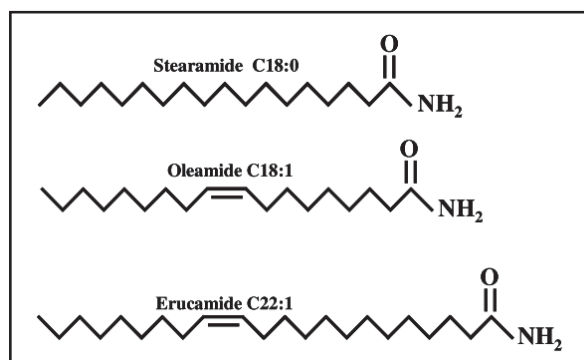


Figure 1-3 A schematic of the three basic slip agent structures Waxes [19].

To enlight the migration mechanism of fatty amides let's take the example of polyethylene. Hydrocarbon chains have high affinity to polyethylene and for this reason, near the surface,

hydrocarbon chains are embedded in polymer with their amide groups facing air after composite synthesis. Slip agent molecules migration entail the formation of a top layer on the surface. The molecules of the second layer orient themselves with amide group facing each other (similar functional groups have the affinity to each other particularly they have both oxygen and hydrogen which easily to form weak hydrogen bonding). Friction coefficient is not reduced until double layer begins to form (Figure 1-4).

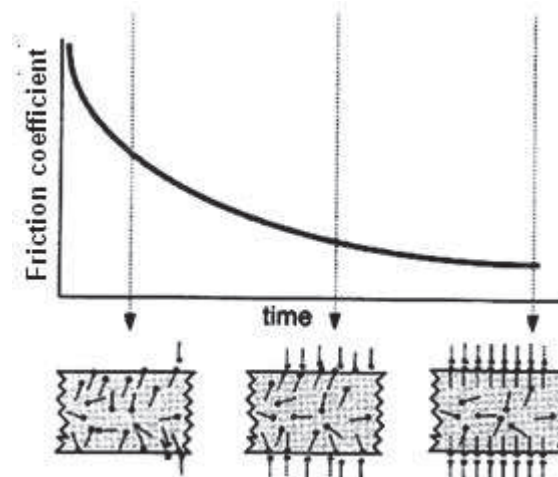


Figure 1-4 surface orientation of slip agent and its effect on coefficient of friction [21].

The energy required to break these weak bonds is low. Surface of films having such lubricated layers slide on each other with ease and this contributes to good slipping properties [21].

## 1.5 Surface coating

The development of high performance materials is required for a growing number of applications where good tribological properties are necessary [22]. Most polymeric materials are sensitive to scratching and the use of protective coatings is an important way to enhance surface properties such as elastic modulus, hardness and fracture toughness [23], [24], [25], [26]. To minimize friction, tribological coatings must also provide low shear stress during sliding at the contact. Broadly, in inorganic-organic composites coatings the organic component provides flexibility whereas the inorganic component is responsible for hardness and mechanical properties. The inorganic components with nanoscale dimensions have already shown a great effect on improving the scratch and wear resistance [22]. In addition, an important parameter in specific industrial applications is to maintain gloss and transparency, which is possible for low nanofiller percentage loading. For instance, a widely used protective coating for solar cell is the hard lacquer coating, where small  $\text{SiO}_2$  or other glass-like particles are embedded in a polymer matrix [25].

## **1.6 Nano-carbon dispersion's issue in thermoplastic**

In order to maximize the utility of CNTs, they must be dispersed uniformly and individually. CNT with a good dispersion will result in a uniform stress distribution and minimize the presence of stress-concentration centers [27]. However, a uniform dispersion of nanocarbon fillers in polymer matrices is a fundamental challenge. In general, several factors that influence the nanocarbon dispersion in a polymer matrix have to be considered in the preparation process of polymer nanocomposites. The entangling of CNTs or graphene during polymer growth process and the attraction between them by van der Waals forces make them aggregate. It prevents nanofillers from being well dispersed within polymers and the obtained composites are poor in their mechanical performances [28]. Several techniques have been developed to improve the dispersion of nanofillers in polymer matrices : the use of surfactant, sonication and chemical functionalization [29][30][31]. Advantages and drawbacks of these techniques will be discussed in the following paragraphs.

## **1.7 Modification of nanocarbon surface**

Aggregate formation can be limited or avoided by modifying the nanocarbon surfaces to decrease the van der Waals effects. Surface modification can enhance their dispersability and modify the properties of resultant nanocomposite. There are mainly two different methods to modify surface properties of nanocarbon. These approaches can be simply divided into physical (non- covalent) and chemical (covalent) functionalization.

Non-covalent can be realized by using many processes such as in-situ polymerization solution mixing. The advantage of non-covalent functionalization is that it has no effect on the final structural properties of material, for example there are possibility of attaching functional groups to graphene without destroying the electronic network [32], [33]. The non-covalent attachment, controlled by thermodynamic criteria, which for some polymer chains is called wrapping (Figure 1-5b) can alter the nature of carbon nanofillers surface and make it more compatible with the polymer matrix. The drawback is that the force between the wrapping molecules and nanotube may be too weak and consequently lowers the efficiency of filler to transfer the load [34].

Chemical functionalization, (Figure 1-5c) is based on the covalent bond of functional groups onto a carbon form of CNTs or graphene sheets. Covalent functionalization of carbon nanotubes was achieved by solvent processing, plasma treatment, etc. The attachment of small molecules on CNTs surfaces has expanded the applications of CNTs since their compatibility with polymer matrices significantly enhanced [35].

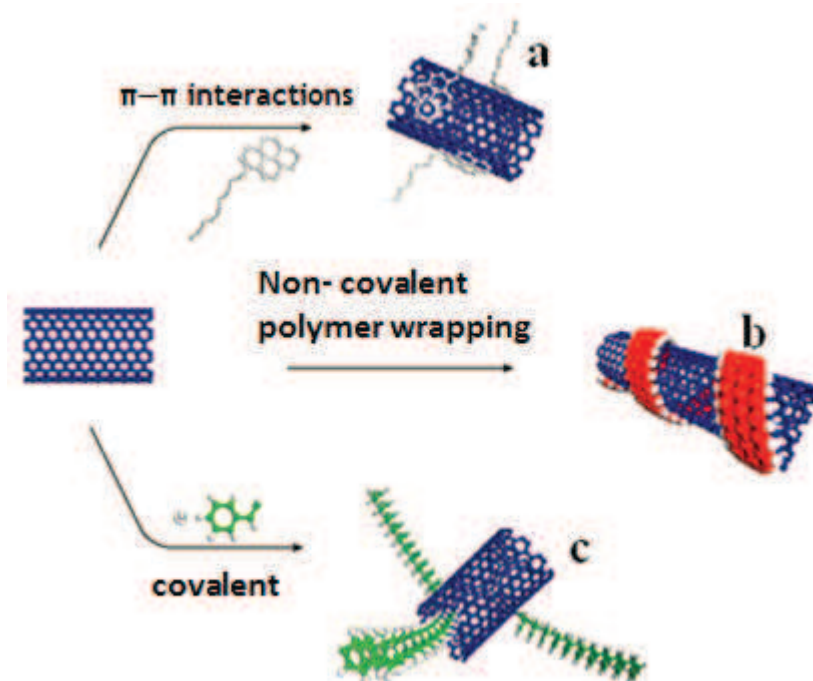


Figure 1-5(a) Aromatic molecules can be appended to nanotubes using certain non-covalent interactions (known as  $\pi$ - $\pi$  interactions). Groups emanating from these molecules interact with the surrounding solvent or matrix (b) Non-covalent interactions (including  $\pi$ - $\pi$  interactions, van der Waals forces and charge-transfer interactions) can be used to wrap polymers around nanotubes (c) chemical groups can be covalently attached to nanotubes [36].

A covalent functionalization can be either "grafting from" or "grafting to". "Grafted from" involves the polymerization of monomers from the surface using initiators, chain transfer agent or catalysts, which are covalently attached to the surfaces of the CNTs. "Grafting to" involves the attachment of chains like polymers to the surface of CNTs previously functionalized adequately to react with the functional groups of polymers [37], [35].

Gonçalves et al.[38] have successfully grafted the surface of GO with PMMA chains by using atom transfer radical polymerization (ATRP). The resulting material GO-PMMA was dispersed in organic solvent and applied as reinforcement particles in the preparation of PMMA composite films. A much more homogeneous distribution of the GO in the PMMA matrix was then achieved. The mechanical analysis of the resulting films, GO-PMMA/PMMA, showed that loading as low as 1% (w/w) of GO in PMMA are effective reinforcing agents, yielding tougher films than those of pure PMMA. The thermal analysis also showed an increase in the thermal stability properties of the films prepared with GO-PMMA fillers in comparison with non-modified fillers providing evidence that strong interfacial interactions between PMMA and GO-PMMA are achieved.

Mammeri et al. [39] demonstrated that the introduction of an appropriate functional group on the surface of CNTs/ methyl methacrylate compatible with the polymer matrix, and the controlled of its length leads to a better miscibility of CNTs in common organic solvents and



in polar polymers like PMMA. The nanoindentation results for the thin films prepared from PMMA and modified CNTs showed significant improvement in the mechanical properties of the resulting nanocomposites.

The disadvantage of covalent functionalization of CNTs is that the structure and the original properties of carbon nanotubes are changed after functionalization process. Functional groups might introduce defects on the surface of the nanotubes and these defects will turn down the effectiveness of the reinforcing component, thus, there will be a tradeoff between the capability of the interface and the durability of the nanofillers. Generally, the covalent attachment of functional groups to the surface of nanocarbons can improve the efficiency of load transfer [33][34].

## **1.8 Fabrication of polymer nanocomposites**

Basically, there are three methods to prepare nanocomposites including melt mixing, solution mixing and in-situ polymerization [40].

### **1.8.1 Melt mixing process**

Melt mixing is a common method employed to disperse nanocarbon fillers easily and uniformly through the polymer matrix by using extruder or an internal mixer. Polymer and nano-reinforcement fillers are added in the extruder and subjected to intense mixing for some time and nanocomposite comes out from the die. In this method, polymer mobility simply comes from thermal energy [24]. This method is suitable for polymers that cannot be processed with solution techniques due to their insolubility in common solvents [41]. Amorphous polymers can be processed above their glass transition temperature and any additives, such as carbon nanotubes can be mixed into the melt state by shear mixing. The shear forces help to break nanotube aggregates or prevent their formation [42]. The advantage of this technique is its speed and simplicity. Melt mixing process may be the more preferred method for producing nanocomposites for commercial use.

### **1.8.2 Solution mixing process**

Solution mixing process is the most common method for preparing polymer nanotubes composites. The difference with the previous one is the use of a solvent to favor nanofiller dispersion. This method mixed nanotubes and polymer in a favorable solvent before evaporating the solvent to form a composite film [43]. Solution mixing method has the advantage that the viscosity of the system can be controlled to be low enough to achieve acceptable dispersion of nanotube in polymer matrix [44]. The solvent used will help the mobility of the polymer chains which can intercalate of the polymer chains with the nano-reinforcement [24]. In general, solution processing method can be summarized by the following steps.

1. Dispersion of nanotubes in either a solvent or polymer solution by energetic agitation.
2. Mixing of nanotubes and polymer in solution by energetic agitation.
3. Controlled evaporation of solvent leaving a composite film.

The choice of solvent is generally made based on the solubility of the polymer. However pristine nanotubes cannot be well-dispersed in most solvents. To get around this problem a number of groups have used an additive such as a surfactant to disperse the nanotubes before mixing with the polymer solution [45]. The disadvantage associated with this method is the large amount of solvent required for the preparation of nanocomposite, which for industrial application may not be environmentally friendly or cost effective [44].

### 1.8.3 In-situ polymerization

The third method which is commonly employed for the preparation of polymer nanocomposites is in-situ polymerization process. This method provides many of the benefits of solution mixing such as good dispersion due to low viscosity of monomer without using solvent. However, the need to use solvent remains if the viscosity of the monomer is too high. If the solvent is used it can interfere with polymerization and reduces the length of resulting polymer chains. In-situ polymerization technique is suitable for preparation of insoluble and thermally unstable polymers, which cannot be processed by solution or melt processing [45]. The low viscosities during this process lead to better dispersion of nanotubes and subsequent polymerization of monomer, which lead to the uniform interaction of polymer around the nanotube. A polymer can be also chemically grafted to the nanotube surface either by acidic functionalities generated on the surface by chemical treatment or by direct grafting of polymer chains onto the surface of nanotubes by using the surface immobilized initiators [44].

In general, an in-situ polymerization can be applied for the preparation of almost any polymer nanocomposites. The nano-filler can be either non-covalently or covalently bond to the polymer matrix [4]. Velasc-Santos et al. incorporate of the unfunctionalized and carboxyl functionalized MWCNTs into a PMMA by the use in-situ polymerization process with radical initiator. FTIR results showed that unfunctionalized MWCNTs could have chemical interaction with a polymer through opening  $\pi$  bonds on MWCNTs during polymerization process. Moreover MWCNTs functionalized with the carboxylic groups have reactive groups on the tip and surface, which are more useful for bonding them with polymer chains when the polymerization is carried out [46]. Many researchers [47], [48], [49], [50], [45] employed in-situ radical polymerization to fabricate MWCNTs-PMMA composites by using radical initiator and they believe that  $\pi$ -bond in carbon nanotubes were initiated by the initiator during polymerization process. Therefore nanotubes can precipitate in polymerization to form strong interface between the MWCNT and polymer matrix.

## 1.9 Fabrication of surface coating

### 1.9.1 Introduction

A coating is important to modify surface properties. Several strategies have been tried by researchers for improving surface properties of products [51]. For instance, most polymeric glass are sensitive to scratching and coating is a common way of improving the scratch behavior of these materials [23]. Scratch protection films are necessary to achieve mechanical properties similar to glass on soft substrates. The mechanical behavior, such as elastic

modulus, hardness and fracture toughness are responsible for the coating resistance of the overall system [25].

## **1.9.2 Surface coating methods**

There are a lot of coating techniques such as spin coating, doctor blading, casting, spray coating, slot-die coating, slide coating and knife-over-edge coating [25].

### **1.9.2.1 Casting**

This is the simplest film-forming technique. The advantage is that no equipment is needed except a horizontal work surface. The procedure is to simply cast a solution onto a substrate followed by a drying step. While it is possible to prepare films of good quality and also thick films, the technique suffers from a lack of control over the film thickness and often picture framing effects are observed near the edges of the film or precipitation during drying. Moreover, in a case the surface tension of the liquid dominates, the drying is inhomogeneous. There is also a requirement that the material to be coated has a high solubility in the solvent used if crystallization and precipitation is to be avoided [25].

### **1.9.2.2 Spin Coating**

The typical spin coating operation involves an application of a liquid to a substrate followed by high-speed rotation of the substrate. Alternatively the liquid solution may be applied while the substrate is spinning. The angular velocity of the substrate with the overlying solution results in the ejection of most of the applied liquid where only a thin film is left on the substrate. The thickness, morphology and surface topography of the final film obtained from a particular material in a given solvent at a given concentration is highly reproducible. These properties are known to depend highly on rotational speed, viscosity, volatility, diffusivity, molecular weight and concentration of the solutes. They have little dependence on the amount of solution deposited, the rate of deposition and the spinning time.

The film thickness  $t$  obtained during a spin coating experiment can be expressed by the experimental relationship:

$$t = kw^\alpha \quad (1-1)$$

Where  $w$  is the angular velocity and,  $k$  and  $\alpha$  are empirical constants related to the physical properties of the solvent, solute and substrate. Typically,  $\alpha$  has a value of around (- 0.5) and the constant  $k$  contains many parameters such as the initial viscosity of the solution. Despite the complexity of film formation, the method allows highly reproducible formation of films and has several advantages over other coating techniques and allows formation of very homogeneous films over a large area (the diameter of the substrate can be as high as 30 cm) [25].

### 1.9.2.3 Doctor Blading

The films obtained by Doctor Blading technique, have controlled thickness. Compared to the spin coating technique Doctor Blading technique is more economic because the loss of coating solution is minimized (less than 5%). The technique proceeds by placing a sharp blade at a fixed distance from the substrate surface that is to be coated (typically 10–500  $\mu\text{m}$ ). The coating solution is then placed in front of the blade that is moved linearly across the substrate leaving a thin wet film after the blade. The final wet thickness of the film is ideally half the gap width but may vary due to the surface energy of the substrate, the surface tension of the coating solution and the viscosity of the coating solution.

The final dry thickness of the coated film ( $d$ ) can be calculated from the empirical relationship:

$$d = \frac{1}{2} \left( g \frac{c}{\rho} \right) \quad (1-2)$$

Where ( $g$ ) is the gap distance between the blade and the substrate, ( $c$ ) is the concentration of the solid material in the solvent in  $\text{g.cm}^3$  and ( $\rho$ ) is the density of the material in the final film in  $\text{g.cm}^{-3}$ . Compared to the spin coating technique, doctor-blade method gives films that are perhaps thermodynamically more equilibrated because of a slower speed of solvent evaporation [25].

### 1.9.2.4 Spray coating

This technique involves forcing the suspension through a nozzle where a fine aerosol is formed. A carrier gas and electrostatic charging may be involved to aid in directing the aerosol at the surface that is to be coated [25]. The main advantage of this method is that coated surface is unlimited in size and the thickness also. The well-controlled process required although to be automated, especially to obtain homogeneous thickness all over the surface.

## 1.10 Conclusions

1. No polymer can provide a reasonable low working wear rate with optimum coefficient of friction required, so there is a need to modify most polymers by suitable filler that can reduce the wear and coefficient of friction.
2. PMMA reinforced with nanocarbon fillers like MWCNTs, graphene and graphene oxide can have excellent tribological properties. To maximize the advantage of nanocarbon filler as effective reinforcements in high strength composites, they must be well dispersed to prevent aggregates formation. Generally several techniques are employed to enhance the dispersibility of nanofillers in polymer matrices, such as the optimum physical blending, in situ polymerization and chemical functionalization [30].

3. Slip additives can control the surface of polymer film and sheet to enhance its tribological performance. Stearamide, Erucamide and Oleamide are types of slip agents that can be produced by the amidisation of long chain fatty acids. The working principle of these additives depends on their migration them to the surface over time and modifies the surface properties.
4. The critical carbon filler content in the matrix can play a major role in determining the mechanical properties of the resultant composite. For example, the mechanical properties can decrease with the increase loading of nanofiller after critical and sometimes, these properties decrease below the neat matrix material. The filler size and critical fiber length also have a great impact on mechanical and tribological properties of composite.
5. Coating is a common way to improve the scratch behavior of polymeric materials and inorganic components with nanoscale dimensions. It brings a great effect on improving the scratch and wear resistance maintaining gloss and transparency of the nanocomposite coating. There are a lot of coating techniques such as spin coating, doctor blading, casting, spray coating, slot-die coating, slide coating and knife-over-edge coating that are employed to form coating surfaces.

## 2 Mechanical and tribological properties of polymer nano-composites

### 2.1 Mechanical properties

To satisfy the tribological requirements, coated surface must have a suitable combination of properties, for example in terms of hardness, elasticity, shear strength, fracture toughness, thermal expansion and adhesion.

For coated systems (Figure 2-1 )there are four different zones, each with different properties which must be considered [52].

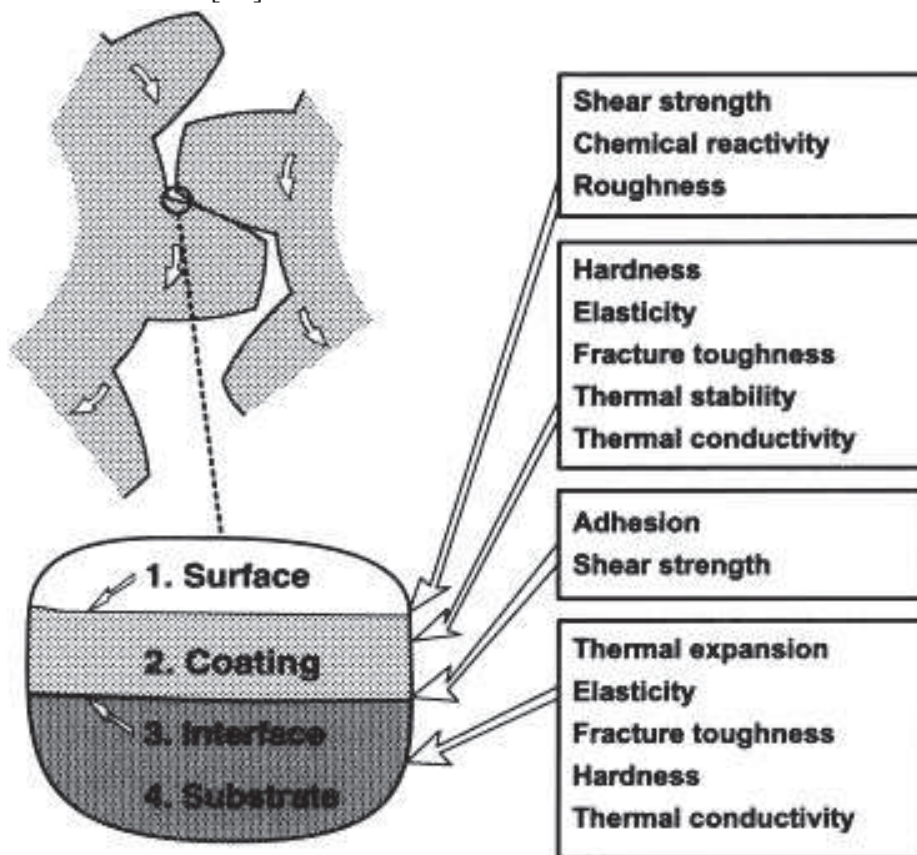


Figure 2-1 Tribologically important properties in different zones of the coated surface [53].

#### 2.1.1 Elastic properties

The mechanical behavior of a polymer is a function of its microstructure or morphology and the elastically work should be done against the forces holding the material together when a glassy polymer is stretched. These forces come from different sources and can be roughly divided into three groups. The intermolecular forces holding chains together to pull neighboring chains apart, for non-polar molecules these are primarily van der Waals polarization forces. To elongate individual chains, work has to be done to bend and stretch

the bonds between the carbon atoms making up the chain backbone. If the chains are randomly kinked as they are in an amorphous polymer, then they can be elongated, if rotation takes place about certain bonds in the chain backbone in which case work has to be done against the steric hindrance to rotation. The overall elastic modulus of the structure will be determined by a combination of these various effects [54].

The mechanical response of amorphous polymers is known to be strongly influenced by testing conditions. For this reason, the development of material constitutive models must consider both temperature and strain rate dependence, in the glassy region, the initial Young's modulus of amorphous polymers,  $E$  is found to decrease with increasing temperature in the following manner [55].

$$\log E(T) = \log E(T_{\text{ref}}) - a(T - T_{\text{ref}}) \quad (2-1)$$

Where  $E(T_{\text{ref}})$  is the Young's modulus at the reference temperature  $T_{\text{ref}}$  and  $a$  is a parameter characterizing the temperature sensitivity of the material.

Polymer composites reinforced with fibers of high Young's modulus are an important class of lightweight materials often characterized by excellent specific mechanical properties [56]. Polymer matrix reinforced with high aspect ratio fiber can increase both Young's modulus and strength of the composite using a stress transfer mechanism from the matrix to the fiber during external loading. The assumption which represents the principle of reinforcement polymer matrix explains that at a given composite strain the fiber carries more stress than the matrix since it is stiffer [57].

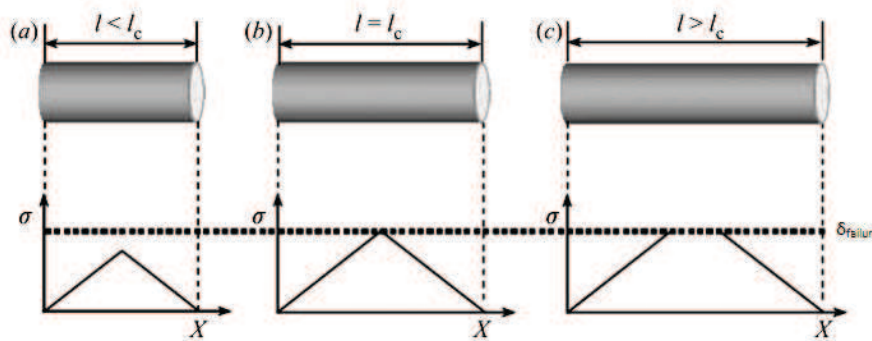


Figure 2-2 (a) Short fibers have insufficient length to reach the failure stress of the fiber ( $\delta_f$ ) as indicated by the dotted line, whereas fibers of (b) critical fiber length  $l_c$  or (c) greater can fracture [57].

Figure 2-2 shows the tensile stress transfer profile along the fiber length during composite straining. As a result, straining of a composite with short fiber will generally cause failure away from the fiber itself, may be within the matrix or at the interface between fiber and matrix. For longer fiber a sufficient length can just cause failure in the fiber, with this length often referred to as the critical fiber length or ( $l_c$ ). The critical fiber length can also be used as an indication of the level of adhesion between the fiber and the surrounding polymer matrix in a composite material. A weak interfacial strength will cause the stress profile to build up slowly along the fiber length, resulting in large ( $l_c$ ) values, whereas very strong fiber-matrix interfaces cause a rapid rise in tensile stress in the fiber during composites straining resulting

in relatively small ( $l_c$ ) values. The relationship between the critical fiber length ( $l_c$ ), interfacial strength ( $\tau_c$ ) and fiber diameter ( $d$ ) and the fracture stress of the fiber ( $\delta_f$ ) has been determined by Kelly and Tyson:[58]

$$l_c = \frac{\delta_f d}{2\tau_c} \quad (2-2)$$

The relationship between the fiber diameter ( $d$ ) and the critical length ( $l_c$ ) indicates how smaller diameters can improve the efficiency of polymer reinforcement [57]. Many works showed that after a critical carbon filler content in the matrix, mechanical properties decrease with the increasing critical loading of nanofiller and sometimes these properties decrease below the neat matrix material [56]. Above a critical filler concentration, nanocarbon fillers tend to agglomerate and 3D network will be formed in the polymer matrix, this 3D network generates the volume fraction of nanocarbon filler and this is called the percolation threshold ( $V_c$ ) [59]. The filler size also has a great impact on mechanical and tribological properties of composite. Nanocomposite with finer fillers would realize the great enhancement in the surface properties, in another words, there is a critical particle size below which the wear resistance of the composite can be improved [60], [61]. Fu et al. studied the effects of particle size, particle/matrix adhesion and weight fraction of particle on composite stiffness, strength and toughness of a range of particulate composites having both micro- and nano-fillers. The results showed that among these three factors, particle/matrix adhesion composite has a significant effect on strength and toughness. This is expected because strength depends on effective stress transfer between filler and matrix [60].

Wang Guihua et al. [62] studied the effect of variety particle size of  $ZnO_2$  filler on the tribological behavior of poly(etheretherketon) (PEEK) and showed that the ability of  $ZnO_2$  to improve the tribological behavior is increased with decreasing the particle size of  $ZnO_2$ . Increasing the particle size in the sample showed low wear resistance because the composite has poor adhesion and transfers to the sliding counterface. The same conclusion is also made by Xing and Li [63]. They used spherical silica particles as a filler to reinforce an epoxy matrix and they showed that the filler with smaller size seemed to be more effective in the improvement of tribological performance of composites.

## 2.1.2 Hardness

### 2.1.2.1 Definition

The hardness of material is its ability to resist local deformation. It is therefore the ability of a material to resist penetration by other bodies. The hardness is traditionally measured by pressing normally an indenter on a surface. The indenter is removed and the shape of the residual imprint is optically examined. Usually, hardness  $H$  is calculated from the projected area  $A$  of indentation and the load  $P$ : [64]

$$H = \frac{P}{A} \quad (2-3)$$



Where (A) is estimated using the indentation area.

Different standards have been formulated for measurement of normal indentation hardness depending on geometrical shapes of the indenter such as Brinell (spherical), Vickers (pyramidal) and Rockwell (conical). Hardness represents the plastic component in the case of metals that mean the hardness is normally associated with the irreversible deformation and hence the induced plastic flow. Such definitions are difficult to apply to polymers as they show a wide range of deformation behaviors, namely elastic, elastic-plastic, visco-elastic or visco-plastic and for a small change extrinsic parameters (Figure 2-3) [65].

On polymer samples, hardness can be measured by nanoindentation techniques and analysed by the Oliver-Pharr model. This model does not take into account the viscoelastic part of polymeric materials but it gives a rather good way of comparison [66]. When a rigid conical indenter is pressed into a solid deformable block it introduces an intense and localized strain field. The resistance provided by the block describes its hardness. For ductile materials, the hardness is normally associated with the irrecoverable deformation and hence the induced plastic flow. With organic polymers such as poly(methyl methacrylate) PMMA a palpable elastic component accompanies the plastic flow [67].

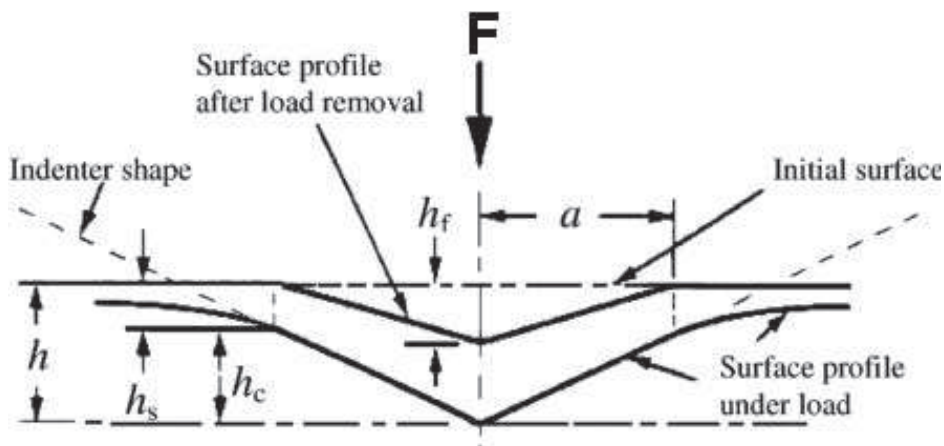


Figure 2-3 schematic representation of a section through an indentation using a conical indenter [68].

The deformation below a Vickers indenter did not followed plasticity theory by shown outward flow of metal, but resembled the deformation that would be expected if there was radial flow of the metal away from the indenter. In 1964 Marsh suggested that this behavior was due to elastic yielding of the hinterland, the deformation resembling the expansion of a spherical cavity into a plastic-elastic solid by an internal (hydrostatic) pressure Figure 2-4a. Hill (1950) showed that the pressure  $p$  at which the cavity expands depends on the ratio of yield stress  $Y$  to the elastic modulus [64].

The variation of  $\frac{p}{Y}$  with the ratio  $\frac{E}{Y}$  is shown in Figure 2-4b. It is seen that when  $\frac{E}{Y}$  small,  $p$  is only  $1.1Y$ . This corresponds to a very elastic material which is able to adjust the plastic strains and so reduces the restriction on flow. This demonstrates the behavior of many plastics.

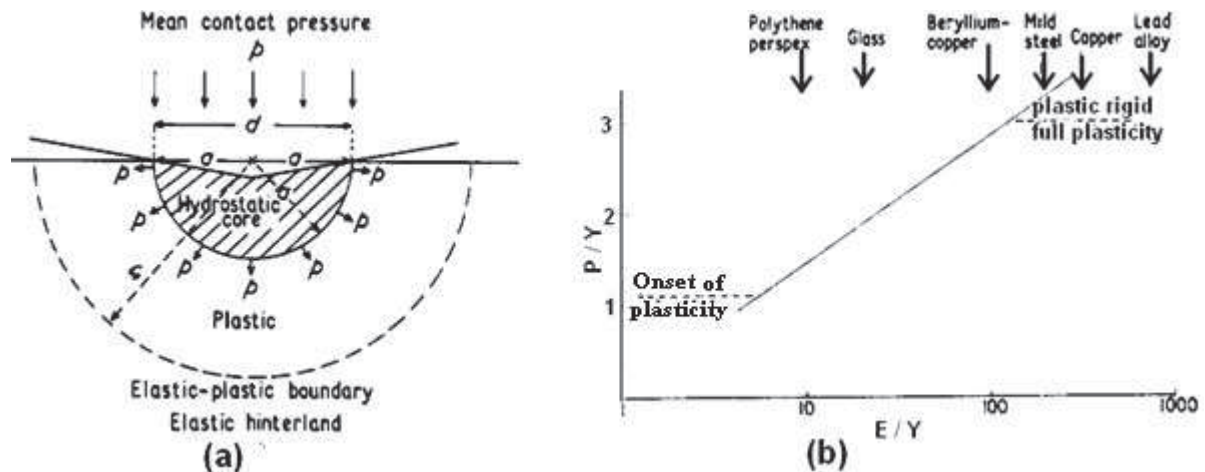


Figure 2-4 (a) The indentation process in an ideal elastic-plastic solid regarded as the expansion of a hemispherical core, (b) the variation of indentation pressure  $p$  with the ratio  $E/Y$  where  $E$  is Young's modulus and  $Y$  the yield stress [64].

### 2.1.2.2 Influence nanofillers on the hardness of the polymer nanocomposites

Carbon nanotubes (CNTs) display perfect chances for developing high performance composite materials. Mammeri et al [39] concluded nanoindentation results of thin films prepared from PMMA and modified MWCNT that the MWCNT can improve the mechanical properties of the composites. The hardness in such nanocomposite increased from 140 MPa for pure PMMA to 186 and 250 MPa for composites reinforced MWCNT-COOH and MWCNT-grafted- PMMA respectively. Das et al [12] study the effect of introducing few layer graphene in PMMA matrix using solution mixing technique. Nanoindentation tests results showed that the hardness was increased from 140 MPa for pure PMMA to 144.9, 145.6, and 153.1 MPa for composites reinforced with 0.2, 0.4, and 0.6 wt. % of few layer graphene. On the other hand, Alam and Verma [69] concluded that the hardness of PMMA/pristine MWCNTs composites prepared by in situ polymerization method was decreased with increasing the volume fraction of MWCNTs. This may be explained by weak interfacial interactions between MWCNTs and polymer (PMMA) matrix.

## 2.2 Tribology of polymer nanocomposite

### 2.2.1 Definitions

When two bodies are in contact under a normal load and a relative motion between the bodies starts, some friction force arises. The ratio between the friction force and the applied normal load to the moving tip is called the apparent friction coefficient  $\mu_{app}$ .

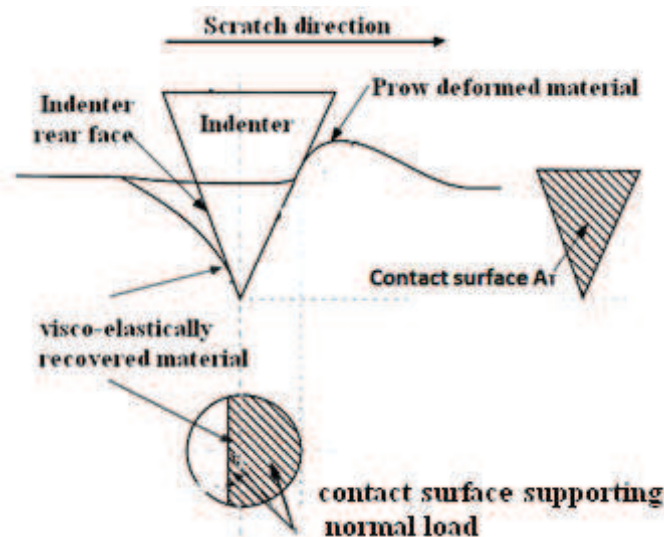
Scratch can be described as an irreversible mechanical deformation process during the movement of a head tip on polymeric surface at constant speed and temperature. Even at low contact loads, most of the polymers are particularly hypersensitive to remarkable surface deformation and damage [70], [71].

In normal indentation the direction of the applied force is normal to the surface and the hardness is measured as the reaction force per unit of contact area between the indenter and the test material, whereas in scratch hardness a tangential force arises in the presence of a normal load. Scratch hardness arises from resistance of the material to the dynamic surface deformation, i.e. ploughing, and from the interfacial friction between the indenter surface and the material.

When the indenter tip moves across the surface of material, the load is not symmetrically supported around the cone apex. A significant amount of elastic/plastic deformation and brittle cracking can occur due to tangential scratch force which acts as tensile force on the rear half of the tip.

Tangential hardness, defined as the ratio of the tangential force and  $A_T$  perpendicular cross-section, upon which the force acts, is also called ploughing hardness or scratch resistance of the material (Figure( 2-5)).

The evolution of area  $A_T$  in the case of viscoelastic- plastic material involves estimating the contribution to friction given by the prow of material which generally forms ahead of the indenter and which may have a considerable effect upon the adhesive component of the resistance to the scratching [72], [73].



Figure( 2-5) Scratching contact geometry for a viscoelastic- plastic material material [74].

In the scratch testing of thin coating, the scratching tip moves across the coated surface under increasing load until a certain load referred to as the critical load ( $F_c$ ). It is characterizes as the beginning of failure event (taking into account that the maximum depth under loading is thickness over 10 to get the mechanical response of the coating).

Gauthier et al., clarified that the ratio of the thickness of the coating to the roughness of the tip is confirmed to be a critical parameter and governed the scratch resistance increase for thin coating [23].

W. Boentoro et al. studied the impact of the film thickness on the critical load in scratch testing for both coatings on glass and on polycarbonate (PC) polymer. For PC, they observed an increase of the critical load for first failure up to 5 N at 2  $\mu\text{m}$  thicknesses while for the

increase from 2 to 4  $\mu\text{m}$  thicknesses, only the critical load for the transverse cracking can be raised to 10 N [75].

### **2.2.2 Influence of nanofillers on nanocomposites tribological properties**

In the pristine or bulk form, only few polymers would satisfy most of the tribological requirements. In fact, it is well-known that an improvement of the mechanical properties can be effectively achieved by introducing “small” inorganic particles in the polymer matrices [76].

Recently, due to high load-bearing capacity, low surface energy, high chemical stability, weak intermolecular and strong intramolecular bonding, carbon nanotube have received a great attention by tribology researches [14]. The favorable tribological performance of these nanocomposites can be attributed to either one or more of the following phenomenon:

1. The presence of CNTs with high aspect ratio enhances the mechanical stability and increases the load bearing capacity of the nanocomposites. It helps the polymer structure to resist plastic deformation and to reduce the adhesive and plough wear.
2. The tubular structure of CNTs make it acts as a spacer thereby effectively reducing the contact with the counter face in the interface between two mating surfaces.
3. CNTs possess excellent self-lubricating properties based on the sliding/rolling effect at the interface between mating surfaces [1], [77], [78].

Since the geometric structure of individual CNT are highly anisotropic in nature, the tribological properties of CNTs-polymer nanocomposites are orientation dependent [6].

Graphene showed great promise in tribological application and is one of the high self-lubricating materials [13]. The weak van der Waals force between the 2D layers can make the inter-layer sliding more easily in multilayer graphene which lead to a reduction in coefficient of friction. And also increase wear resistance due to the reinforcement effect with graphene [79].

Depending on the required service for composite material, there are two different roles for filler throw, and this can be achieved through the selection of the matrix and the filler:

#### **2.2.2.1 Hard and strong filler in a softer matrix (bulk modification)**

The function of the filler here is to strengthen the polymer matrix and thus increase the load bearing capacity of the composite. This system showed a better result in terms of load-bearing capacity and toughness. Issue that has significant effect on the reinforced composite is critical concentration. Many experimental results have shown that the enhancement of properties can take place up to a specific weight or volume fraction of filler after which the reinforcement efficiency decreases [1] [80]. Table 2-1 showed the effect of some nanocarbon fillers on the mechanical properties of polymer nanocomposites.

<i>Nanocomposites</i>	<i>Filler weight fraction (%)</i>	<i>Processing method</i>	<i>Elastic modulus (%increase)</i>	<i>Tensile strength (%increase)</i>	<i>References</i>
Graphene in the PMMA matrix	0.5	In situ polymerization	150	115	[81]
PMMA-grafted MWNTs in the SAN matrix	1	solution casting from THF	51	99	[82]
Graphene grafted Octadecylamin in the PMMA matrix	0.5	In situ polymerization	/	67	[83]
MWNTs grafted Octadecylamin in the P(MMA-co-EMA) matrix	10	solution-mixed	135	49	[84]
MWNTs pristine in the P(MMA-co-EMA) matrix	10	solution-mixed	9.2	12.8	[84]
GO-grafted MWNTs in the PMMA matrix	1	solution-mixed	16	20	[38]
GO in the PMMA matrix	2	In situ polymerization	29.9	15	[17]

Table 2-1 Mechanical properties for nanocarbon filler reinforced polymer matrix

### 2.2.2.2 Soft and lubricating fillers in hard and strong matrix

The low shear strength and self-lubricating properties of filler which is used in this type of composite can reduce the coefficient of friction and wear. Sufficient amount of fillers should be located at the interface to reduce the coefficient of friction and increase the wear resistance. In this kind of system, a controlled diffusion of the lubricant to the surface is critical for improving the coating life time. The disadvantage of this type of composite is clearly the reduction in the strength and load carrying capacity of the material in the composite form. Therefore, the addition of this type of fillers beyond a certain percentage (by volume or by weight) may give counterproductive results for tribological performance due to the fall in the bulk properties [1], [77].

Fatty acid amides are functional organic additives used to decrease the frictional properties of film by migration to the film surface. Maria X. Ramirez et al. [20] performed a comparative study between the effect of Erucamide and Behenamide on the friction coefficient of low density polyethylene film and they concluded that the film containing Erucamide have coefficient of friction lower than the film containing Behenamide. By using the AFM technique to qualitatively examine the structure of Erucamide and Behenamide crystals on the film surface, they clearly evidenced that Erucamide crystals are much larger than the Behenamide crystals and Erucamide crystals showed a layered or plate-like formation while Behenamide crystals showed a bumpy structure. This may explain the difference in tribological behavior between them. Mansha et al. [85] showed the effect of many types of fatty acid amides on the surface properties of PMMA and they concluded that the coefficient of friction of PMMA can be reduced by: i) the use of appropriate plasticizer and ii) lower

amounts of fatty acid amides. In addition they clarified that the bulk yield stress and yield strain are not changed significantly by fatty acid amides.

### 2.2.3 Tribological analysis and relevant scales

The tribology of a contact involving surfaces in relative motion can be understood as system with input and output data. Input data are the geometry of the contact on the macro and microscale, the material properties based on the chemical composition and structure of the various components involved and the environmental parameters. The experimental imposed parameters such as normal load, velocity and temperature and the measured parameters as tangential force can be used as a starting point for the analysis of a tribological contact (Figure 2-6) [53].

During the sliding contact some settings will change (the output data), surface layers are formed, strain hardening takes place, local temperature increases causing softening, etc. and a new set of parameters that control the friction and wear can be obtained after one sliding event [86]. The three relevant scales of friction called macroscopic, local and molecular friction scales are important to understand and analysis the dissipative mechanisms. For each scale, a related type of friction is involved.

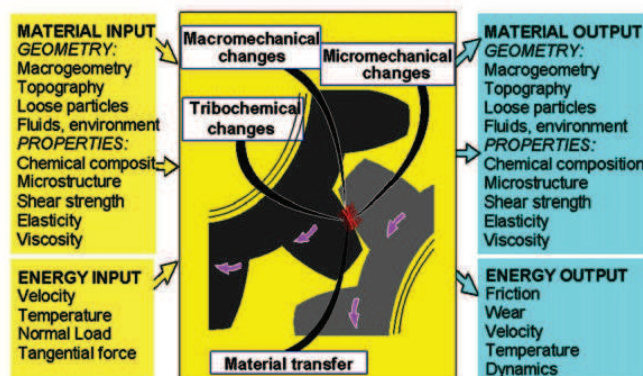


Figure 2-6 The tribological process in a contact between two surfaces including mechanical and tribochemical changes and material transfer, The changes are determined by material and energy input parameters and result in a comparable set of partially changed output parameters[86].

#### 2.2.3.1 Macroscopic friction scale

The macroscopic scale is that of the relative motion between two macroscopic bodies. The contact areas consist of a large number of elementary discrete local contact areas with different geometries, but the friction of each of these elementary contacts is only an apparent value. This apparent value is itself the sum of a true local friction (Figure 2-7) (the ratio between the interfacial shear stress at the interface and the local pressure) and the viscous and/or elastic-plastic and/or plastic flow of the material around the local contact area. Measurements of the macroscopic friction show a dependency on temperature and sliding velocity and attempts were made to give a physical sense to this dependency [87], [88].

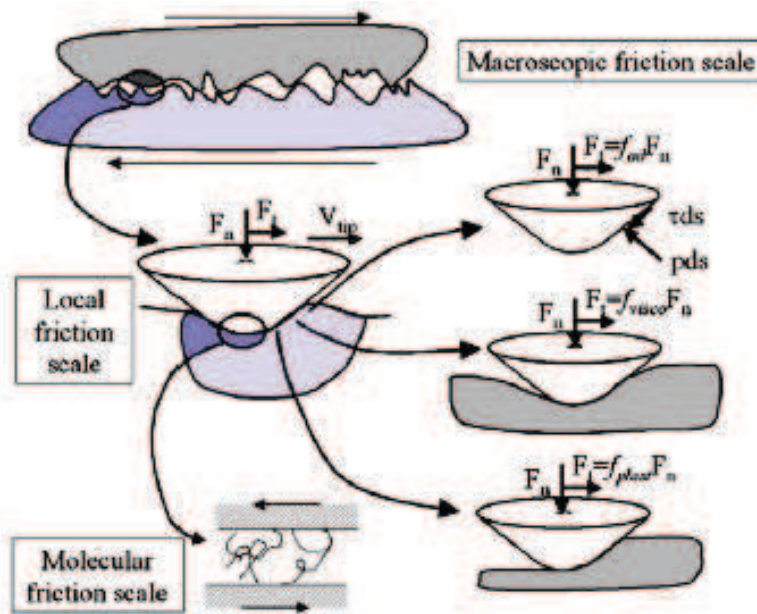


Figure 2-7 The three relevant scales of friction called macroscopic, local and molecular friction scales.[87]

### 2.2.3.2 Local friction scale

The sources of the friction and wear phenomena observed on the macrolevel are found in the mechanisms that take place at the micro level. The friction mechanisms explain the stress and pressure forming at the asperity to asperity level, the crack generation and propagation, material liberation, and particle formation.

In typical engineering contacts, these phenomena are at a size level of approximately  $1 \mu\text{m}$  or less, down to the nanometer range [89].

At the local scale, the contact zone is a smooth flat surface with ideal continuous contact between the bodies. For polymers when the glass temperature transition is reached, the local friction shows a peak and the growth of the friction is similar to that of the mechanical loss factor  $\tan \delta$ , this friction peak is attributed to adhesion hysteresis, due to the energy dissipated in the loading– unloading cycle.

The experimental apparent friction is the ratio of the tangential force to the applied normal load. This friction comprises an adhesive component between the surface and the moving tip and a ploughing component, the latter is connected to the contact mechanics which control the shape of the contact. Provided the adhesive and ploughing parts of the friction do not interfere with each other, the apparent friction is classically written as: [90]

$$\mu_{app} = \mu_{adh} + \mu_{plough} \quad (2-4)$$

The local friction is defined as the ratio of the local shear stress  $\tau$  to the local pressure  $p$  and may be written as: [88]

$$\mu_{loc} = \frac{\tau_{Local}}{p_{Local}} \quad (2-5)$$

To a first approximation, the local friction is equal to the adhesive friction. The ploughing friction may be decomposed into one term due to the viscoelasticity and another due to the plasticity. Hence the friction may be written as:[87], [90]

$$\mu_{\text{app}} = \mu_{\text{adh}} + \mu_{\text{visco}} + \mu_{\text{plastic}} \quad (2-6)$$

#### 2.2.4 Tribological measurement: direct observation of the contact during scratching

In the case of solid polymers, the material underneath the moving tip may display various types of behavior: elastic, viscoelastic, elastoplastic (elastic and plastic strains are present in the contact area) or fully plastic [91]. During scratching the true contact area between the moving tip and the material is somewhat difficult to predict and is therefore generally considered to be the front half of the part of the tip in contact with the surface.

As the polymer materials are viscoelastic and viscoplastic like polymers, recovery of the groove can occur. The amount of recovered material which will support the tip depends on the nature of the material, when it is perfectly plastic, there is no recovery after deformation and hence no load bearing support at the rear half of the tip. In the case of an elastic plastic or viscoelastic, viscoplastic material, there is partial support in the trailing zone (Figure 2-8).

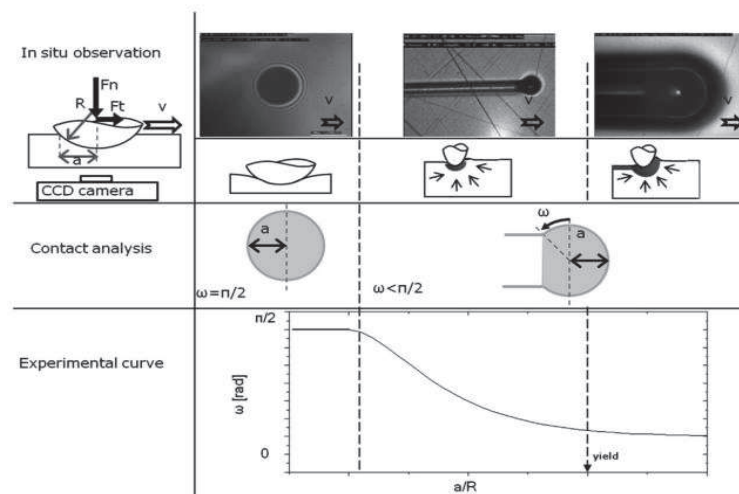


Figure 2-8 Sketch of typical snapshots during sliding of a spherical rigid indenter on a transparent polymeric surface in the elastic, elasto-plastic and plastic regime. The omega angle  $\omega$  is characteristic of the rate of plastic flow in the contact [92].

Moreover, the geometry of the groove left on the surface depends on the relative levels of the contact strain and the yield strain of the material [93].

The recovery of the groove and the symmetry of the contact area can be estimated by means of an angle  $\omega$  varying from (0 to  $\pi/2$ ) (Figure 2-8).

The cross section of a groove is not identical to the profile of the grooving tip for viscoelastic and viscoplastic material. The partially elastic deformation of the surface recovered partly instantaneously and partly after a very short time depending on the plastic rate in the elastic – plastic contact. The depth of a groove is less than the penetration of the tip during its motion.



Relaxation measurements for polymethylmethacrylate (PMMA) at room temperature indicated that the relaxation of grooves is negligible after a few tenths of a second and we therefore called these grooves viscoplastic scratches. As a result, the rear contact left a groove narrower than the contact area and after this elastic relaxation the edges of the plastic flow left on the surface lay parallel (Figure 2-9 and Figure 2-10) [93].

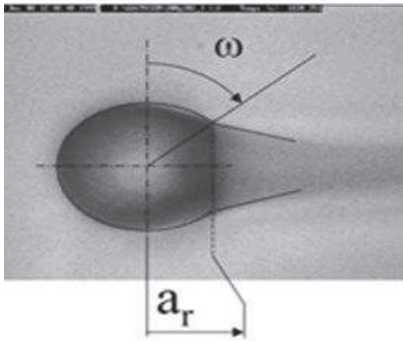


Figure 2-9 Photograph of the moving tip during viscoelastic grooving [93]

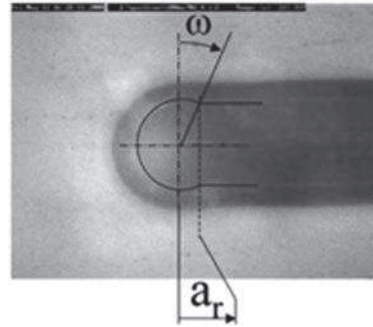


Figure 2-10 Photograph of the moving tip during plastic scratching with a spherical tip of radius 100 μm [93]

The true contact area is the sum of a front area (half disc of radius)  $a_f$  and rear area  $a_r$  (part of the rear half disc) (Figure 2-11) [91].

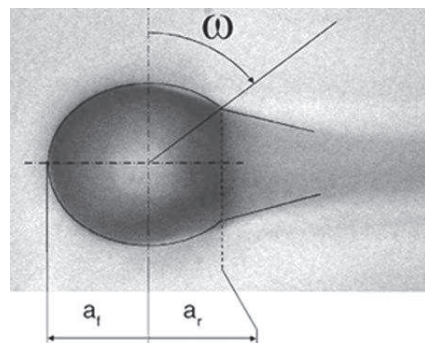


Figure 2-11 Photograph of the contact area during scratching. This area has a front part defined by the length  $a_f$  and  $a_r$  rear part defined by the angle  $\omega$  or the length  $a_r$  [88].

When the contract is almost elastic and the mechanical loss factor low, the rear area can be identical to the front area, and the ratio ( $a_r/a_f$ ) is 1, while for an elastic–plastic contact, this ratio is: [88]

$$\frac{a_r}{a_f} = 1 - \left[ 1 - \sqrt{\frac{2 \cdot C \cdot Y}{E^*} \tan \theta} \right] \frac{\varepsilon - \varepsilon_e}{\varepsilon - \varepsilon_p} \quad (2-7)$$

For plastic contact:

$$\frac{a_r}{a_f} = \sqrt{\frac{2 \cdot C \cdot Y}{E^*} \tan \theta} \quad (2-8)$$

Where  $Y$  is the yields stress,  $E^*$  the normalized elastic modulus ( $\frac{1}{E^*} = \frac{1-\nu_1^2}{E_1} + \frac{1-\nu_2^2}{E_2}$ ),  $\theta$  the apex angle of the conical scratching tip and  $C$  the coefficient connecting the yield stresses measured in a hardness test and under compression ( $C \approx 2$  for polymer).  $\epsilon_e$  and  $\epsilon_p$  denote the contact strains at the end of the elastic contact area and at the beginning of the plastic contact area [88].

#### 2.2.4.1 True contact strain

When the tip moves, energy is consumed mainly in two zones: first zone at the interface a very thin layer subject to extremely high shear strain, a high strain rate and adhesive slipping, and the second is a larger and deeper volume beneath the tip where viscoelastic and viscoplastic yield occurs, this zone is roughly spherical and its size is comparable to that of the groove left on the surface [94].

The local strain rate ( $\dot{\epsilon}$ ) may be simply estimated as the tip speed  $V_{tip}$  divided by the groove width  $L_g$ : [94]

$$\dot{\epsilon} = \frac{V_{tip}}{L_g} \quad (2-9)$$

However, in the interfacial zone, the strain rate may be several decades higher than in zones far from the tip. Tabor has shown that in the case of normal indentation, the constant ratio of hardness to yield stress for a perfectly plastic solid may be applied to a solid hardening under strain, provided the yield stress is replaced by the flow stress measured under simple compression at a representative strain  $\epsilon_r$ .

For a conical tip, where  $\beta$  is the angle between the tip and the surface: [95][94]

$$\epsilon_r = 0.2 \tan \beta \quad (2-10)$$

For spherical tip, where  $(R)$  is the radius of the tip and  $(a)$  radius of the surface contact area [95][94].

$$\epsilon_r = 0.2a/R \quad (2-11)$$

Briscoe et al. they suggested that in a viscoelastic material the proportionality constant can be lower than 0.2 [93].

#### 2.2.4.2 Viscoplastic scratch and Viscoelastic grooves

As compared to metals or ceramics, polymers like PMMA exhibit large viscoplastic and viscoelastic contributions to the imposed deformation during both indentation and scratch tests and the cross section of the groove left on the surface is not identical to the profile of the

grooving tip. Depending on the level of yielding during the contact time, the deformation of the surface, which is partially elastic, recovers partly instantaneously and partly after a short delay, thus the depth of the groove is less than the penetration of the tip during its motion and the relaxation of groove. In case of real scratching measurements of the relaxation of grooves in PMMA at room temperature indicated that the relaxation of grooves in PMMA is negligible after short time and thus these grooves are named a viscoplastic scratches (Figure 2-12) [96], [93].

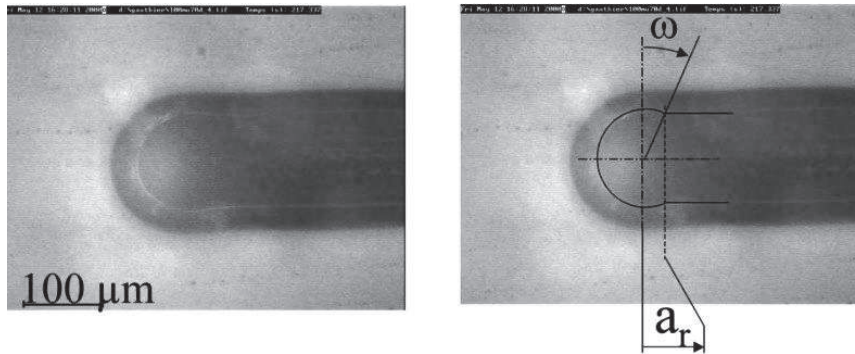


Figure 2-12 Photograph of the moving tip during plastic scratching at 70°C with a spherical tip of radius 100 μm. The edges of the groove stay parallel for a very short interval after contact, since the mean strain is sufficient to generate plastic flow around the tip [93].

The nature of the strain inside the half spherical volume under the contact area determines the nature of the process involved and in all cases, the bulk material displays elastic behavior. In the case of elastic sliding, as shown on polymer at very low contact strain, there is no groove left on the surface and the contact is a full disk: the rear angle  $\omega$  is  $\pi/2$  and the rear length is comparable to the frontal length.

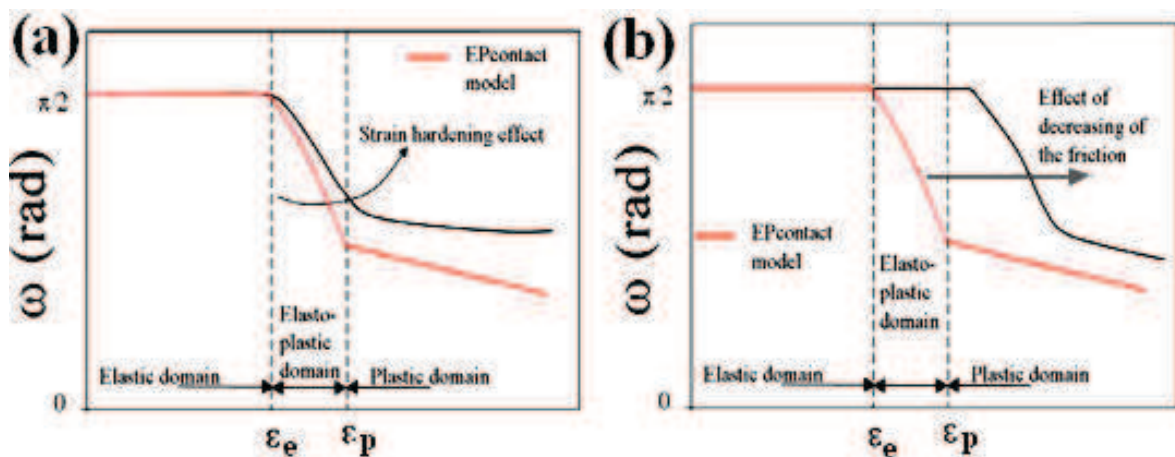


Figure 2-13 Show that the  $\omega$  angle versus the contact strain (a) the material shows strain hardening (b) elastic and elasto-plastic domains are increased in case of lower friction [88].

The contact strain can be represented by the ratio of the contact radius to the tip radius for a spherical tip. In the case of a viscoelastic contact, the rear angle  $\omega$  is equal to  $\pi/2$  for elastic deformation. If the material displays strain hardening,  $\omega$  increases Figure 2-13a [23]. As the strain rate and temperature variation, even under constant loading, the contact area may also vary considerably and the strain near the contact may change from viscoelastic to viscoplastic and a reduction in friction results in an increase in the elastic and elasto-plastic domains (Figure 2-13b) [85], [88].

## 2.2.5 Tribological properties of coatings

The macromechanical tribological mechanisms describe the friction and wear phenomena by taking into account the stress and strain distributions in the entire contact. That is the total elastic and plastic deformations, the total wear particle formation process and its dynamics.

Four main parameters can be defined to control the tribological contact behavior in contacts between two surfaces which one or both are coated:

1. The relationship between coating-to-substrate hardness.
2. Coating thickness.
3. The surface roughness.
4. The size and hardness of the debris in the contact that can come from external sources or be produced by the surface wear interactions themselves.

The relationship between these four parameters will result in a number of different contact conditions characterized by specific tribological contact mechanisms [53].

### 2.2.5.1 Hardness of the coating

The hardness of the coating and its relationship to the substrate hardness is the most important parameters that can influence the tribological behavior of a coated surface. It is better to discuss hard and soft coatings individually. When a ball is sliding on a soft plate, the frictional force is ideally the product of the shear strength and the contact area, as shown in Figure 2-14a.

A harder layer material will result in a decreased contact area but increased shear strength, and therefore no significant effect on friction (Figure 2-14b). Adding thin soft coating can cause reduction in the friction at the contact, due to the reduction of the contact area and the interfacial shear strength, as shown in Figure 2-14c [53].

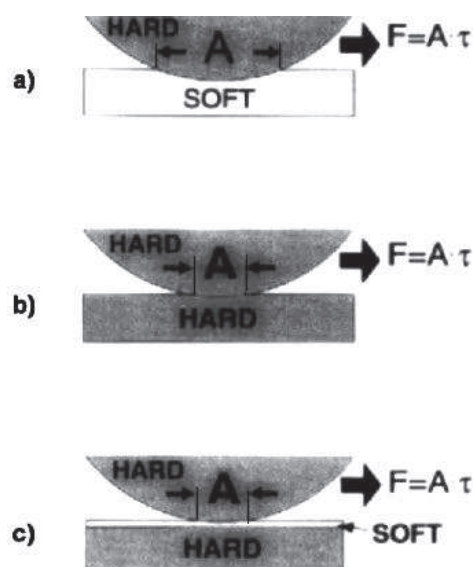


Figure 2-14 The friction is not greatly dependent on hardness, but low friction can be obtained by depositing a thin soft film on a hard plate in an idealized sliding contact [98].

When a soft substrate coated by a hard layer, the role of the hard coating here is to avoid ploughing on both a macro and a micro scale which can lower the friction and wear.

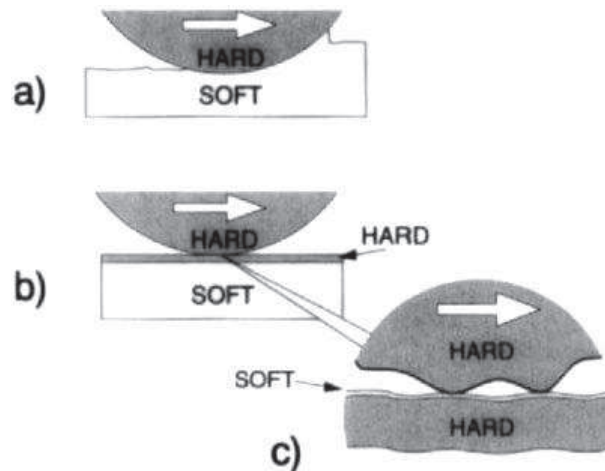


Figure 2-15 (a) A hard slider moving on a soft face results in ploughing (b) The ploughing can be hindered with a hard coating on the soft substrate (c) A soft microfilm at the top of the hard coating results in reduced friction [53][98].

In particular, hard coatings can act as an abrasive resistance coating, while low friction can be done with hard coatings if a low shear strength microfilm is created on the top of the coating, as a result, the shear will take place in the microfilm and the load is entirely supported by the hard coating (Figure 2-15) [53], [86].

### 2.2.5.2 Thickness of the coating

Assuming, the thin soft film was deposited on a hard substrate with a smooth surface and no debris existing in the contact zone, if the film is thin enough, the effect of ploughing of the film will be small, consequently, the friction can be determined by the shear strength of the film and the contact area, which is related to the deformation properties of the substrate (Figure 2-16).

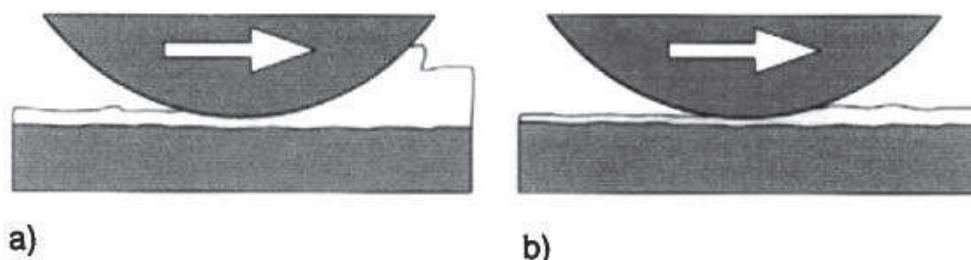


Figure 2-16 The contact of a hard slider moving on a hard flat surface coated by a soft coating is characterized by (a) ploughing for thick coatings and (b) shearing for thin coatings.

For a sphere sliding on a hard plate coated with a soft coating, the contact area is determined by the Hertzian equation. Roberts (1989 and 1990) has shown that the coefficient of friction in this situation can be calculated from the equation: [99]

$$\mu = \frac{\pi\tau}{Fn^{1/3}} \left( \frac{3R}{4E'} \right)^{2/3} \quad (2-12)$$

Where  $\tau$  is the shear strength of the coating,  $F_n$  the normal load,  $R$  the radius of the sphere and  $E'$  the reduced modulus of elasticity of the contact materials. The above equation shows that there are two main criteria to achieve low friction, first the film should have the property of low shear strength and the second it should be applied onto surfaces of high hardness or high elastic modulus.

For thick soft films, the friction increases with film thickness increase up to an optimum value due to the decrease in load-carrying capacity of the surface and increase in the ploughing as shown in Figure 2-16a.

The increasing in the coefficient of friction is due to the elastic or plastic deformation of the film and due to the increased contact area at the interface between the sphere and the coating where the shear takes place. The mechanism of ploughing will be the same mechanism of soft bulk materials scratched by a hard indenter.

When a soft smooth substrate coated with a hard coating layer with no debris present, if the coating is very thin, as shown in Figure 2-17b, it will be unable to support the load. The role of the coating here is to separate the substrate from the counterface and to prevent ploughing using hard coating with suitable thickness. Consequently, the obstruction of ploughing can reduce both the friction and the wear.

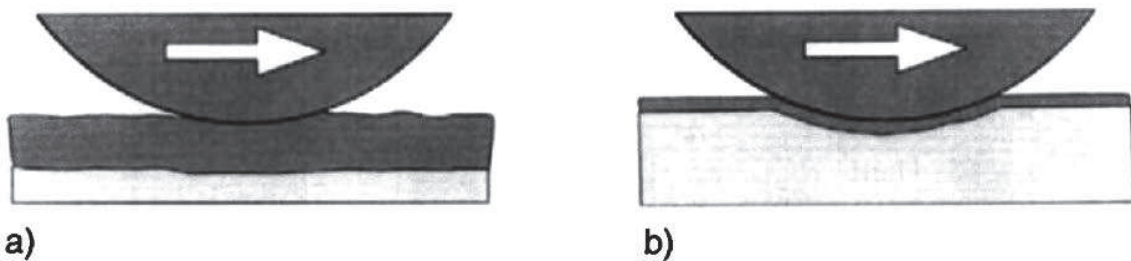


Figure 2-17 The contact of a hard slider moving on a soft substrate coated by a hard coating is characterized by (a) load support from the coating for thick coatings and (b) substrate deformation for thin coatings.

With hard coating higher shear strength introduced at the contact interface, this can be the explanation for the very high coefficients of friction which often occur in sliding contacts of thin hard coatings. The increase in friction due to increase the shear strength which generally seems to be more controlling than the reduction in friction due to decreased ploughing, and after loaded the coating will deviate accordance with the deformation of the substrate and the substrate will either deform elastically or plastically and as the coating does not support the load the deformation can be calculated as for bulk materials.

While the deformation of the substrate will be smaller if the hard coating is more thick due to its stiffness that can carry part of the load Figure 2-17a. Ploughing of the coating hindered by the high hardness and the contact area between the coating and the sphere, where the shear takes place, is reduced due to decreased deflection [98].

## 2.3 Conclusions

In normal hardness, the load is symmetrically supported about the apex of the cone and also the value of the indentation width is a little changed after unloading. In the scratch hardness where indenter moved across the surface of material, the load is not symmetrically supported about the cone apex and a significant amount of elastic/plastic deformation and brittle cracking can occur due to tangential scratch force which act as tensile force on the rear half of the tip [100], [101], [102].

Attack angle have a great effect on the local strain and hence on the mode of material deformation, generally, higher attack angle or low apex angle of the tip would create cutting and chip formation mode, while low attack angle would promote elastic-plastic deformation mode coupling with the viscous behavior [102].

The major difference between polymeric and other classes of materials is the capacity of the groove left on the surface to recover and this capacity is one way to improve the scratch resistance of polymeric surfaces [103].

Friction coefficient has a great impact on the deformation features that produced by scratch and any changes in the coefficient of surface friction can change the stress state polymer substrate near the surface during the scratch process. An increase in coefficient of surface friction shifts and localizes the stress field toward the surface [102].

Four main parameters can be defined to control the tribological contact behavior in contacts between two surfaces which one or both are coated, The relationship between coating-to-substrate hardness, coating thickness, the surface roughness and the size and hardness of the debris in the contact that can come from external sources or be produced by the surface wear interactions themselves [104].

Modify most polymers by suitable filler that can reduce the wear rate and depending upon the design requirement, either increase or decrease the coefficient of friction. The roles of filler are strengthening of the matrix (high load carrying capacity), improvement in the subsurface crack-arresting ability (better toughness) lubricating effect at the interface by decreased shear stress [105].

In order to coat polymeric surface with nanocomposite protective layers there are many limitations such as realize the perfect dispersibility of nanofiller in the polymer matrix, good interfacial bonding between the matrix and fillers and the difficulty of coating polymers to provide additional capabilities such as improved scratch resistance.

In our research, we have attempts to enhance the surface properties for coating solution by used many types of nanocarbon fillers as a reinforcement agent, due to their excellent properties. So we have some challenges such as enhance the dispersibility and compatibility of the filler with polymer matrix and find the best way of coating polymeric surface suitable as anti-friction coating and maintaining sufficient transparency.





# **Section two Experimental works**



## 3 Experimental work

### 3.1 Material and methodology

#### 3.1.1 Materials

The following materials were purchased from Sigma-Aldrich:

- The monomer methyl methacrylate (MMA) [purity 99% - C<sub>5</sub>H<sub>8</sub>O<sub>2</sub>, mol. wt. 100.12 g/mol] and the polymerization initiator 2,2'-azobisisobutyronitrile (AIBN) [C<sub>5</sub>H<sub>12</sub>N<sub>4</sub>, mol.wt. 164.21 g/mol].
- Octadecylamine (ODA), N,N'-dicyclohexylcarbodiimide (DCC) [purity 97% , mol.wt. 269.51 g/mol], 2-bromo-2-methylpropionylbromide [mol.wt. 206.33 g/mol], thionylchloride SOCl<sub>2</sub> [purity 99%, mol.wt. 118.97 g/mol], N, N, N', N'', N''-pentmethyldiethylenetriamine, (PMDETA) [purity 99%, mol.wt. 173.3], N, N-dimethylaminopyridine (DMAP) [purity 99%, mol.wt. 122.17 g/mol], glycol (HOCH<sub>2</sub>CH<sub>2</sub>OH) and CuBr.
- Solvents: chloroform (CHCl<sub>3</sub>) [purity 99.9%], Tetrahydrofuran (THF) [purity 99.9%], N, N-dimethylformamide (DMF), and methanol [purity 99.9%].
- Tetrahydrofuran (THF), N, N-dimethylformamide (DMF), chloroform (CHCl<sub>3</sub>), glycol (HOCH<sub>2</sub>CH<sub>2</sub>OH) they were distilled before used.

#### 3.1.2 Few layers graphene (FLG)

Few layers graphene (FLG) are synthesized by mechanical ablation of pencil lead on a harsh glass surface with simultaneous ultrasonication [106].

To remove the impurities such as inorganic binder present (15%) in the pencil lead carbon, FLG was purified in three steps. The first step is refluxing it for 24 h at 110 °C with aqueous sodium hydroxide (40 wt. %). The mixture was then washed with distilled water until pH 7, the resulting solid was dried overnight at 80°C. In the second step, 1.5 g FLG (from the first step) was dispersed in 100 mL mixture of HCl / HNO<sub>3</sub> (3:1 by volume ratio) and refluxed for 17 h at 110°C. The excess acid was removed by filtration and washed with distillation water several times until pH 7. The resulting solid was dried overnight at 80 °C. The final step consists of short ultrasonication of the product in toluene and separation of the heavy weakly ablated part, which settle-down after 0.5 h in toluene. The overall yield from the initial pencil lead carbon is 60%.

#### 3.1.3 Graphene oxide (GO)

The way to prepare graphene oxide involves two steps. First, graphite powder is oxidized to produce graphite oxide, which can be easily dispersed in water or another polar solvent due to the presence of hydroxyl and epoxide groups on the sheets of the graphite oxide and carbonyl and carboxyl groups located at the edges. Second, the bulk graphite oxide is exfoliated by sonication to form colloidal suspensions of monolayer, bilayer or few-layer GO sheets in different solvents [107]. (Figure 3-1) showed the scheme of preparing graphene oxide from graphite.

We used Hummers method to prepare graphene oxide [108]. Typically, 5 g of graphite (mesh 100), 8.75 g of NaNO<sub>3</sub> and 375 cm<sup>3</sup> of H<sub>2</sub>SO<sub>4</sub> were mixed in a flask maintained in an ice bath. 25 g of KMnO<sub>4</sub> were slowly added over 1 h and the mixture was stirred for additional 2h in the ice bath. The ice bath was removed and the mixture was stirred at room temperature for 5-6 days until it became pasty and brownish. It was slowly diluted water. The temperature was increased to 98°C, the color changed to brown. To complete the oxidation, 15 cm<sup>3</sup> of 30% wt. aqueous solution of H<sub>2</sub>O<sub>2</sub> was added. The mixture was centrifuged, the supernatant discarded. The resulting gel was resuspended in 30% wt. HCl (20 mL HCl and 180 mL water) and stirred overnight. The suspension was centrifuged, the supernatant removed and the resulting solid was re-suspended in water. The solid was rinsed by repeated cycles of centrifugation, removal of supernatant and overnight re-dispersion of the solid in water until the pH 7. The solution was then filtered and dried under vacuum at ambient temperature for several days to get brown solid flaky of graphene oxide.

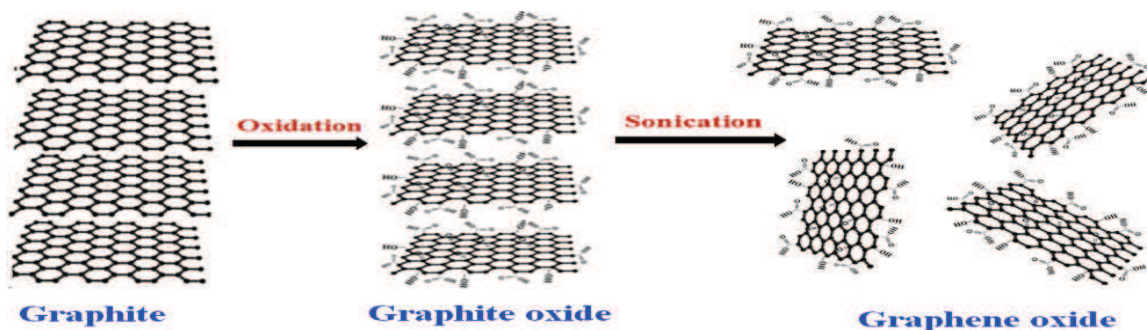


Figure 3-1 Scheme for preparing graphene oxide (GO) from graphite [107].

### 3.1.4 Multiwall carbon nanotubes (MWCNTs)

MWCNTs (with 30-50 nm outer diameter and length of 10–20 μm) were purchased from Nanocyl Company. They contain 0.75 % of COOH group.

Many MWCNTs processes cause considerable residual metallic catalyst which can be detrimental to performance. To eliminate impurities in the MWCNTs and in order to produce MWCNTs-COOH with high percentage of carboxylic groups, MWCNTs were treated with a 68% HNO<sub>3</sub> aqueous solution for 30 min in a sonication bath. The solution was then refluxed for 24 h at 100 °C. The resulting dispersion was diluted in water and filtered. The solid was then washed until neutral pH and dried in vacuum at 40°C overnight. These acid-treatments are known to potentially shorten the length of MWCNTs and introduce hydroxyl functional groups to MWCNTs. It also makes MWCNTs more dispersible in common organic solvent.

### 3.1.5 Erucamide

Erucamide [CH<sub>3</sub>(CH<sub>2</sub>)<sub>7</sub>CH=CH(CH<sub>2</sub>)<sub>11</sub>CONH<sub>2</sub>, Mol wt. 337.58 g/Mol] having melting point of 79°C was purchased from Croda Chemicals [85]. It offers distinct benefits and advantages when used for specific processing situations. Erucamide has a low vapor pressure and is less

volatile, making it suitable for higher temperature processing. Furthermore, Erucamide is prone to thermal oxidation during processing and contributes low color and odor to the final product.

### 3.1.6 Surface modification of nanofiller

#### 3.1.6.1 Functionalization of FLG with octadecylamin

Chemically grafted nanosheets of graphene with long alkyl chains were expected to have enhanced solubility in various organic mediums and compatibility with polymer matrix [83]. After acid treatment process the increase of functional groups such as carboxylic and hydroxyl groups can be observed on the graphene sheets, which facilitate further covalent functionalization.

The amidation reaction was carried out by the DCC (N,N'-dicyclohexylcarbodiimide) activated coupling reaction between carboxylic moieties on the FLG nanosheets and the amine group of ODA molecule.

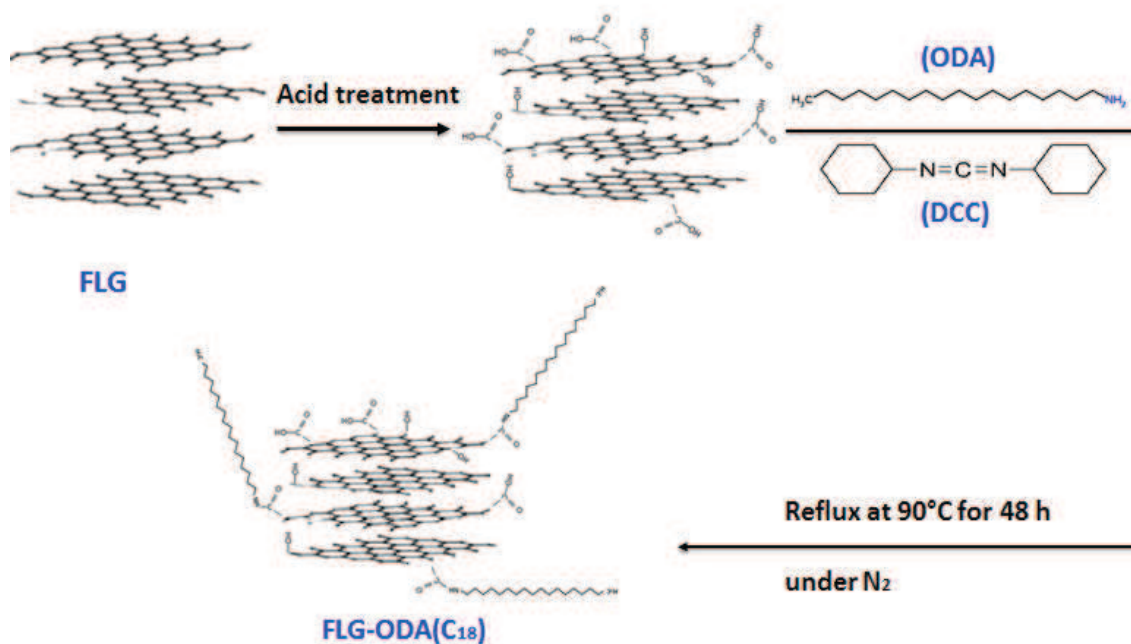


Figure 3-2 Scheme representing of functionalization FLG with octadecylamin.

Typically, 0.15 g of purified FLG was dispersed in 200 mL of anhydrous DMF by 1 h ultrasonication. 5 g of ODA (Octadecylamin) and 2 g of DCC (N, N'-dicyclohexylcarbodiimide) were added. The mixture was then stirred at 90 °C under N<sub>2</sub> for 48 h. The result solid was washed with excess ethanol to remove unreacted amine and dried under vacuum overnight (Figure 3-2).

The direct conversion of a carboxylic acid to an amide is difficult because amines are basic and tend to convert carboxylic acids to their highly unreactive carboxylates. In this reaction, the carboxylic acid adds to the DCC molecule to form a good leaving group which can then

be displaced by an amine during nucleophilic substitution. DCC induced coupling to form an amide linkage is an important reaction in the synthesis of peptides. In general case side product can be formed during the reaction due to the action of the coupling agent.

### 3.1.6.2 Functionalization of MWCNT with PMMA by “grafting-from” method via ATRP

We used the in-situ atom transfer radical polymerization (ATRP) “grafting from” approach to functionalize MWCNTs with PMMA chains [109]. The general strategy for grafting the polymers from MWCNTs via ATRP can be realized by five steps as summarized in Figure 3-3:

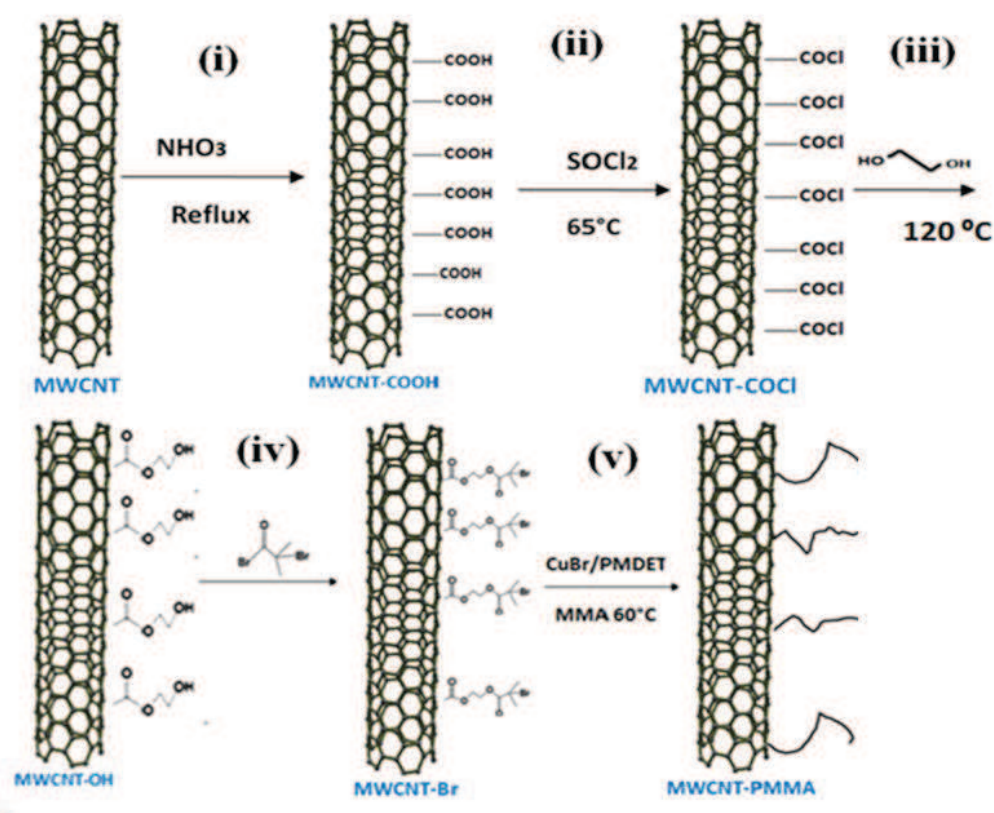


Figure 3-3 Atom transfer radical polymerization (ATRP) “grafting from” modification method of carbon nanotubes.

**(i) Preparation of MWCNT-COOH:** MWCNTs as received have an outer diameter of about 30-50 nm, an average length of 10-20  $\mu\text{m}$  and contain only 0.75 % of carboxylic groups (COOH). In order to increase the percent of carboxyl groups, 1 g of MWCNTs were dispersed in 10 mL of aqueous  $\text{HNO}_3$  (68%) solution during 30 min using the sonication. The system was then refluxed for 24 h at  $100^\circ\text{C}$ . Afterwards, the resulting dispersion was diluted in water and filtered. The solid was next washed until neutral pH and dried under vacuum at  $40^\circ\text{C}$  overnight.

**(ii) Generation of MWCNT-COCl from MWCNT-COOH:** Carbonyl chloride groups functionalized MWCNT (MWCNT-COCl) was prepared via reaction of thionyl chloride with

carboxyl-contained MWCNT (MWCNT-COOH). Typically, 0.6 g of MWCNT-COOH was suspended in 20 mL of  $\text{SOCl}_2$  and stirred at  $65^\circ\text{C}$  for 24 h, under nitrogen. The solid was then separated by filtration, washed with anhydrous THF and dried under vacuum at room temperature for 2h.

**(iii) Synthesis of MWCNT-OH from MWCNT-COCl:** hydroxyl groups were introduced onto the surface of MWCNT by the reaction of MWCNT-COCl with glycol generating MWCNT-OH. Typically, 0.5 g of MWCNT-COCl was mixed with 20 mL of glycol and stirred at  $120^\circ\text{C}$  for 48 h. The obtained solid was separated by vacuum filtration with a  $0.22\ \mu\text{m}$  Millipore polycarbonate membrane. The resulting solid was washed with anhydrous THF three times and dried under vacuum at room temperature overnight.

**(iv) Synthesis of MWCNT-Br from MWCNT-OH:** in order to form sites for ATRP initiation (MWCNT-Br), 0.5g of MWCNT-OH was mixed with 10 mL of distilled  $\text{CHCl}_3$ , 0.0365 g of DMAP and 0.303 g of triethylamine were added. Then 0.684 g of 2-bromo-2-methylpropionyl bromide dissolved in 5ml  $\text{CHCl}_3$  was added dropwise at  $0^\circ\text{C}$  during 1h.

The mixture was stirred for 3 h at  $0^\circ\text{C}$  followed by stirring at room temperature during 48 h. Afterwards, the solid was separated from the mixture by filtration, washed with  $\text{CHCl}_3$  five times and dried under vacuum at  $40^\circ\text{C}$  overnight.

**(v) Synthesis of MWCNT-PMMA from MWCNT-Br:** in order to synthesize the MWCNT-PMMA, 0.1g MWCNT-Br and 28.6 mg of CuBr were placed in a 10 mL dry flask containing a magnetic stirrer. All the liquid products, 0.03466 g of PMDETA, 1.014 g MMA and 1 mL of DMF were placed in another dry flask. Both flasks were sealed and degassed under argon. The mixture of MMA and PMDETA in DMF was injected into the first flask with a degassed syringe. The flask was immersed in an oil bath at  $60^\circ\text{C}$  immediately and kept stirring for 24 h. The viscosity increased during the reaction. The mixture was diluted with  $\text{CHCl}_3$  and filtered using a  $0.22\ \mu\text{m}$  Millipore polycarbonate membrane. This last step was realized three times.

The thickness of the polymer layer grafted on the MWCNTs can be controlled by the feed ratio of MMA to MWCNT-Br.

## 3.2 Fabrication of polymer nanocomposite samples

Polymer nanocomposite dedicated to coating was prepared by three different ways: in-situ polymerization, in-situ polymerization in solvent and solution mixing technique. The choice of the method to prepare the coating depends on the filler's concentration and the required thickness of the coating layer.

### 3.2.1 In-situ polymerization without solvent (Dispersion- reaction)

The analytical grade MMA monomer was dried and purified by distillation under reduced pressure before a polymerization. Typically, PMMA/nanocarbon nanocomposites were prepared by in-situ polymerization by adding nanocarbon filler to the monomer (MMA) with various weight percentages with respect to MMA monomer. Then the mixture was sonicated by using bath sonication for 3h. The mixture was put into the bottom 3-neck flask, and 0.2% of radical initiator AIBN (with respect to MMA monomer) was added prior to air removal by



evacuating and backfilled with N<sub>2</sub> three times. The reaction lasted 25 to 40 min at 70 °C under nitrogen. When the viscosity dramatically increased the mixture was cooled quickly at once to room temperature in the case of using the solution for coating. After coating, the samples are heated up to 65°C for 24 h. A final post heating step was performed for 1h at 110°C to complete the polymerization process.

### **3.2.2 In- situ polymerization in solvent (Dispersion-reaction-precipitate)**

The second method we used was in-situ polymerization in the presence of the solvent, typically DMF was used for this purpose. The advantage of this method is the ability to disperse the nanofillers in the pre-polymerization blend low viscosity. Another advantage is being able to bring up the nanotube distribution as the reaction viscosity increases. The reaction can also produce covalent crosslinking between the matrix and the nanofillers which lead to enhance the interfacial interaction according to Wang et al. [81].

In this method, DMF was mixed with MMA in the ratio 5mL DMF/1 g MMA. An appropriate amount of nanocarbon was added to the mixture by using bath sonication for 3 h at room temperature. The mixture was then poured with N<sub>2</sub> gas for 20 min followed by a heating step up to 70 °C, then 0.2 wt. % of the initiator AIBN (based on weight of MMA) was added in order to start the polymerization. After 24 h the mixture was precipitated into cooled methanol and the product was recovered by vacuum filtration and dried under vacuum overnight. The resultant product was ground in a mortar to produce a fine powder. The same procedure was employed to prepare a control sample (pure PMMA).

### **3.2.3 Solution mixing (Dispersion – dispersion – precipitates)**

Solution mixing is the most common method to prepare polymer/ nanocarbon composites. It consists of mixing the nanocarbon fillers and the polymer in a suitable solvent before evaporating the solvent to form a composite film. This method relies on an efficient dispersion of nanocarbon fillers. The choice of solvent is generally made based on the solubility of the polymer [45]. Figure 3-4 showed solution mixing process to prepare FLG/PMMA composite coating.

Solution process begins by dispersing the fillers in a solvent, typically THF. This solution is mixed with a solution of PMMA dissolved in the same solvent. The nanocomposite is then recovered via precipitation in cooled methanol, filtration and drying under vacuum overnight at room temperature. Depending on the wt. % in the final composite, each type of nanofiller was initially dispersed in THF (0.5 mg/mL) by tip sonication (40 % power) for 20 min and bath sonication at room temperature for 3 h. These solutions were then combined with enough of a solution of PMMA in THF (1g/10mL) by shear mixing (by used shear mixer, Silverson machines) at 6500 rpm for 60 min in an ice bath to evacuate the frictional heat from the polymer.

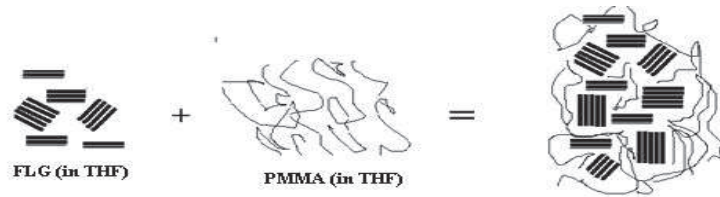


Figure 3-4 Shows solution mixing technique to prepare FLG/PMMA composite coating.

The composite solution for PMMA was then coagulated with cool methanol (300mL), filtered under vacuum and dried overnight to yield a solid flaky composite (Figure 3-5).

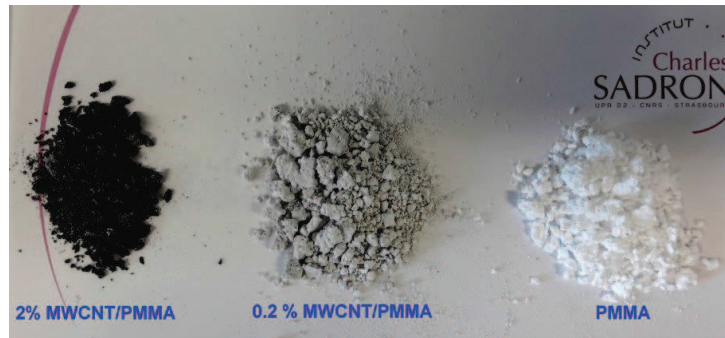


Figure 3-5 Photograph showed powder of composites and pure PMMA prepared by solution mixing method.

The diagram (Figure 3-6) illustrates the methods of preparation of coating solutions.

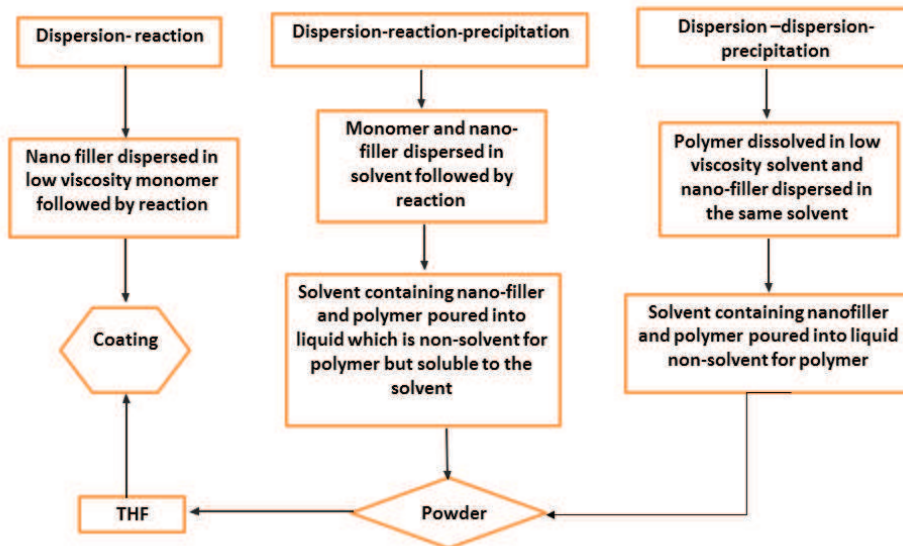


Figure 3-6 Schematic diagram for preparation methods of composite coating.

### 3.3 Characterization techniques of the nanofillers and composite samples

#### Fourier Transform Infrared Spectroscopy (FTIR)

The FTIR spectra were measured with a Bruker Optics Vertex 70. The samples were dispersed as neat powder and compressed in KBr. The spectra were recorded from 400 to 4000  $\text{cm}^{-1}$ .

#### Photoelectron Spectroscopy (XPS)

Structural characterization of functionalized MWCNTs was evaluated by X-Ray Photoelectron Spectroscopy (XPS). Measurements were performed with an ESCA200 spectrometer (VG microtech) system using a monochromatized aluminium  $\text{K}\alpha$  anode.

#### Thermogravimetric Analysis (TGA)

Thermogravimetric analysis (TGA) was carried out on a METTLER TC10A TG50. The analyzer was heated up to 800  $^{\circ}\text{C}$  under 1 atm of air pressure with a heating rate of 20 $^{\circ}\text{C}/\text{min}$ .

#### Gel Permeation Chromatography (GPC)

To determine polymer molecular weight distributions Gel Permeation Chromatography (GPC) technique (Shimadzu LC2-AD) was used. The polymers were dissolved in THF.

#### Scanning electron microscopy (SEM)

SEM micrographs were recorded with a JFOL 2600F microscope operating at an acceleration voltage of 15 KV and an emission current of mA. The samples were covered a thin layer of sputtered gold in order to avoid charging problem.

#### Transmission Electron Microscopy (TEM)

A solution or suspensions of nanocarbon filler in THF was sonicated during 10 min. Five microliters of the solution were deposited onto a Lacey-Formvar/carbon-covered copper grid (300 mesh). The suspension was left for 2 min and finally blotted with filter paper. The grids were observed with a Technai G2 microscope (FEI) at 200 kV. Images were acquired with an Eagle2K ssCCD camera (FEI).

#### Differential Scanning Calorimetry (DSC)

Differential scanning calorimetry (DSC) was carried out by Cathy Settel from the polymer characterization facility at Charles Sadron Institute. She used a DSC Perkin Elmer 8500. At a heating and cooling rate of 20 $^{\circ}\text{C}/\text{min}$  four steps were performed:

Heating from -10 to 180  $^{\circ}\text{C}$  at a rate of 20  $^{\circ}\text{C}/\text{min}$ .

Cooling from 180 to -10  $^{\circ}\text{C}$  at a rate of 20 $^{\circ}\text{C}/\text{min}$ .

Heating from -10 to 180  $^{\circ}\text{C}$  at a rate of 20 $^{\circ}\text{C}/\text{min}$ .

Cooling from 180 to -10  $^{\circ}\text{C}$  at a rate of 20 $^{\circ}\text{C}/\text{min}$ .

### 3.4 Sample preparation for surface mechanical measurements

Two types of substrates were used for coating (Figure 3-7):

- Commercial PMMA supports (Arkema, 26 mm x 76 mm x 8 mm)
- Glass slides

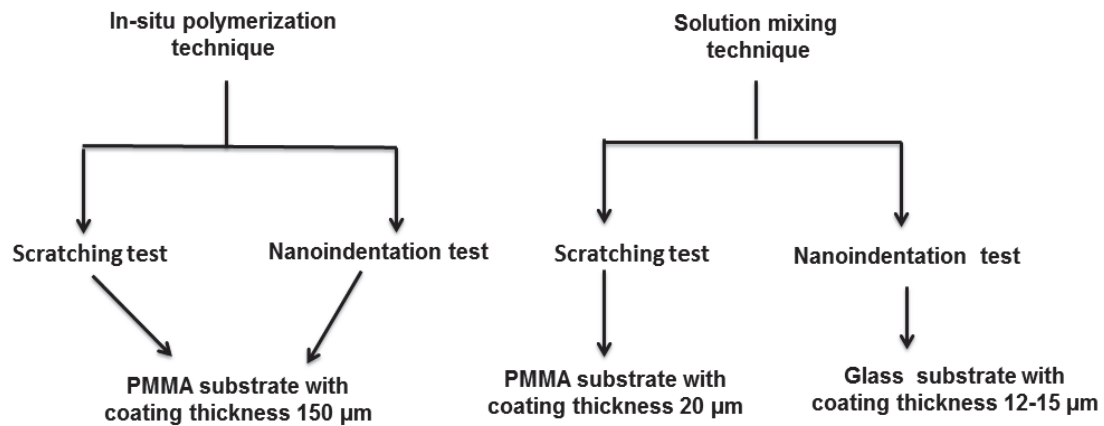


Figure 3-7 Scheme for samples that used in the surface and mechanical tests.

The choice of the technique of coating depends on the method of preparation of the coating solution and on the required coat thickness.

When the coating material is prepared by solution mixing, only spin coating method is suitable to produce very thin coating (few nanometers to  $3\mu\text{m}$ ) and Doctor blade technique for coat thickness between  $10\mu\text{m}$  to  $100\mu\text{m}$  (Figure 3-8).

When the coating material is prepared by in-situ polymerization none of the two above techniques is suitable. Thus we coated by cast technique, which yielded thicknesses more than  $150\mu\text{m}$ .



Figure 3-8 Scheme showing the ranges of the thickness that can be produced with different coating techniques.

### 3.4.1 Cast coating by in situ polymerization

Thick coatings ( $> 150\mu\text{m}$ ) are needed to get a complete set of tribological measurements to characterize the effect of embedded fillers on mechanical surface properties. In this regard, thick coated samples were prepared by cast coating during in situ polymerization. The substrate PMMA were cleaned by ethanol and dried by  $\text{N}_2$ . To create the mold on the commercial PMMA an adhesive tape with thickness of  $\sim 150\mu\text{m}$  was stuck as a gasket on edges of the commercial PMMA. The top was covered by a microscope glass slide. Viscous solution was prepared by in situ polymerization method (described in section 3.2.1) poured by a syringe in the home-made mold (Figure 3-9 a). Then, the samples were heated at  $65^\circ\text{C}$  for 24 h and 1h at  $110^\circ\text{C}$  to complete the polymerization process (Figure 3-9 b).

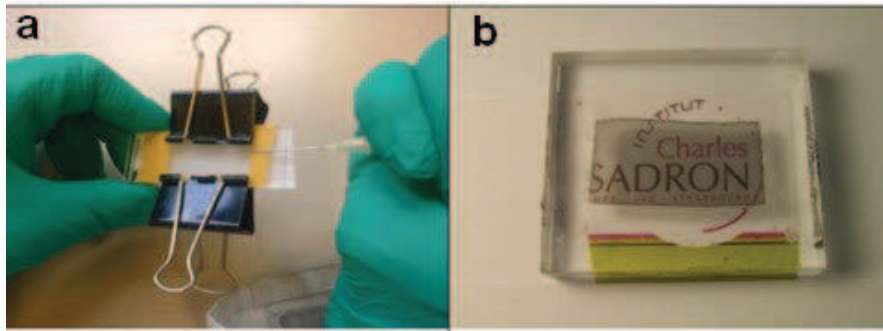


Figure 3-9(a) Cast coating during the polymerization process (b) polymer substrate coated with the composite coating.

Figure 3-10 show the optical microscopy image with dimension (1470  $\mu\text{m}$  length  $\times$  1100  $\mu\text{m}$  width) of a cross-section of a PMMA substrate coated with 0.2 % FLG-C18/PMMA composite cast during polymerization.

This method yields smooth surfaces (mean roughness  $\approx$  11.32 nm) and the interface between the coating and the substrate is homogeneous.

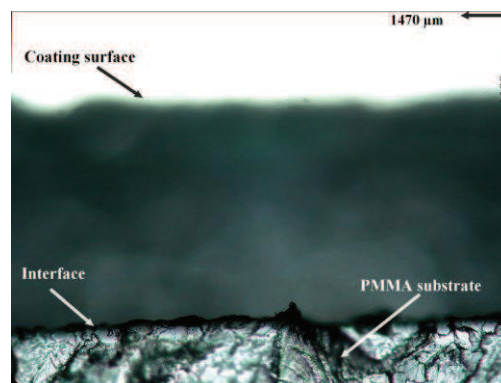


Figure 3-10 Optical microscopy images of PMMA substrate with 0.2 % FLG-C18/PMMA composite coated by cast during polymerization method. (the Image does not represent the real roughness of the surface due to the effect of the cold cutting).

### 3.4.2 Doctor Blade technique

Thinner coatings (15-50  $\mu\text{m}$ ) were prepared by Doctor Blade technique with solutions obtained from composite powders (prepared either by the solution mixing, §3.2.2, or in situ-polymerization in solvent, §3.2.3).

In both case the composite powders were dissolved in dry tetrahydrofuran THF (1 g / 5 mL) and sheared by a mixer at 6500 rpm for 30 min. This step was performed in ice bath to evacuate the frictional heat from the polymer. Figure 3-11 shows the Doctor Blade apparatus. The coating thickness is controlled by the gap between the blade and the top surface of the substrate (Figure 3-11b).

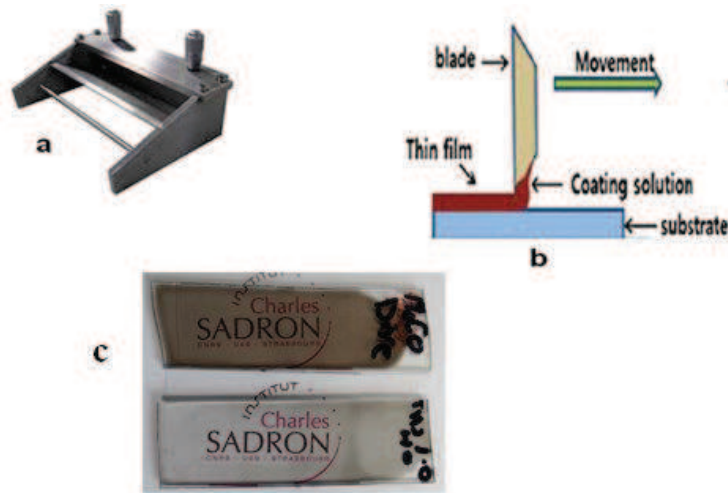


Figure 3-11 (a) Doctor Blade equipment (b) film casting by Doctor Blade technique (c) PMMA substrate coated with 20  $\mu\text{m}$  thickness of PMMA nanocomposite.

All coated samples were dried at ambient temperature for 24 h to make the surface of the coating layer more stable and then at 70  $^{\circ}\text{C}$  under vacuum for 48 h. Figure 3-11c presents an example of 20  $\mu\text{m}$  thick coated sample. The neat PMMA control samples were prepared in the same manner. Figure 3-12 shows an optical microscopy image of a cross-section of the commercial PMMA coated with 100  $\mu\text{m}$  thickness of 0.1% MWCNT-g-PMMA/PMMA composite which was prepared by Doctor Blade technique.

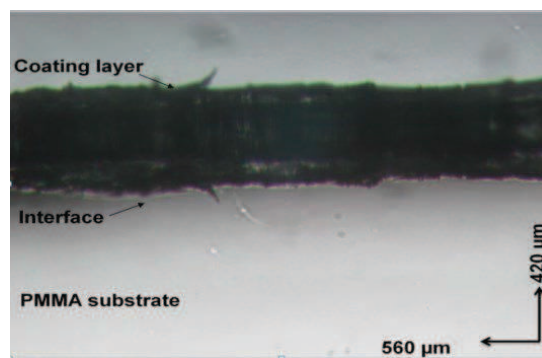


Figure 3-12 Optical microscopy image of PMMA substrate coated with 0.1% MWCNT grafted PMMA/PMMA layer by used Doctor Blade method, with picture dimension (560 length  $\times$  420 width).

Regarding the PMMA/Erucamide mixture, bulk MMA monomer was used and no THF was added. 1g of pure PMMA powder was dissolved in 6 mL MMA and Erucamide was added at different percentages. The mixture was stirred until the components completely dissolve and the solution became quite transparent with a viscosity suitable for coating.

To prepare samples for nanoindentation test, the same above procedure was used but on a glass substrate with coating thicknesses are 12-15  $\mu\text{m}$  (Figure 3-13).



Figure 3-13 Glass substrate coated with composite coating by used Doctor Blade method.

Before depositing the coating, the glass slides are cleaned by immersion in Piranha solution (mixture of  $H_2SO_4:H_2O_2$ , 3:1) for 24 h and another 24 h in the solution of (HCl 1 mL: water 2 mL). Hydrochloric acid may attack and etch the surface of the glass. We checked the roughness of glass by AFM by measuring Rms, it was 1.73 nm before acid treatment and 4.97 nm after acid treatment. Finally, the glass was washed with distilled water and put in drying oven. Relatively an acceptable adhesion between the glass plate and composite coating after the above cleaning steps.



Figure 3-14 The mean roughness of a microscope glass slide (a) before and (b) after treatment with acidic solutions.

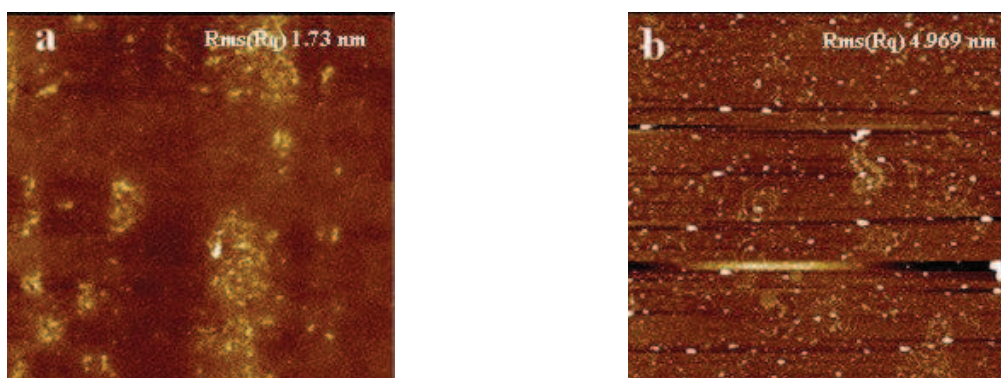


Figure 3-15 AFM images of a microscope glass slide (a) before (b) after treatment with acidic solutions with Rms (Rq) of 1.730 nm and Rms (Rq) of 4.97 nm respectively.

### 3.5 Techniques and equipments to characterize mechanical properties of the coated samples

#### 3.5.1 The conditions for analysis the contact mechanics in the coating

The penetration depth during the scratching test for a coating surface should not exceed the value of  $0.1t$ , where  $t$  is the coating thickness, to eliminate the substrate effect (Figure 3-16).

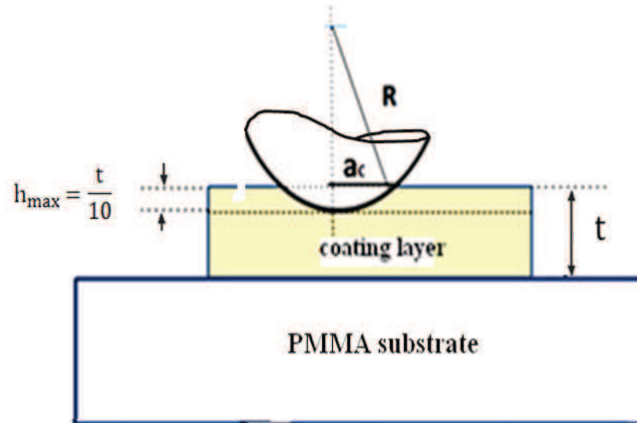


Figure 3-16 Maximum penetration depth during scratching coating surface.

From the average coating thickness ( $t$ ) we can estimate the maximum penetration depth  $h_{\max} = \frac{t}{10}$  below which the effect of the substrate is negligible on the measured mechanical properties. For scratching tests, the tip radius ( $R$ ) of the spherical indenter is known and therefore it is possible to calculate the critical contact radius ( $a_c$ ) at the maximum penetration depth,  $h = \frac{t}{10}$ , as following:

$$(R - h_{\max})^2 + a_c^2 = R^2$$

Leading to:

$$a_c = \sqrt{R^2 - \left(R - \frac{t}{10}\right)^2}$$

For each experiment on the coated samples, the  $a_c$  was calculated and this value allows to calculate the maximum imposed strain  $0.2 a_c/R$  (or the ratio  $a_c/R$ ) above which the experimental results are not exploitable to explain the single coating response.



### 3.5.2 Nano-indentation tests

Nanoindentation testing is a method to measure the mechanical properties of a material such as hardness and Young's modulus on the microscopic scale using Ultra Nano Hardness Tester (UNHT), manufactured by CSM Instruments (Switzerland), with capacity of 30  $\mu\text{N}$  to 100 mN having a load resolution of 5  $\mu\text{N}$  (Figure 3-17).

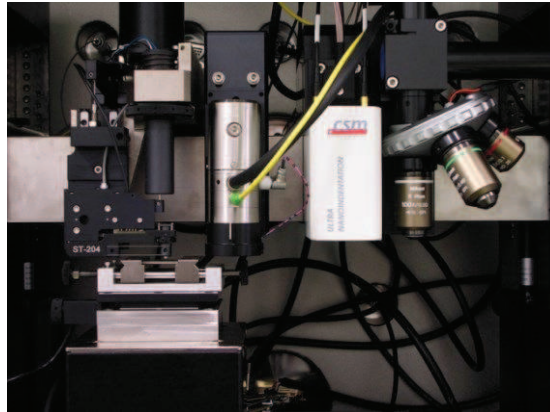


Figure 3-17 The photograph of nanoindentation/scratch apparatus.

The indentation procedure was developed by Oliver and Pharr (O&P) [66]. When this technique is used to characterize coating films, there are general rules to be applied:

- The indentation depth should be deep enough to minimize the surface effect (tip apex defect, surface roughness...). We used a Berkovich tip (diamond three-sided pyramid) with an effective cone angle  $70.3^\circ$ . This apex defect entails that results below 300 nm depth are not taken into account.
- The indentation depth should be less than 10% of the film thickness when the sample is deposited on a hard substrate. Otherwise, the measured value is usually larger than it should be, due to the effect of the support.
- To avoid sink-in or pile-up effect appearing in the unloading curve as a bulge (“nose”), nanoindentation tests were performed at a high unloading rate after long holding time.

Nanoindentation measurements were carried out at room temperature. We have used an already established method where an indenter tip with a known geometry is driven by applying an increasing normal load. When reaching a pre-set maximum value, the normal load is reduced until partial or complete relaxation occurs. A matrix of eight indentation points separated by 50  $\mu\text{m}$  (in order to avoid any possible interference between neighbouring indents) was created to check reproducibility and ensure the statistical results. For each point ten cycles of quadratic loading- unloading were performed. The first load starts at 0.5mN and unloads to 5%, the final load reaches 30 mN (pause time 30s), time to unload 30s. The time pause between each cycle is 50s (Figure 3-18).

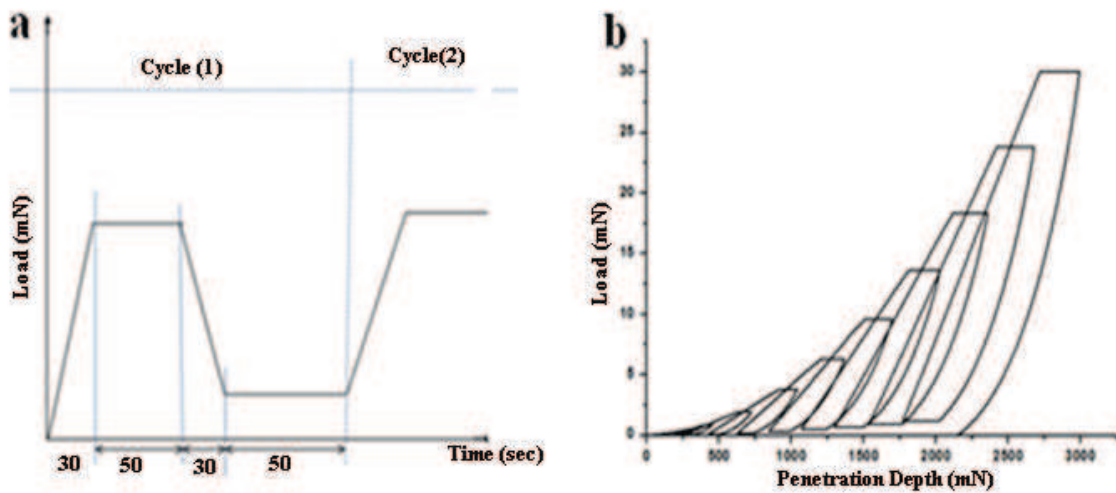


Figure 3-18 a) Scheme represents the cycle load–unload, time to maximum load 30s, time to unload 30s, pause 50s pause between cycles 50s. b) Load–displacement curves.

The hardness ( $H$ ) can be computed as  $H = \frac{P_{max}}{A}$

Where  $P_{max}$  the maximum normal load and  $A$  is the contact area at the maximum load.

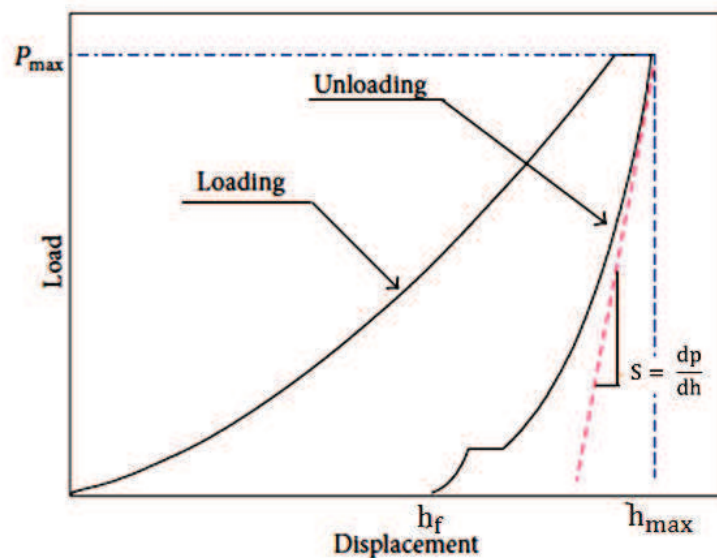


Figure 3-19 Schematic illustration of indentation load–displacement data showing important measured parameters[110].

By considering the non-rigid indenters response, the elastic modulus ( $E$ ) can be directly calculated through the following equation:

$$\frac{1}{E_r} = \frac{1 - \nu^2}{E} + \frac{1 - \nu_i^2}{E_i}$$

Where ( $E_r$ ) is the reduced modulus of indentation contact, ( $\nu$ ) Poisson's ratio, the elastic modulus for diamond indenter ( $E_i$ ) and Poisson's ratio ( $\nu_i$ ).

The reduced modulus of elasticity ( $E_r$ ) can be calculated from the unloading curve with Oliver-Pharr method using the following equation:

$$E_r = \frac{\sqrt{\pi} dp}{2 dh \sqrt{A}}$$

Where  $\frac{dp}{dh}$  is the slope of the unloading curves (Figure 3-19) [110], [66].

### 3.5.3 Scratch tests

The surface properties were analyzed from a homemade sclerometer, the micro-visio-scratch (MVS) apparatus. It consists of a commercial servomechanism bearing a small transparent box with temperature control, which contains the sample and the scratching tip (Figure 3-20). It is fitted with a built-in microscope, allowing in situ observation of the contact area and the groove left on the surface. The input parameters are the normal load  $F_n$ , tip geometry, temperature and the sliding speed, whereas the output parameters are the tangential force, groove geometry and the true contact area.

Scratch test may be performed over a large range of speeds ( $10^{-3}$  to 15 mm/s) and within a temperature range covering the  $\alpha$  and  $\beta$  polymer relaxation peaks of a broad spectrum of polymers (-40°C to 100°C).

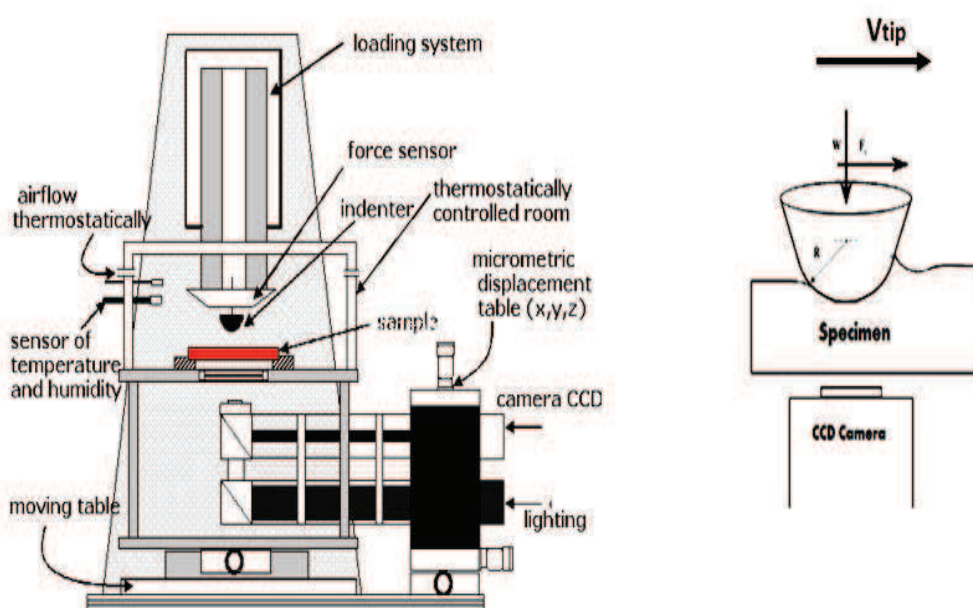


Figure 3-20 A schematic diagram (on the right) and photograph (on the left) of scratch apparatus.

The normal load  $F_n$  applied to the moving tip can be selected from 0.05 to 25 N by adjusting the compression of springs of 3 different stiffness. The tip can be driven in at a constant speed while normal load increases step by step or at a constant normal force (while tip speed increases step by step). Sliding and scratching tests are characteristically carried out at mounting normal load at a constant speed for a given temperature. [85], [90], [111].

The shape and the width of the contact area can be estimated from the true contact area which is photographed in situ at every loading step (Figure 3-21). When it is perfectly plastic (Figure 3-21c) there is no recovery after deformation and hence no load bearing support at the rear half of the tip. In the case of an elastic plastic or viscoelastic (Figure 3-21b) viscoplastic material, there is partial support in the trailing zone. The recovery of the groove and the symmetry of the contact area can be estimated by means of an angle  $\omega$  varying from (0 to  $\pi/2$ ).

If the ratio of the local shear to the local pressure is termed the ‘true friction coefficient, then the apparent friction coefficient may be written as [23]:

$$\frac{F_t}{F_n} = \mu_{app.} = \frac{C + D\mu}{A + B\mu}$$

Solution of this relationship between the true and apparent friction coefficients requires calculation of the four integrals A, B, C and D, which are the local pressure and shear elementary action integrals, together with knowledge of the rear angle  $\omega$ , the real contact area and the geometry of the tip. A, B, C and D take into account the macroscopic contact shape.

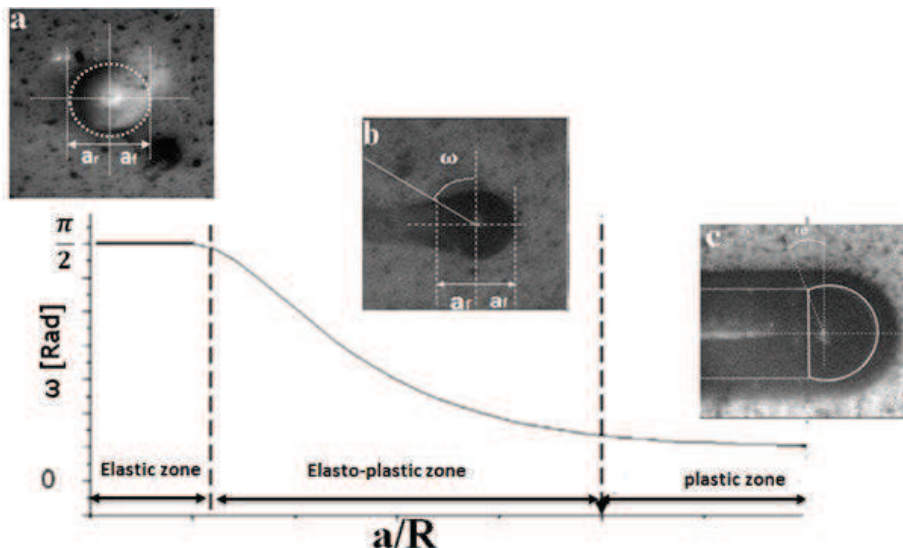


Figure 3-21 Photograph of the rear contact angle  $\omega$  as a function of the mean contact strain (a) elastic sliding (b) viscoelastic grooving, (c) plastic scratching with a spherical tip of radius 100  $\mu\text{m}$  for PMMA nanocomposite coating.

### 3.5.4 Instron Uniaxial tensile testing machine

Tensile test is the most common technique to determine a lot of properties of material such as yield stress and strain, shear resistance, elastic modulus. This test is used for characterizing all kinds of materials. Instron Uniaxial tensile testing machine, model 4500 (Figure 3-22) is used to characterize bulk mechanical properties, with a capacity of 10 kN and a velocity ranging from  $10^{-3}$  mm/s to 3 mm/s. Samples can be experimented for traction, compression, shear, bending, flexion/relaxation, mechanical spectrometry and dynamic mechanical analysis (DMA) from 0.002 Hz to 5 Hz. An environmental chamber allows the measurements from -70°C to 125°C and the machine is provided with two load cells of 10 kN and 200 N.

For the tensile test, the samples was prepared as mentioned in section 3.5.2. The strain rate was maintained at 20% per min.

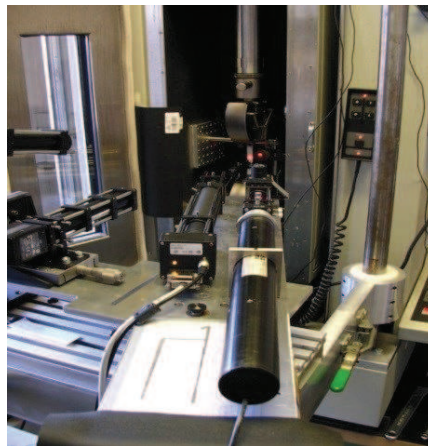


Figure 3-22 Photograph of the Instron Universal Testing Machine model 4500.

# **Section three: Results and discussion**



## 4 Few layer graphene (FLG)

### 4.1 Chemical and structure characterization

Few layers graphene (FLG) obtained after mechanical ablation of pencil lead type B9 and purification contain some oxygen groups and  $sp^3$  carbons that belong to the defects in the structure. FLG obtained by this process has lateral size of few micrometers, consists of 1 up to 20 and occasionally up to 50 sheets [106]. The oxygen groups (carboxyl and hydroxyl) can be functionalized by an amidation reaction to graft a long alkyl chain to the graphene sheets. The length of the grafted alkyl chain is obtained with ODA molecules which hold 18 carbons. The functionalization of graphene with octadecylamine, called here FLG-C18 can improve the solubility of nanosheets in most organic solvents such as THF and in polymeric matrix (Figure 4-1).

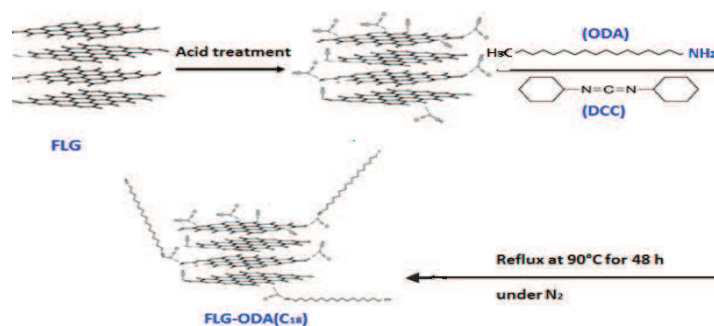


Figure 4-1 Scheme of the functionalization steps of FLG with Octadecylamine.

The morphologies of FLG-C18 samples were characterized by transmission electron microscopy (TEM). The FLG product was dispersed in THF solvent, when the suspension was sonicated during 10 min. Five microliters of the solution were deposited onto a Lacey-Formvar/carbon-covered copper grid (300 mesh) for the TEM analysis (Figure 4-2).

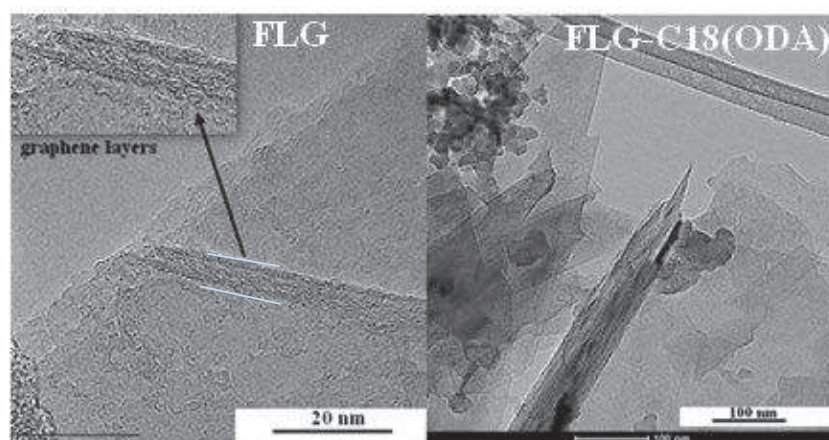


Figure 4-2 Transmission electron micrographs of FLG sheets.



The average size of the FLG sheets is about 2  $\mu\text{m}$  and the number of graphene layers does not exceed 20 with an average number of 5–8 layers. Some monolayers are also detected within the analyzed sample.

The amidation reaction was achieved by the DCC-activated coupling reaction between carboxylic moieties on the FLG nanosheets and the amine group of ODA molecule. The initial reactants and the product were analyzed by FTIR and TGA. As presented in (Figure 4-3) FTIR spectra of ODA show characteristic bands of amide groups around 3350  $\text{cm}^{-1}$  and 1620  $\text{cm}^{-1}$ . These peaks are not present on the FLG spectra, and appear on the ODA modified FLG (FLG-C18). Moreover the bands 2925 and 2850  $\text{cm}^{-1}$  represent the C-H stretch of alkyl chain. These results confirm the presence of ODA moiety on the FLG.

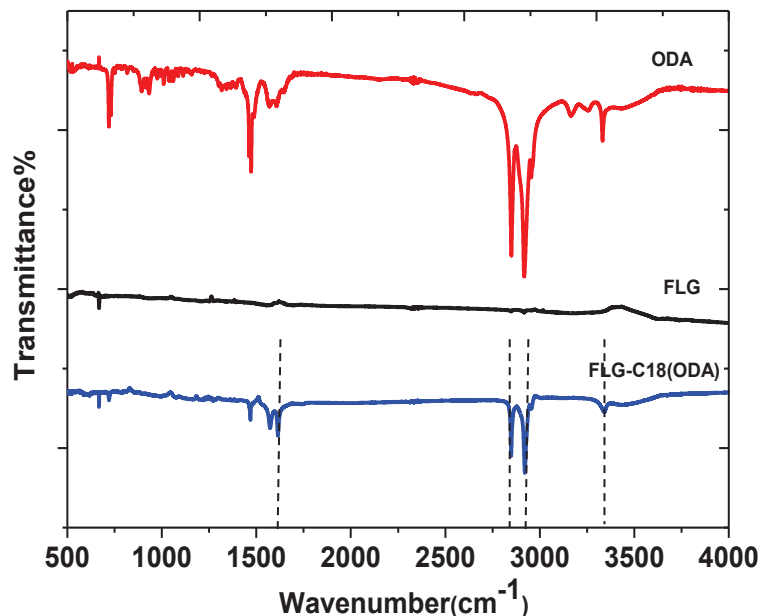


Figure 4-3 FTIR spectrum of (a) Octadecylamine (ODA) (b) few layer graphene (FLG) (c) functionalized few layer graphene (FLG-C18).

Figure 4-4 displays the thermogravimetric results of ODA, pristine FLG and FLG functionalized with ODA. The FLG exhibits a quite good thermal stability and the mass loss starts at 400 $^{\circ}\text{C}$ . The ODA weight loss starts at low temperature around 150  $^{\circ}\text{C}$  which is consistent with data observed by Salam et al. [112].

The FLG-C18 compound shows an in-between behaviour: a first weight loss process starts above 200  $^{\circ}\text{C}$  with the breaking of the N-H bond from the ODA functionalized group. The estimation of the weight loss is around 40 % which give the amount of functionalized FLG. A second weight loss process above 400  $^{\circ}\text{C}$  is very similar to the FLG.

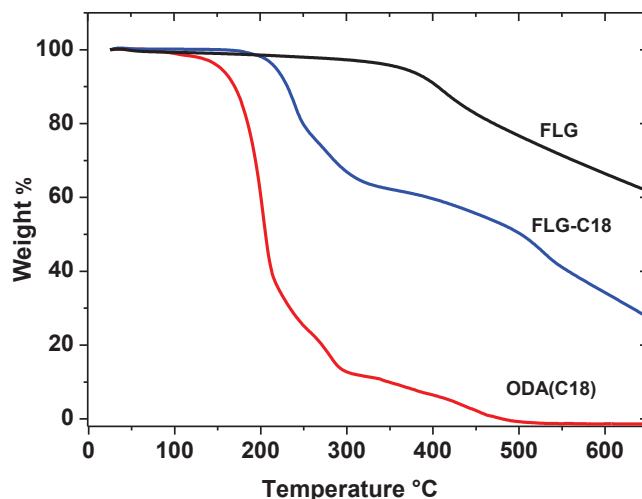


Figure 4-4 TGA curves of FLG, functionalized FLG with ODA, and ODA.

Last, according to the XPS measurements, Table 4-1, the N1s proportion increases from 0.5% for FLG (after mechanical ablation and purification) to 3 % after functionalization with ODA (FLG-C18).

	<i>C1s</i>	<i>N1s</i>	<i>O1s</i>
FLG	94.9	0.5	4.6
FLG-C18	93.1	3.0	3.9

Table 4-1 Elemental atomic composition of FLG and modified FLG.

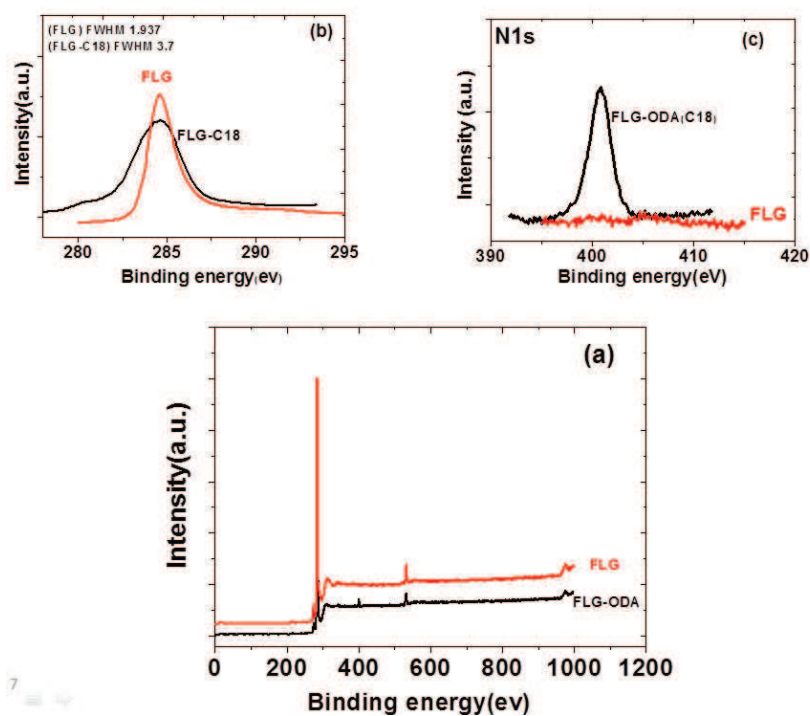


Figure 4-5 XPS spectra of FLG and FLG functionalized octadecylamine a) full spectra b) C peak c) N peak.

Very high peak of N at 401 (ev) with amount of 3% of N, the carbon C1s peak of FLG-C18 is wider than C1s peak of FLG before the functionalization, and Full width at half maximum (FWHM) of FLG-C18 is 3.7 compare to FWHM= 1.937 of FLG. Thus, the important changes in the XPS spectra can be observed, however due to the strong charge effect during the measurement and excessive percentage of N1s, the peaks are not deconvoluted and the measurements needs to be performed again to be confirmed.

The combined results obtained by FTIR, TGA and XPS confirmed the success of the amidation reaction which will enhance the dispersibility of FLG in the MMA monomer or in the solvent THF.

## 4.2 Characterization of PMMA/FLG composites

Two kinds of PMMA/FLG-C18 coatings were prepared, by in-situ polymerization and solution mixing composites (section 3.2.1 and 3.2.3). Prior to mechanical studies, the structures of the composites are checked by GPC and DSC (analysis from the ICS polymer characterization platform).

	<i>Mw</i>	<i>Mn</i>	<i>Mw/Mn</i>	<i>Tg</i> °C
PMMA in situ polymerization (lab.)	7.163*10 <sup>5</sup>	1.938*10 <sup>5</sup>	3.69	110
0.1FLG-C18	4.293*10 <sup>5</sup>	1.819*10 <sup>5</sup>	2.3	112
0.2FLG-C18	2.231*10 <sup>5</sup>	1.714*10 <sup>5</sup>	1.302	112

Table 4-2 Results of GPC and DSC analysis for neat PMMA and FLG-C18/PMMA nanocomposites with various graphene contents prepared by in situ polymerization technique.

The GPC test showed that the molecular weight of the composites prepared by in situ polymerization technique changed a lot, while for all composites prepared by solution mixing technique the molecular weight is almost constant (Table 4-3). This significant change in molecular weight for the composites prepared by in-situ polymerization technique demonstrates that the nanocarbon fillers can participate in polymerization reaction. This is consistent with the results of researchers [47], [48], [49], [50] believe that  $\pi$  – bond in carbon nanotubes were initiated by the AIBN initiator used during polymerization process, and this results in obstructing the growth of PMMA.

DSC results showed that the *Tg* for pure PMMA and all the composites prepared by solution mixing technique increased by about 10 °C compared to pure PMMA and the composites prepared by in-situ polymerization technique (except the height FLG loaded composite).

	$M_w$	$M_N$	$MW/MN$	$T_g^{\circ}C$
Pure PMMA Powder (lab.)	$1.262 \cdot 10^5$	$8.918 \cdot 10^4$	1.415	119.78
0.1 % FLG-C18	$1.242 \cdot 10^5$	$8.773 \cdot 10^4$	1.416	/
0.5 % FLG-C18	$1.301 \cdot 10^5$	$9.850 \cdot 10^4$	1.321	124.72
1 % FLG-C18	$1.242 \cdot 10^5$	$9.038 \cdot 10^4$	1.348	114.7

Table 4-3 The results of GPC and DSC analysis for neat PMMA and C18-graphene/PMMA nanocomposites with various graphene contents prepared by solution mixing technique.

#### 4.2.1 Surface mechanical properties of in situ-polymerization coats

PMMA substrates were coated during the polymerization process, with thickness  $\approx 150 \mu\text{m}$ . Surface mechanical properties, Young's modulus and hardness, are measured by the nanoindentation technique for PMMA substrates coated with pure PMMA and with PMMA reinforced with various weight percentage of FLG-C18 (0.05, 0.1 and 0.2 wt%). Figure 4-6 displays Young's modulus and hardness versus penetration depth of the tip from nanoindentation experiments. The data were fitted (Oliver Oliver-Pharr model) [66] with a Poisson's ratio value of 0.3. In both plots the results in the first 500 nm depth are not considered as it is the tip's apex default. For coating thicknesses  $\sim 150 \mu\text{m}$  we can probe the coating up to  $15 \mu\text{m}$  to get its own mechanical response (as respect to the substrate). The overall penetration depth is  $3 \mu\text{m}$ , the results are only related to the coating properties. Pure PMMA and PMMA / 0.05 wt% FLG-C18 have quite the same mechanical responses and this may be due to the low weight percentage of FLG-C18 in the composite. For 0.1 and 0.2% reinforcement fillers, there is a 15% increase of the Young's modulus, which is not negligible at these low filler percentages. In addition, the surface hardness progressively increases with the filler percentage in the composite.

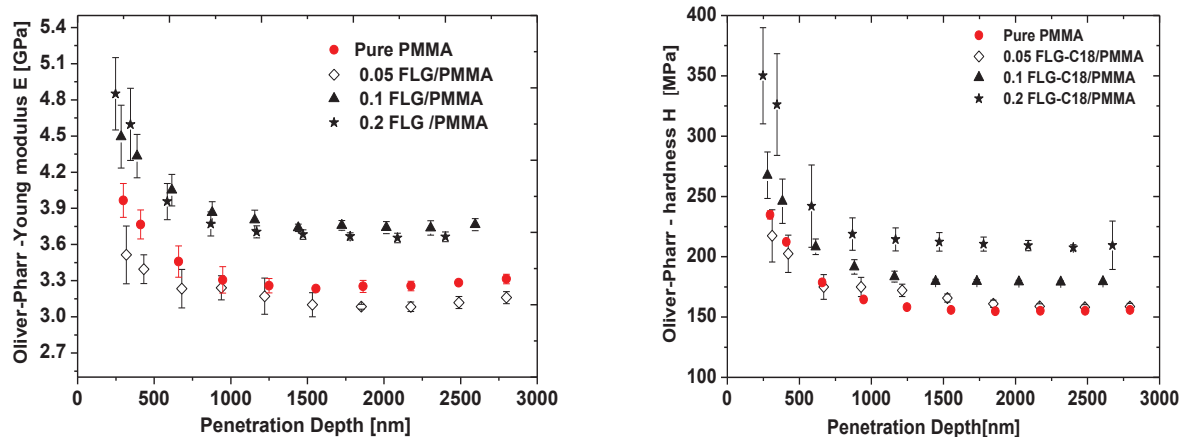


Figure 4-6 Variation of Young's modulus (on the left) and of hardness (on the right) for samples coated by in-situ polymerization process measured by nanoindentation.

It is important to mention that the addition of nanocarbon filler to the polymer matrix perhaps will not follow the mixture rule in terms of improving the properties due to the agglomeration and poor dispersion.

The surface response to shear is characterized by friction tests. Figure 4-7 shows the evolution of the apparent friction coefficient  $\mu_{app}$  as a function of the  $a/R$  ratio for two tip radius ( $R = 98$  and  $250 \mu\text{m}$ ) at room temperature, scratch / sliding speed  $0.03\text{mm/s}$ . The normal load range is  $0.05 \text{ N}$  to  $3 \text{ N}$ . The experimental results indicate that at low percentage of FLG-C18 ( $0.05\%$ ) there is no observed effect on the friction coefficient and the composite behave like the pure PMMA. With the introduction of  $0.1\%$  and  $0.2\text{wt}\%$  of FLG-C18 the friction coefficient significantly decreases. This huge decrease in friction may be attributed to the self-lubricating of FLG and due to the easy share of graphene nano- layers during scratch tests.

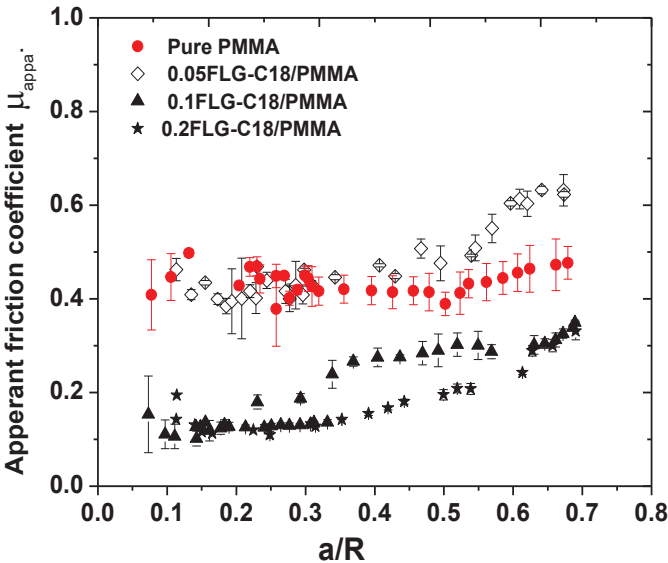


Figure 4-7 Effect of few layer graphene (FLG) on the apparent friction coefficient, for two tip radius ( $R = 98$  and  $250\mu\text{m}$ ) at room temperature, slip/scratch speed  $0.03\text{mm/s}$  and normal load from  $0.05 \text{ N}$  to  $3 \text{ N}$ .

Looking at the contact snapshots it is noticeable that the coating composites progressively became non transparent (the analysis is no more possible above  $0.2\%$ ) (Figure 4-8).

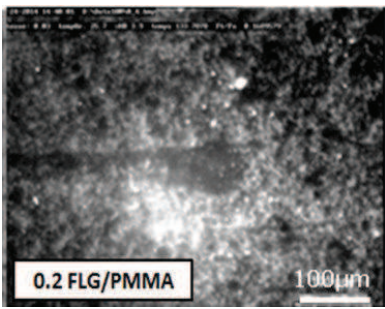


Figure 4-8 Photograph of  $0.2 \text{ FLG/PMMA}$  composite coats prepared by in situ polymerization technique. (Coating thicknesses  $\sim 150 \mu\text{m}$ ).

A local friction coefficient,  $\mu_{loc}$ , gives information regarding the local sheared interface under the contact without the ploughing effect of the tip. It is defined as the ratio of the local shear stress  $\tau$  to the local pressure  $p$ .

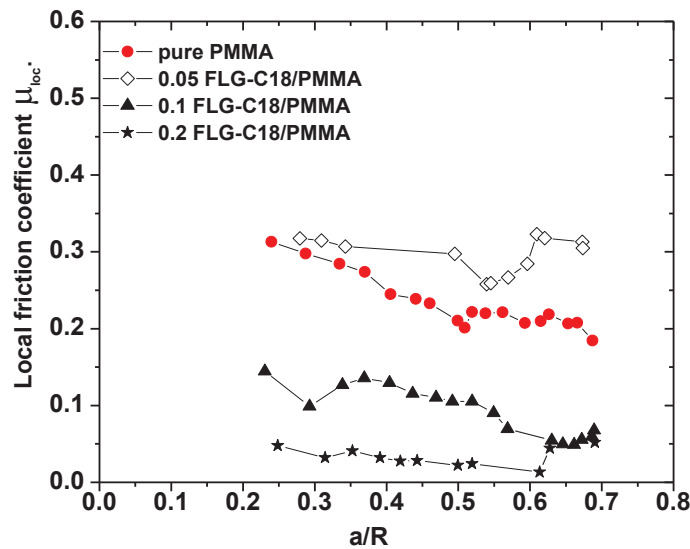


Figure 4-9 Estimation of the local friction coefficient as a function of the contact strain represented by the ratio ( $a/R$ ) with tip radius  $98\mu\text{m}$ .

Figure 4-9 presents the calculated local friction coefficients as a function of the  $a/R$  ratio for the previous experiments. The local coefficient of friction does not clearly depend on the contact strain. The experimental results indicate that the local friction coefficient for coating composites with different percentages of FLG-C18 (0, 0.05, 0.1 and 0.2 wt. %) was 0.26, 0.3, 0.13 and 0.04 respectively, and that can show the role of few layer graphene (FLG) in decreasing the local interfacial shear stress.

The rear contact area ( $\omega$ ) represents the nature of the contact between the sliding tip and the polymer surface. It is apparent from the experimental results that the introduction of FLG-C18 can modify the nature of the contact and improve the elasto-plastic of the contact (Figure 4-10). There is a slight shift in the elastic domain, the experimental results reveal that the elasto-plastic domain for pure coating begins at  $a/R$  ratio (0.14), while for the composite coating at ratio  $a/R$  (0.21).

At the same value of contact strain ( $a/R = 0.35$ ), the values of rear contact angle ( $\omega$ ) changes significantly with the introduction of FLG-C18. It is about 0.45 radian for pure PMMA and 0.05% FLG-C18/PMMA composite that have a higher value of friction coefficient, 0.42 and 0.5, respectively. The increase of the weight percent of FLG-C18 in the composite to 0.1 (friction coefficient about 0.23) induces the  $\omega$  increase to about 0.7 and 0.85 radians for composite containing 0.2% of FLG-C18 (friction coefficient of 0.14). It can be concluded that the decrease in friction coefficient is associated with increased value of the rear contact angle.

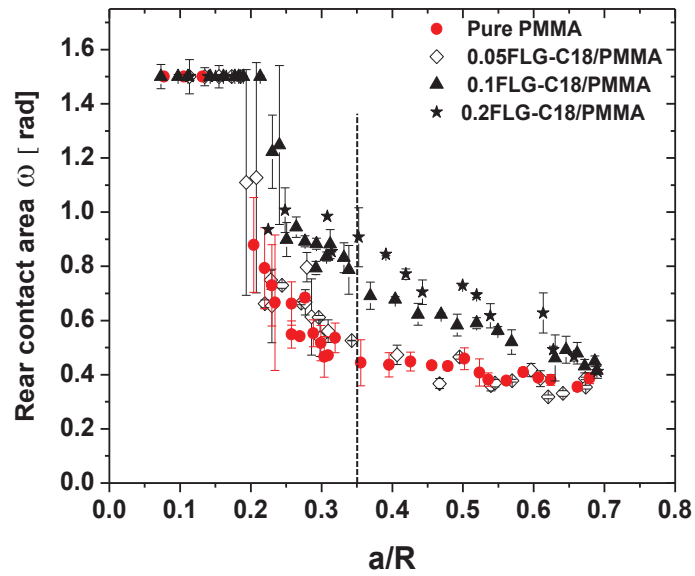
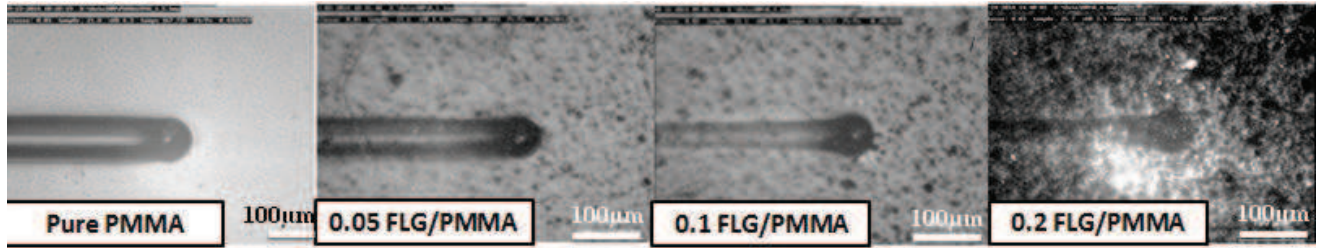


Figure 4-10 Variation of rear contact angles  $\omega$  with contact strain (defined by the  $\frac{a}{R}$  ratio where  $a$  is the mean contact radius and  $R$  is the tip radius). The selected images at ( $\sim 0.35$ ) contact strain with different percentage of FLG-C18.

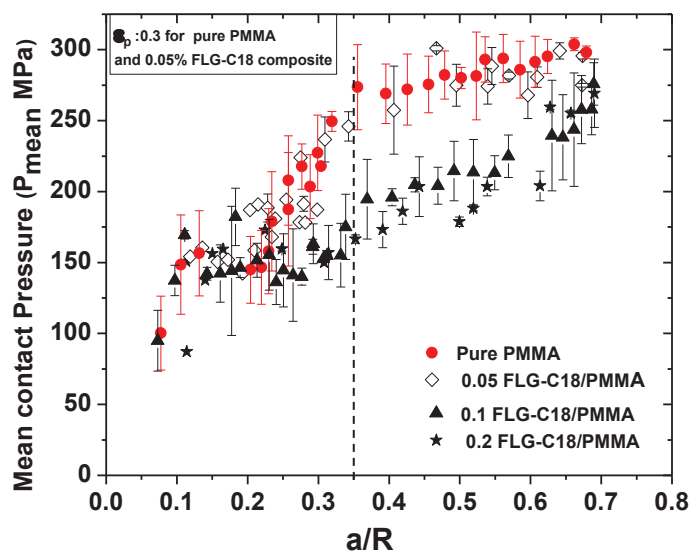


Figure 4-11 Variation of the contact pressure with  $a/R$  ratio.

The pure coating and composite coating begun suffer a plastic yield at the rear contact angle ( $\approx 0.35$  radian).

The in-situ photographs of the contact at the a/R ratio (0.35) explained that the nature of the contact is plastic for pure PMMA coating, while the contact is elasto-plastic for the composites with 0.1 and 0.2wt% of FLG-C18, except the composite with 0.05% FLG-C18 it seems plastic at this value of a/R.

The contact pressure is the ratio of the normal load to the true contact area, which is the sum of the front and rear areas. Figure 4-11 shows the mean contact pressure as a function of the a/R ratio. On the samples coated with pure PMMA and 0.05% FLG-C18 composite, the contact pressure increases from 100 to 250 MPa and then seems to take a stable path as the a/R ratio exceeds 0.35. In the samples coated with composites containing 0.1 and 0.2 % of FLG-C18, the contact pressure increases continuously.

#### 4.2.2 Surface mechanical properties of solution mixing coatings

We used solution mixing technique to prepare coating composites reinforced with weight percentage more than 0.2 % of FLG-C18. All samples were coated by Doctor Blade technique on glass substrate (see Figure 3-13 section 3.4.2) for nanoindentation tests and on PMMA substrates (see Figure 3-11 section 3.4.2) for scratch test.

After the last drying step the coating thicknesses are 12-15  $\mu\text{m}$ , which entails that we can probe the coating up to 1.2  $\mu\text{m}$  to get its own mechanical response by nanoindentation technique.

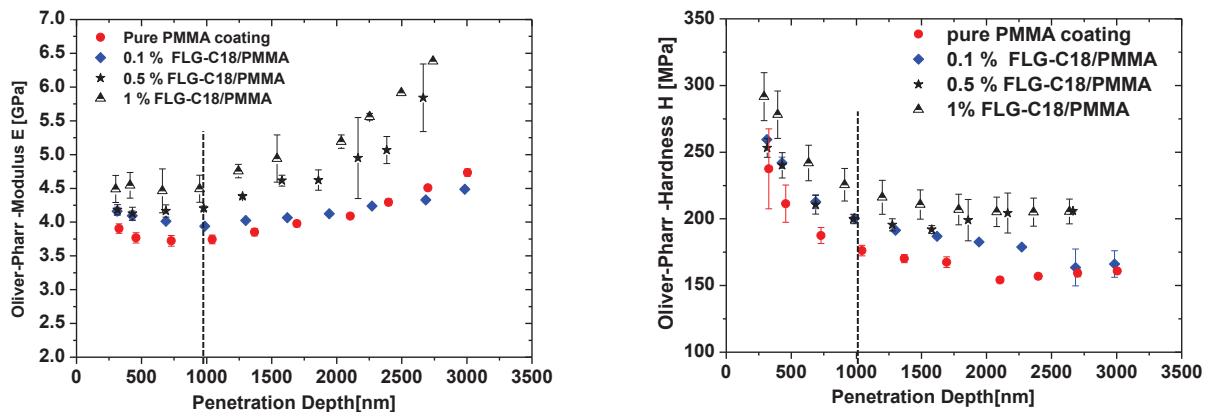


Figure 4-12 Variation of Young's modulus (on the left) and of hardness (on the right) for samples coated by solution mixing process.

Figure 4-12 shows an increase in the composite Young's modulus when the contact depth increases above 1.5  $\mu\text{m}$  which is clearly related to the influence of the glass substrate. So the results that have been adopted were obtained at a penetration depth of 1  $\mu\text{m}$  to avoid the effect of the substrate.



The experimental results show an increase in the Young's modulus and hardness for the coating composites compared to pure PMMA coating. For example, the PMMA reinforced with 0, 0.1, 0.5 and 1 wt % of FLG-C18 have a Young's modulus of 3.74, 3.9, 4.2 and 4.49 GPa and hardness of 175, 200, 200 and 219 MPa, respectively.

Scratch tests were performed on PMMA substrate coated with PMMA/FLG-C18 composites which contain 0, 0.1, 0.5 and 1% of FLG-C18. After the last drying step the coating thicknesses are 20  $\mu\text{m}$ . All the experiments were made at room temperature, 4% humidity and sliding speed 0.03 mm/s. The normal load range is  $0.05 \text{ N} < F_n < 1.5 \text{ N}$  and we use two tip radius, 250  $\mu\text{m}$  and 98  $\mu\text{m}$ . Each point represents the average of three tests.

Figure 4-13 shows a clear decreasing of the friction coefficient of coating composites by a factor of 2 or 3.

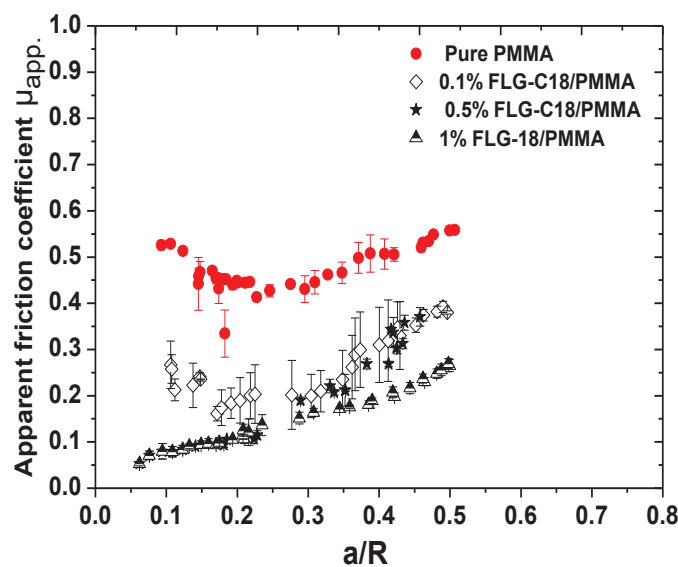


Figure 4-13 Effect of few layer graphene (FLG-C18) on the apparent friction coefficient, with two tips (98  $\mu\text{m}$  and 250 $\mu\text{m}$  Radius).

The plastic scratching contact strain is a function of the geometrical strain which is related to the  $a/R$  ratio and the local friction coefficient, so the plastic strain beneath the indenter is rapidly affected by the local friction. With low friction coefficient, the displacement on a greater depth and the plastic strain level are reduced especially for low  $a/R$  ratio. Moreover, the lowered friction can greatly reduce the shearing strain beneath the moving tip in the contact area.

The introduction of FLG-C18 in PMMA has a great impact on the local friction coefficient (Figure 4-14). For example, at  $a/R$  ratio 0.35 the composite with 1% FLG-C18 has local friction coefficient of 0.07 while for pure PMMA coating is 0.32 at the same value of  $a/R$ . This may be due to the self-lubricating nature of FLG-C18 that can decrease the interfacial shear stress during the scratch process.

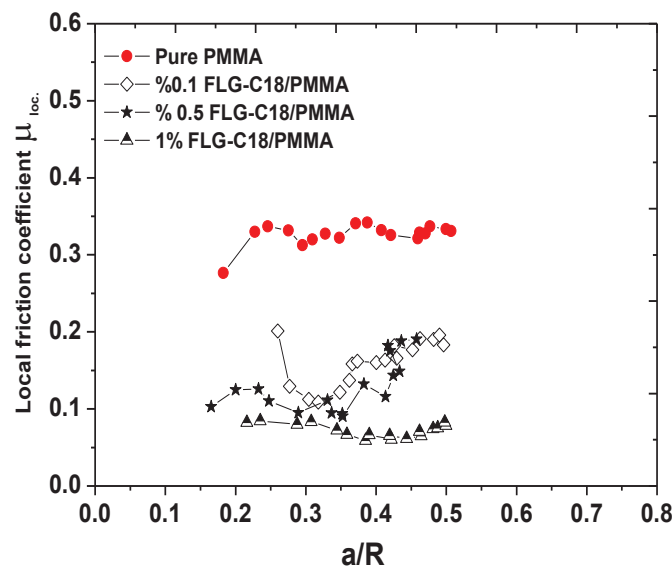


Figure 4-14 Effect of few layer graphene (FLG-C18) on the local friction coefficient, tip radius 98 $\mu$ m.

The evolution of the rear contact angle as a function of the ( $a/R$ ) for PMMA coated samples with different percentages of FLG-C18 is presented in Figure 4-15.

In the case of a viscoelastic contact, the rear angle  $\omega$  is equal to  $(\pi/2)$  for elastic deformation. Whatever the percentage of FLG-C18, there is no significant change in the end of elastic domain. In contrast, the elastic–plastic domain seems to expand in the case of the increased percentage of FLG-C18 in the coating. The plastic domain begins at a higher contact strain for higher percentage of FLG-C18 in the coated samples.

In situ photographs of the contact at the ratio  $a/R$  (0.35) explained that the nature of the contact is plastic for pure PMMA coating, while the contact is elasto–plastic at the same value of ( $a/R$ ) for composite with 0.1, 0.5 and 1 wt%.

Figure 4-16 shows the mean contact pressure as a function of the ratio  $a/R$ . For the samples coated with pure PMMA the contact pressure increases from 100 to 233 MPa and then seems to take a stable path as the  $a/R$  ratio exceeds 0.34, whereas in the samples coated with composites containing FLG-C18, especially 1 wt % FLG-C18, the contact pressure increases continuously.

The FLG-C18 plays a double role, it reduces the coefficient of friction and increases the durability of the coating compared with the pure coating, as is evident from Figure 4-16.

The contact pressure increases continuously and this is consistent with the results of the examination of nanoindentation which indicated the increase of the modulus and hardness for the FLG-C18/PMMA composites.

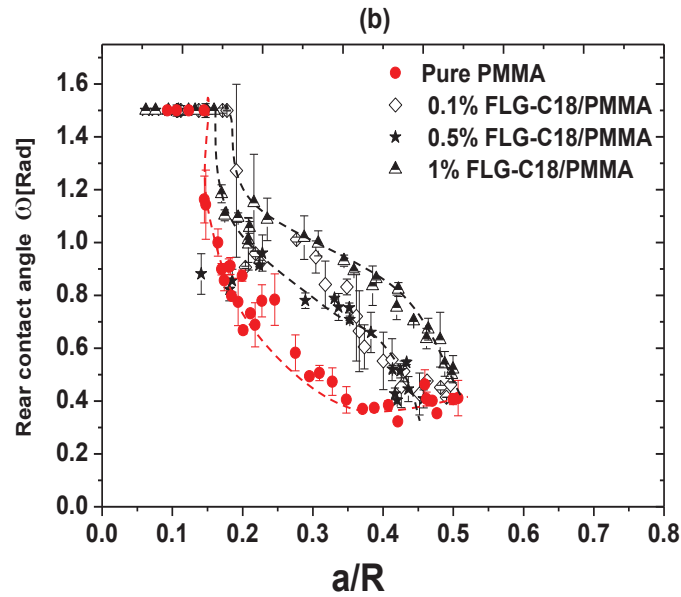
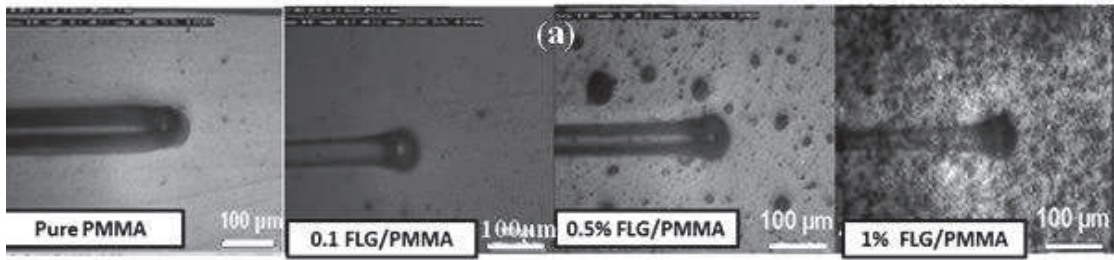


Figure 4-15 a) The selected images at  $a/R$  ( $\sim 0.35$ ) for different percentage of FLG-C18. b) Rear contact angle versus  $(a/R)$  for coated samples with PMMA reinforced with different percentage of FLG-C18.

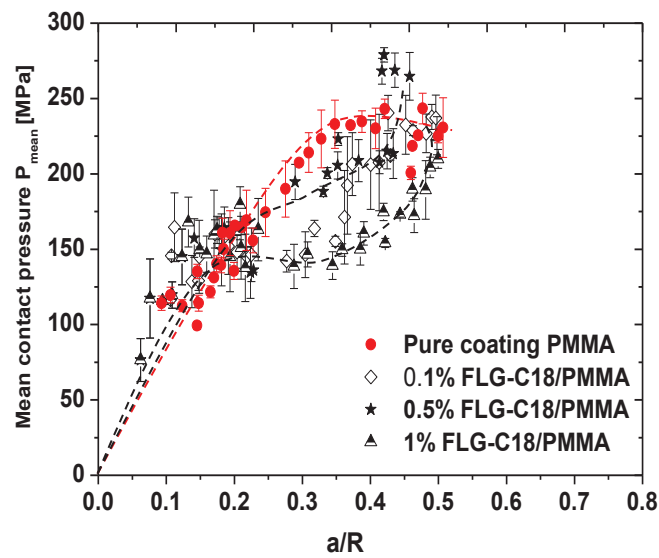


Figure 4-16 Mean contact pressure versus contact strain for coated samples with PMMA reinforced with different percentage of FLG.

### 4.3 Comparative study of the effect of different techniques of coating

In order to compare the effect of the preparation technique of coating solution on the surface behavior of the coated samples, two coating composites prepared by in-situ polymerization and by solution mixing, with the same percentage of the filler (0.1% FLG-C18). Scratch tests were performed on PMMA substrate coated with PMMA/FLG-C18 composites.

The examination of surface roughness revealed that the samples prepared by in-situ polymerization technique have a lower roughness (11.0 nm) (Figure 4-17) compared to the samples prepared by solution mixing technique (89.34 nm) (Figure 4-18)

This difference in roughness can appear due to the use of glass slide as a cover for casting coating during the in-situ polymerization coating (section 3.4.1), which leads to make the roughness of the resultant surface coating almost similar to the roughness of glass slide (typically 7.4 nm).

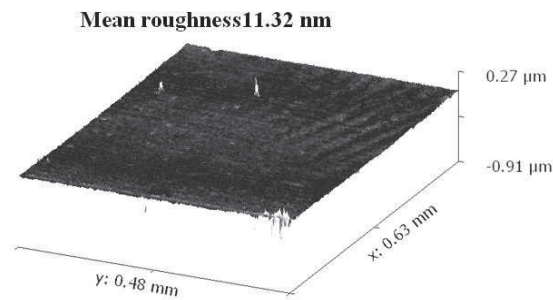


Figure 4-17 Mean roughness of coating composite prepared by in situ polymerization technique.

While in the case of solution mixing technique, the coating layer is deposited on the PMMA substrate without using a glass slide, Moreover, a drying step which is employed to remove the solvent from coating layer perhaps leads to increase the roughness of the resultant coating surface.

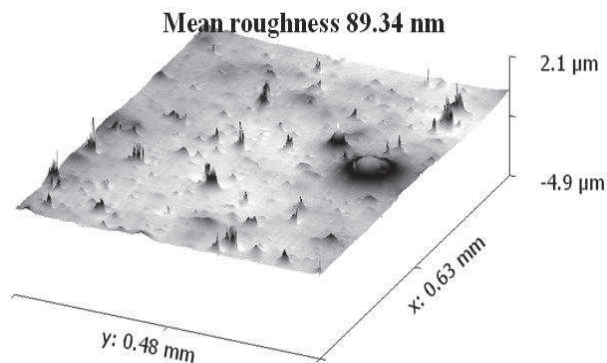


Figure 4-18 Mean roughness of coating composite prepared by solution mixing technique.

The surfaces responses to shear are characterized by friction tests. All the experiments were made at room temperature, 4% humidity, sliding speed of 0.03 mm/s,  $0.05 \text{ N} < F_n < 1.5 \text{ N}$  and with two tip radius of  $250 \mu\text{m}$  and  $98 \mu\text{m}$ .

Figure 4-19 showed apparent friction coefficient and local friction coefficient for pure PMMA coating and for composite coating reinforced with the same percentage of FLG-C18 (0.1wt %) coated by two different techniques.

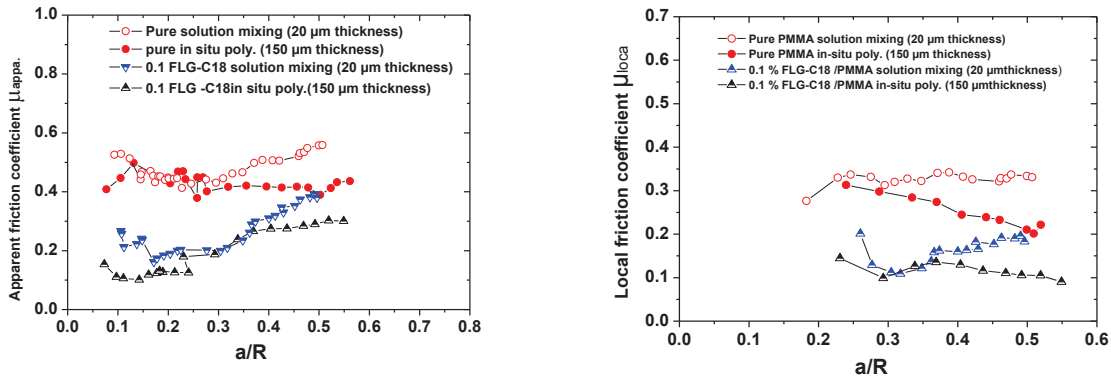


Figure 4-19 The apparent friction coefficient (with tip Radius  $98 \mu\text{m}$  and  $250 \mu\text{m}$ ) (left) and the local friction coefficient with tip Radius  $98 \mu\text{m}$  (right), for samples coated by two different techniques.

In general, it seems from the experimental results, that the two types of coating have the same friction coefficient.

Figure 4-20 shows the evolution of the rear contact angle as a function of the ratio  $a/R$  for polymer coated samples by two different techniques.

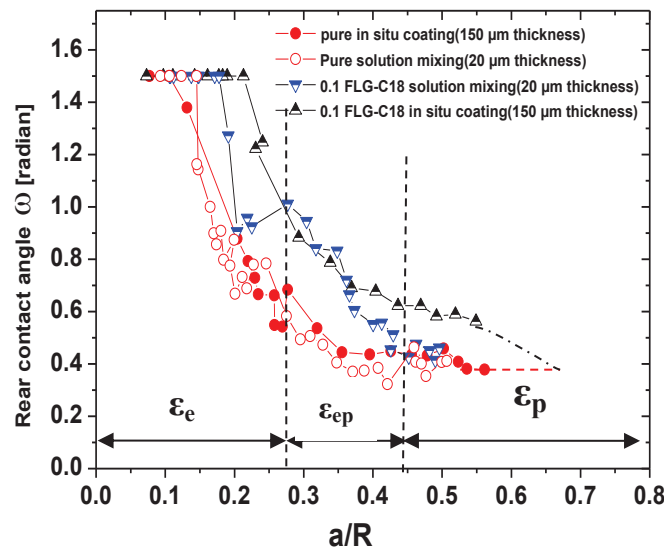


Figure 4-20 Rear contact angle versus contact strain for samples coated by two different techniques.

For coating composite by in situ polymerization, elastic domain ( $\epsilon_e$ ) ends at  $\frac{a}{R} = 0.25$ , while for composite coating by solution mixing technique at  $\frac{a}{R} = 0.2$ . The plastic domain ( $\epsilon_p$ ) begin at  $\frac{a}{R} = 0.42$  for solution mixing coating, while for in-situ polymerization coating the plastic domain begin at  $\frac{a}{R} = 0.7$  (section 4.2.1).

#### 4.4 Comparative study of the effect of coating thickness on the surface mechanical properties

In order to study the effect of change the ratio of coating thickness to weight percent of reinforced filler on the surface behavior of the coated samples. Two composites coating were prepared, first have thickness 150  $\mu\text{m}$  reinforced with 0.1 FLG-C18/PMMA and the second have thickness 20  $\mu\text{m}$  reinforced 1% FLG-C18/PMMA.

Young's modulus and hardness are measured by the nanoindentation technique, the results showed that the Young's modulus and hardness for the composites reinforced with 1% of FLG-C18 was 4.5 GPa and 225 MPa respectively. While the Young's modulus and hardness for composite reinforced with 0.1% of FLG-C18 was 3.75 GPa and 180 MPa respectively. For Scratching tests the experiments were made at room temperature, 4% humidity, sliding speed of 0.03 mm/s,  $0.05 \text{ N} < F_n < 1.5 \text{ N}$  and with two tip radius of 250  $\mu\text{m}$  and 98  $\mu\text{m}$ . Figure 4-21 shows the effect of increasing the percentage of FLG-C18 by 10 times with decreasing the thickness of the coating by 8 times on friction coefficient, the results indicated that the two composites coating almost have the same friction coefficient. Increasing the percentage of FLG-C18 can modify the nature of contact (modifying the strain hardening) due to increasing Young's modulus and hardness (Figure 4-22). The in situ photographs of the contact at the  $a/R$  value of 0.35 explained how the increasing of the percentage of FLG-C18 can modify the nature of contact. The transparency for both coatings samples is almost same.

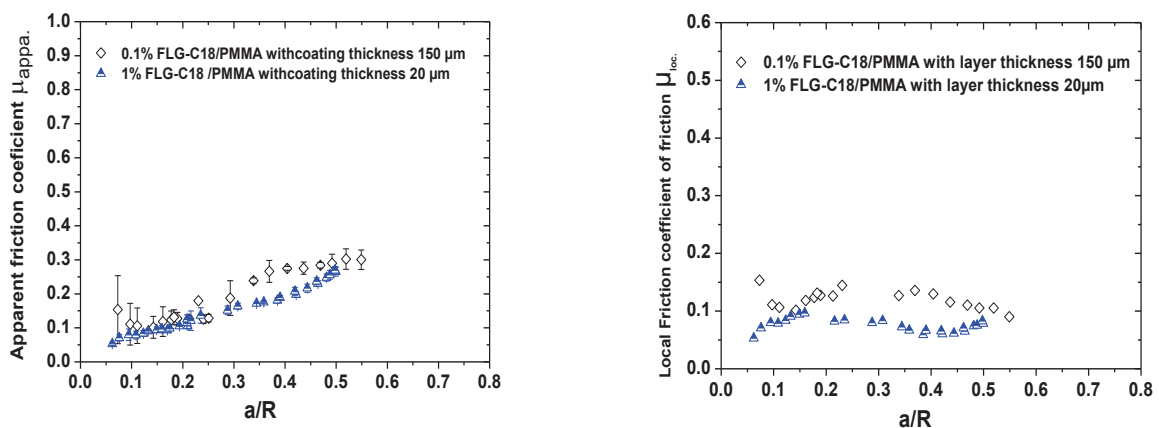


Figure 4-21 The apparent friction coefficient (left) and the local friction coefficient (right) versus  $a/R$  value.

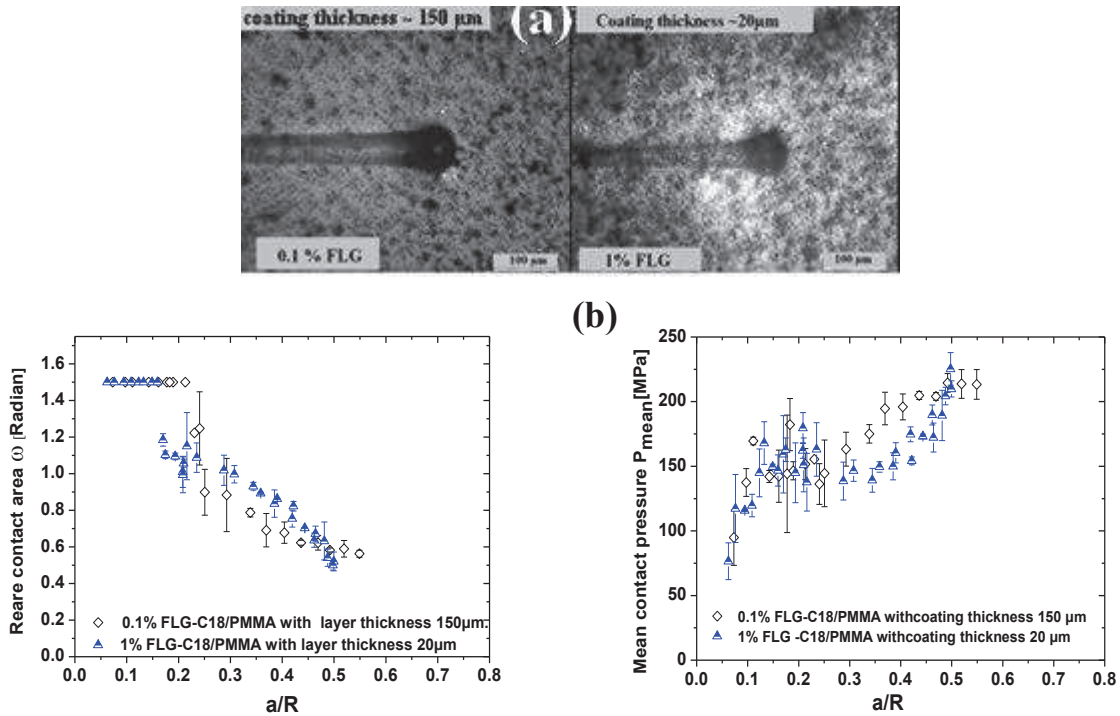


Figure 4-22 a) The selected images at  $a/R$  (~0.35), b) Rear contact angle (left), mean contact pressure (right) versus  $a/R$  values.

## 4.5 Conclusions

1. Few layers graphene (FLG) obtained by mechanical ablation of pencil lead (B9) and purification was functionalized with Octadecylamine groups to improve its dispersibility in THF solvent and MMA monomer. The success of the functionalization process was confirmed by FTIR, TGA and XPS analyses.
2. Two techniques for coating were employed to prepare composite coatings, in-situ polymerization and solution mixing technique.
3. Young's modulus and hardness for coating prepared by in situ polymerization technique were measured by the nanoindentation technique for PMMA substrates coated with pure PMMA and with PMMA reinforced with various weight percentage of FLG-C18 (0.05, 0.1 and 0.2 wt%). Young's modulus and hardness were increased by 15% and 36% respectively with increasing the FLG-C18 percentage in the composites as compared with pure coating that was prepared by the same technique. Regarding, the samples that were coated by solution mixing technique, the Young's modulus and hardness were measured by the nanoindentation technique on glass slide substrates coated with pure PMMA and with PMMA reinforced with various weight percentage of FLG-C18 (0.1, 0.5 and 1 wt%). Young's modulus and hardness were increased by 21 % and 26 % respectively with increasing the FLG-C18 percentage in the composites as compared with pure coating that was prepared by the same technique.

4. Samples that were coated by in-situ polymerization technique have lower surface roughness than the samples coated by solution mixing technique.
5. The introduction of FLG-C18 in composite coating can decrease the coefficient of friction with increasing the percentage of FLG-C18, due to the weak van der Waals force between the 2D layers in the FLG-C18 that can make the inter-layer sliding more easily in multilayer graphene.
6. The decrease of the coefficient of friction was accompanied by a modification in the nature of the contact and improves the elasto-plastic behavior at the contact.
7. A plastic domain begins at higher contact strain ( $a/R$ ) for higher percentage of FLG-C18 in the coated samples.
8. The in-situ polymerization technique for coating is more effective to decrease the coefficient of friction than the solution mixing technique.
9. Generally, the experimental results confirmed that FLG-C18 can play a double role by reducing the coefficient of friction and also caused increasing in the mechanical properties of the composite coating.
10. The upper limit of the weight percent of FLG-C18 was 1% that can be used in coating layer with average thickness of 20  $\mu\text{m}$  and 0.2 % with average thickness 150 $\mu\text{m}$  which maintained acceptable transparency.



## 5 Graphene oxide (GO)

There are many primary methods for producing GO, all of which generate a product with a larger interlayer spacing than graphite, and has several oxygen-based functional groups decorating the surface such as carboxylic acids, epoxides and alcohols [113]. (GO) was synthesized from graphite by Hummers method [108].

Compare to the FLG, graphene oxide contains higher amount of monolayer graphene and a higher lateral size of sheets and higher number of functional groups such as hydroxyl and epoxide on their basic planes and also carbonyl and carboxyl groups located at the sheet edges, these functional groups can be helpful to form a stronger interfacial interaction with the polymeric matrix like PMMA.

PMMA nanocomposites with excellent tribological properties can be fabricated with graphene oxide because they are regarded as derivatives of self-lubricating graphite, which has a layered structure and exhibits a low friction and wear rate when used as solid lubricants [107], [11]. The main objective of this part is to prepare GO/PMMA composite coating and study its surface and mechanical properties.

### 5.1 Chemical and structure characterization

The microscopic morphologies of samples were characterized by transmission electron microscopy (TEM). GO product was dispersed in THF solvent, by the sonication during 10 min, and next five microliters of the suspension were deposited onto a Lacey-Formvar/carbon-covered copper grid (300 mesh) for the TEM analysis.



Figure 5-1 Transmission electron micrograph of graphene oxide sheet in solvent (THF).

The single and multi-lamellar layer structures of graphene oxide sheets were observed in the TEM images Figure 5-1, and slight wrinkles were observed.

At the macro level, GO has a brown and very thin lamellar structure and the yellow color was more significant in relatively low concentrations.

The chemical structures of materials were measured by Fourier-transform infrared spectra analyzer FTIR. The spectra of initial graphite and GO are shown in (Figure 5-2

The GO sheet showed the absorption bands of the carboxyl C=O ( $1727\text{ cm}^{-1}$ ), aromatic C=C ( $1624\text{ cm}^{-1}$ ), alkoxy C–O ( $1056\text{ cm}^{-1}$ ), and hydroxyl –OH ( $3350\text{ cm}^{-1}$ ) groups. The presence of oxygen-containing functional groups, such as C=O and C–O, further confirmed that the graphite indeed was oxidized into GO, with was consistent with the literature data.

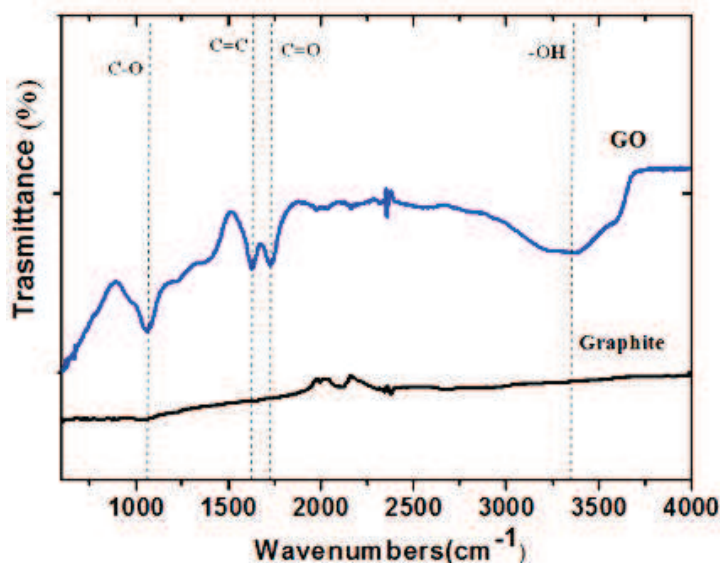


Figure 5-2 FTIR spectrum of graphene oxide and graphite.

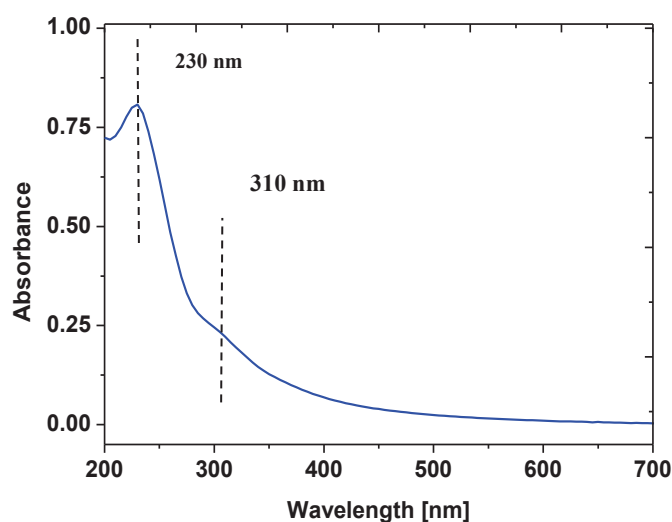


Figure 5-3 UV-vis absorption spectra of graphene oxide.

UV-vis spectra of GO dispersions in water are presented in Figure 5-3. The result showed two kinds of absorptions observed in these spectra to identify GO. The first one, at 230 nm corresponding to  $\pi - \pi^*$ , the second is a shoulder at  $\sim 310$  nm, corresponding to an  $n-\pi^*$ .

C1s XPS spectrum of GO consists of two different chemically shifted component and can be simply deconvoluted into four peaks  $sp^3$  ( $C = C$ ) in aromatic rings (284.7 eV), C-O (286.7 eV), (C=O) 288.2 eV, and O-C=O (289.2 eV) respectively (Figure 5-4).

The XPS spectra confirms the formation of GO, the percentage of O in the GO sample almost 45% best on the area of C1s and O1s peaks.

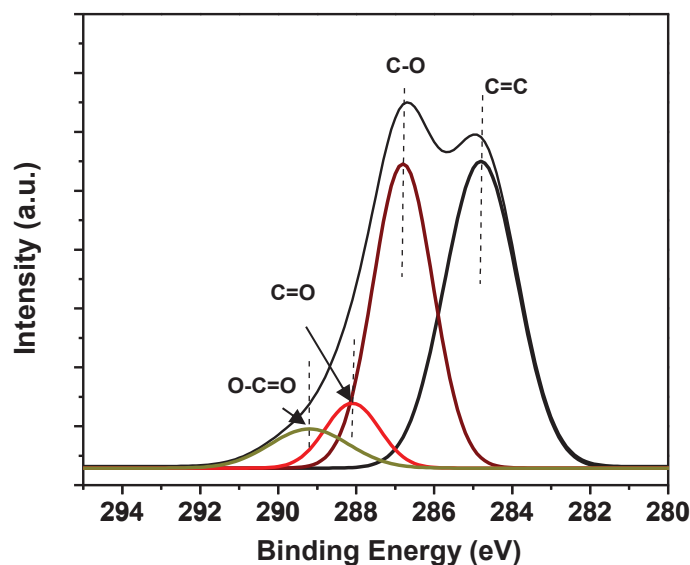


Figure 5-4 C1s XPS spectra of GO.

## 5.2 Characterization of PMMA/GO composites

Two kinds of PMMA/GO coatings were prepared, i.e. by in-situ polymerization and solution mixing technique (section 3.2.1 and 3.2.3). Prior to mechanical studies, the structures of the composites are checked by GPC and DSC (analysis from the ICS polymer characterization platform).

	<i>M<sub>w</sub></i>	<i>M<sub>n</sub></i>	<i>M<sub>w</sub>/M<sub>n</sub></i>	<i>T<sub>g</sub></i> °C
Pure PMMA Powder (lab.)	1.262*10 <sup>5</sup>	8.918*10 <sup>4</sup>	1.415	119.78
0.1 % GO	3.393*10 <sup>5</sup>	1.569*10 <sup>5</sup>	1.987	124.05
0.5 % GO	1.286*10 <sup>5</sup>	9.606*10 <sup>4</sup>	1.339	124.6
1 % GO	1.366*10 <sup>5</sup>	9.932*10 <sup>4</sup>	1.366	111.89

Table 5-1 Results of GPC and DSC analysis for PMMAs prepared via solution mixing technique with and without GO.

The results of GPC revealed that the molecular weight is almost constant for all the composites prepared by solution mixing technique. This indicates that the quality of the PMMA matrix is not affected during the process of PMMA/GO composite preparation (Table 5-1). DSC results showed that the increase in the T<sub>g</sub> by 5°C for samples reinforced with 0.1 and 0.5% of GO, the increase of the weight percent of GO to 1% entail a decrease 8°C of the glass transition temperature compared to pure PMMA.

### 5.3 Surface mechanical properties of in situ polymerization coatings

Surface mechanical properties, Young's modulus and hardness, are measured by the nanoindentation technique for PMMA substrates coated with pure PMMA coating and for PMMA reinforced with various weight percentage of GO (0.05, 0.01 and 0.5 wt%). The data were fitted with the Oliver-Pharr [66] model with a Poisson's ratio value of 0.3. After the last drying step during the polymerization process, the coating thicknesses are ~150 μm which entails that we can probe the coating up to 15 μm to get its own mechanical response.

The obtained experimental results revealed that there is almost a 9% increase with addition of 0.5 GO on the elastic modulus. With regard to hardness, there is 17.5% increase in surface hardness with increasing the percentage of GO in the samples (Figure 5-5).

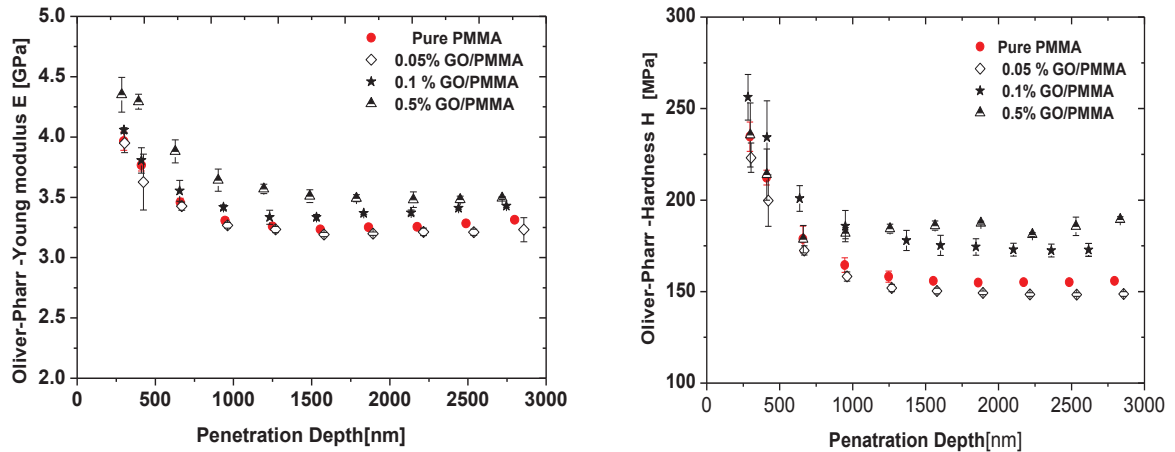


Figure 5-5 Variation of Young's modulus (on the left) and of hardness (on the right) for GO/PMMA composite reinforced with different wt. % of GO prepared by in situ polymerization process.

The surface response to shear is characterized by friction tests. Figure 5-6 shows the evolution of the apparent friction coefficient  $\mu_{app}$  as a function of the  $a/R$  ratio for two tip radius ( $R = 98$  and  $250 \mu\text{m}$ ) at room temperature, sliding speed  $0.03\text{mm/s}$ ) and normal load between  $0.05\text{ N}$  to  $3\text{ N}$ . The experimental results indicate that introducing graphene oxide in PMMA can decrease the coefficient of friction. For example, for the samples coated with PMMA composite with 0, 0.05, 0.1 and 0.5 % GO, at the same value of  $a/R$  (0.3) the apparent friction

coefficient decreased from 0.42 for pure coating to 0.23, 0.12 and 0.12 for all composites respectively. At the same value of (a/R) the local friction coefficient decreased from 0.33 for pure coating to 0.1, 0.02 and 0.02 for all composites respectively (Figure 5-7).

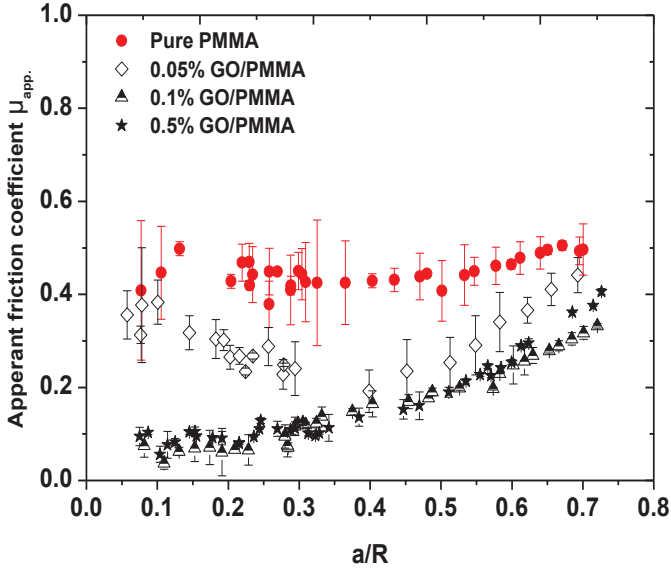


Figure 5-6 Effect of graphene oxide (GO) on the apparent friction coefficient for two tip radius ( $R = 98$  and  $250\mu\text{m}$ ) at room temperature, sliding speed  $0.03\text{mm/s}$  and normal load from  $0.05\text{ N}$  to  $3\text{ N}$ .

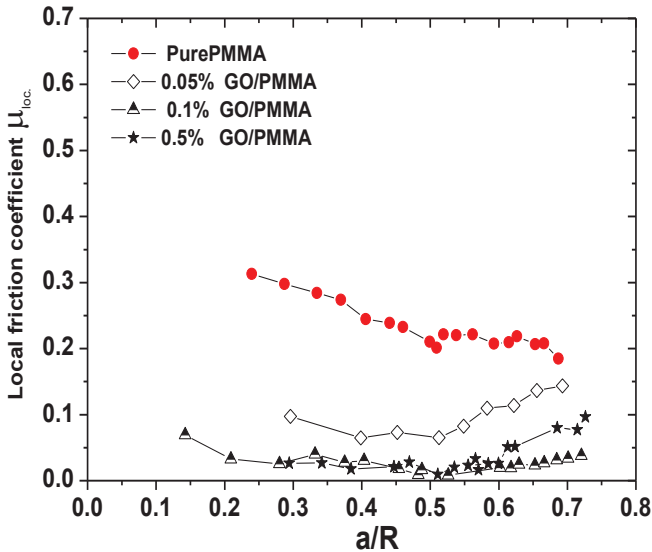


Figure 5-7 Effect of graphene oxide (GO) on the local friction coefficient with tip radius ( $R = 98\ \mu\text{m}$ ).

Looking at the contact snapshots it is noticeable that there are large and thick graphene oxide layers especially at height weight percent (0.5%) of GO. This perhaps is due to agglomeration of graphene oxide sheets during the polymerization process took relatively long time (16 to 20 h to complete the solidification). The presence of graphene in this form in the composite coating, explains the large decrease of the coefficient of friction.

The rear contact angle ( $\omega$ ) is the indicator of the nature of the contact between the sliding tip and the polymer surface. The experimental results indicated that the introduction of graphene oxide can modify the nature of the contact and improve the elasto-plastic behavior at the contact (Figure 5-8). The elastic domain has expanded, the elasto-plastic domain for pure coating begun at  $a/R$  value of 0.14, while for the composite coating it begun at  $a/R$  0.21. At the same value of  $a/R$  (0.3), the value of  $\omega$  changes significantly with the introduction of GO. It is about 0.46 radian for pure PMMA coating having the higher value of friction coefficient 0.42 while for composite contain of 0.05% of GO, it is about 0.8 for friction coefficient about 0.23. The increase of the weight percent of GO in the composite to 0.1 and 0.5% doesn't change the value of  $\omega$ , despite that the coefficient of friction was decreased from 0.23 for 0.05 wt% of GO to 0.11 for 0.1 and 0.5 wt% GO. The in situ photographs of the contact at the  $a/R$  of 0.3 explained that the nature of the contact is plastic for pure PMMA coating, while the contact is elasto-plastic at the same value of  $a/R$  for all percentage of GO in the composites, and also no significant change in the shape of contact with increasing the weight percent of GO is observed.

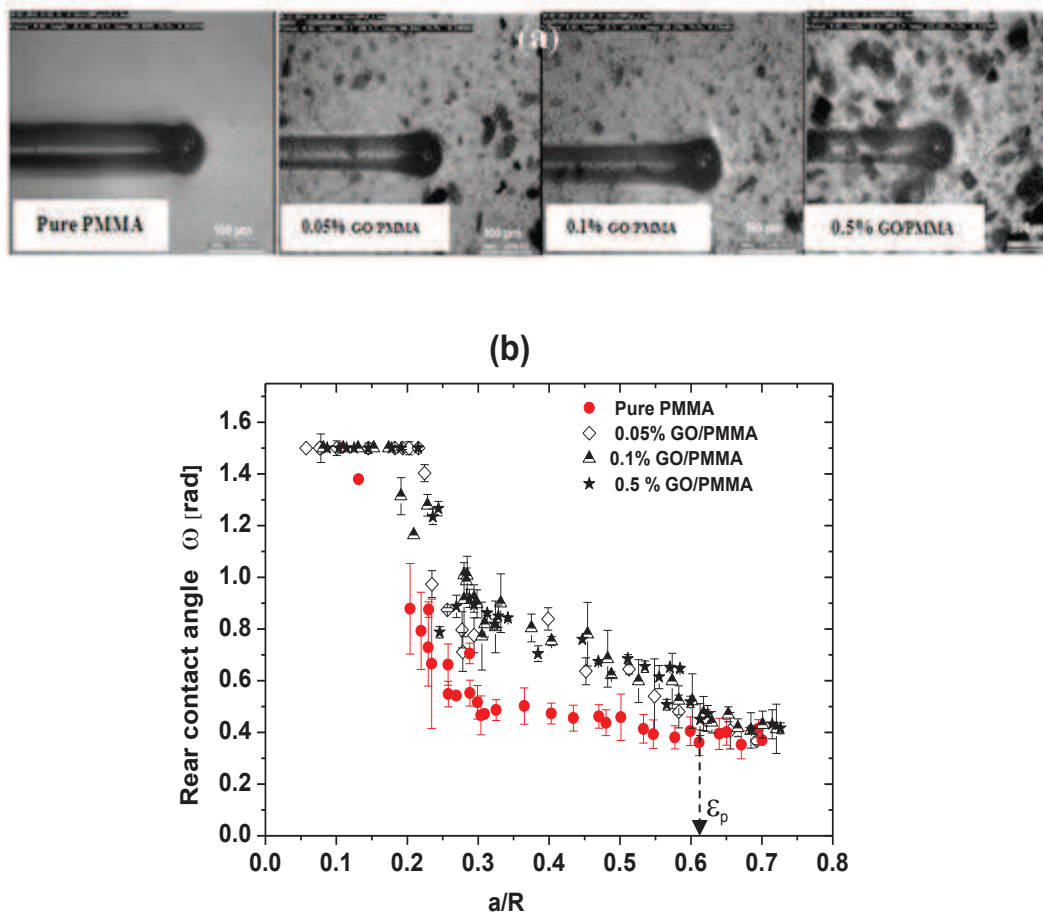


Figure 5-8 a) The selected images at  $a/R$  ( $\sim 0.30$ ) for different percentage of GO. b) Rear contact angle versus  $a/R$  for coated samples with PMMA reinforced with different percentage of GO.

The slope of the contact pressure— $a/R$  curve at the elastic and visco-elastic region of polymers is a function of both the Young's modulus and the friction coefficient [23].

Figure 5-9 shows the mean contact pressure as a function of the  $a/R$  ratio. On the sample coated with pure PMMA, scratched by two tips ( $250\ \mu\text{m}$  and  $98\ \mu\text{m}$ ), the contact pressure increases from 100 to 250 MPa and then seems to become almost constant as the ( $a/R$ ) ratio exceeds 0.35. Whereas in the samples coated with composites the contact pressure increases continuously up to  $a/R = 0.6$  and the elastic-plastic domain seems to expand and then all the mean contact pressure tend to be equal.

There is no large difference in the mean contact pressure observed with changing the concentration of GO in the composite coating from 0.05 to 0.5 wt%.

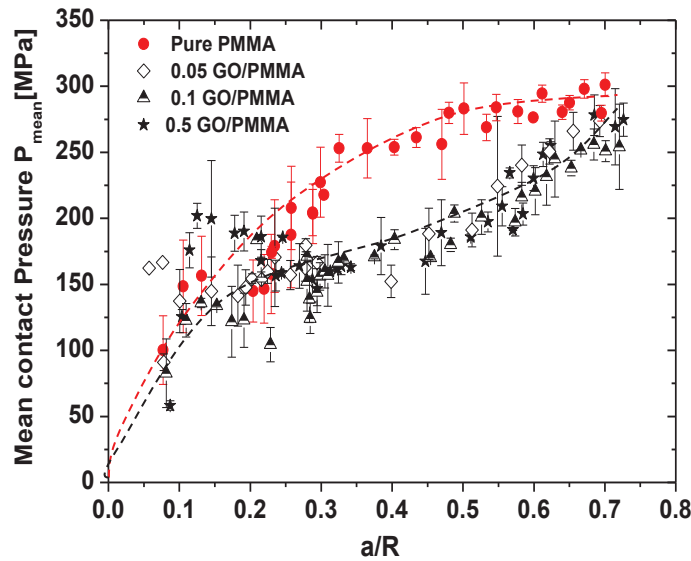


Figure 5-9 Variation of the contact pressure with  $a/R$  ratio for coated samples with PMMA reinforced with different percentage of GO.

## 5.4 Surface mechanical properties of solution mixing coatings

The solution mixing technique was employed to prepare coating composites reinforced with variety percentages of GO (0.1, 0.5 and 1wt %). All samples were coated by Doctor Blade technique on (glass substrate) for nanoindentation tests and on (PMMA substrates) for a scratch test.

After the last drying step the coating thicknesses are  $12\text{-}15\ \mu\text{m}$  which entails that we can probe the coating up to  $1.2\ \mu\text{m}$  to get its own mechanical response by nanoindentation technique. Figure 5-10 shows an increase in the composite Young's modulus when the contact depth increases above  $1.5\ \mu\text{m}$ , which is clearly related to the influence of the glass substrate, so the results that have been adopted correspond to the penetration depth of  $1\ \mu\text{m}$  to avoid the effect of the substrate.

The experimental results show an increase in the Young's modulus and hardness (Figure 5-10) for the composite coating compared to pure PMMA coating. For example PMMA reinforced with (0, 0.5 and 1wt %) GO have a Young's modulus 3.74, 3.86 and 4.74 GPa and hardness 175, 190, and 197 MPa respectively.

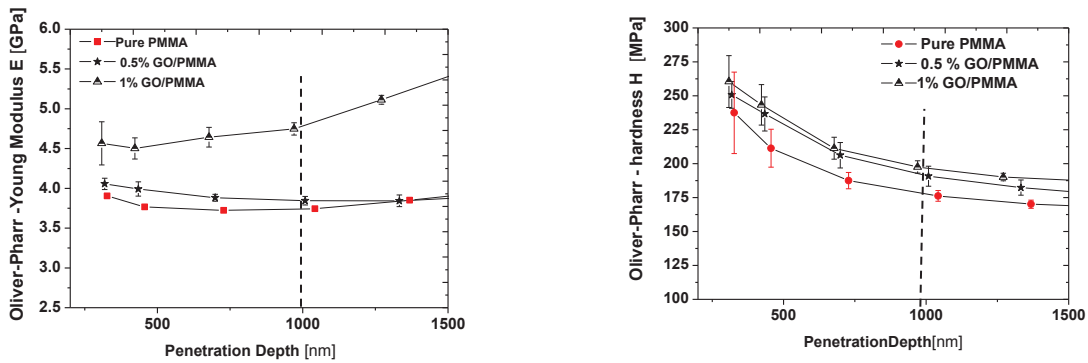


Figure 5-10 Variation of Young's modulus (on the left) and of hardness (on the right) for GO/PMMA composite reinforced with different wt. % of GO prepared by solution mixing process.

Figure 5-11 shows the evolution of the apparent friction coefficient  $\mu_{app}$  as a function of the  $a/R$  ratio for two tip radius ( $R = 98$  and  $250 \mu\text{m}$ ) at room temperature, sliding speed  $0.03\text{mm/s}$ , normal load from  $0.05 \text{ N}$  to  $1.5 \text{ N}$  and coating thickness  $20\mu\text{m}$  on PMMA substrate. The experimental results indicate that the apparent friction coefficient for the composites reinforced with graphene oxide (GO) decreases with increasing the weight percent of GO and lowest friction coefficient obtained was for composite coating reinforced with 1 wt. % of graphene oxide.

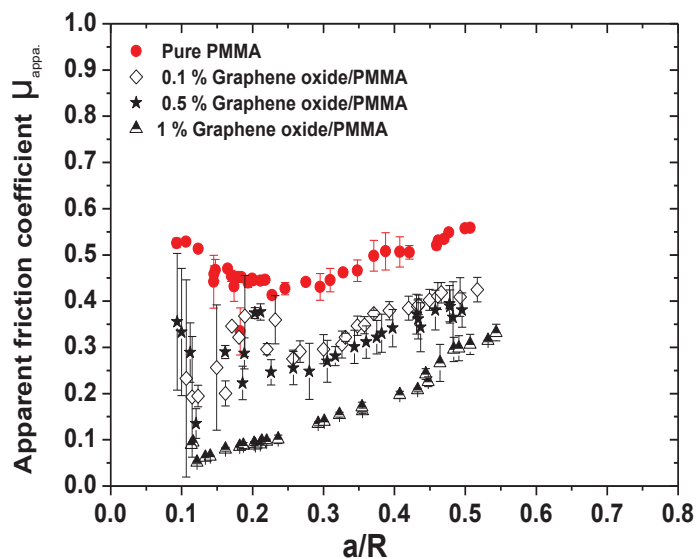


Figure 5-11 Effect of graphene oxide (GO) on the apparent friction coefficient, with two tips ( $98 \mu\text{m}$  and  $250\mu\text{m}$  Radius).

Figure 5-12 showed that the local friction coefficient also decreased with increasing the weight percent of graphene oxide (GO). For example, at contact strain of 0.35 the local



friction coefficient decreased from 0.27 for pure coating to 0.04 for 1% GO/PMMA composite.

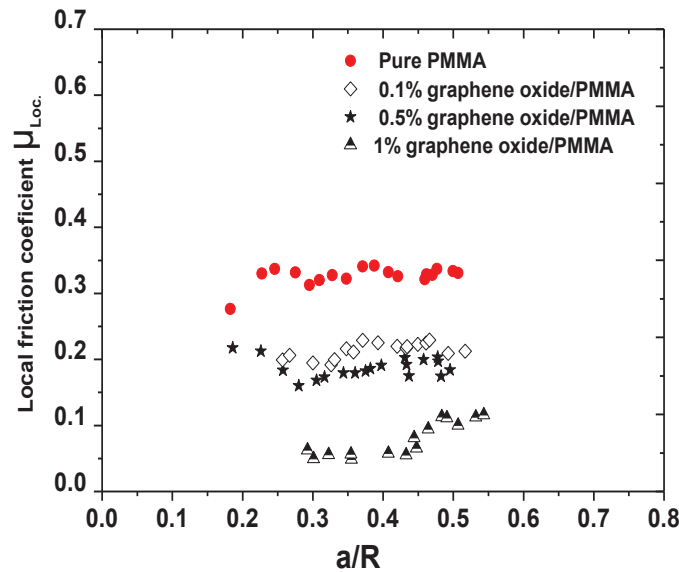


Figure 5-12 Effect of graphene oxide (GO) on the local friction coefficient of composite coating prepared by solution mixing technique with tip radius 98 $\mu$ m.

Rear contact angle ( $\omega$ ) represents the nature of the contact between the sliding tip and the polymer surface. The experimental results revealed that:

- The introduction of GO can modify the nature of the contact and improves the elasto-plastic in the contact.
- The elastic domain for pure coating ends at 0.14 a/R value, while for 1% GO/PMMA composite at (a/R = 0.20).
- The value of  $\omega$  at the same value of a/R (0.35), changed significantly with the introduction of GO. It is about 0.42 radian for pure PMMA coating having higher value of friction coefficient 0.45 and with increasing the weight percent of GO in the composite the value of  $\omega$  increased to about 0.62, 0.7 and 0.8 radian for composites containing 0.1, 0.5 and 1 % of GO which having friction coefficient about 0.35, 0.3 and 0.162 respectively, thus it can be concluded that the decrease in friction coefficient is associated with increased value of the rear contact angle (Figure 5-13).
- Plastic domain for pure coating and also for 0.1% composite begun at a/R of 0.35 while for 0.5 and 1% it begun at a/R of 0.48 and 0.54 respectively.

The in situ photographs of the contact at the a/R of 0.35 shows that the nature of the contact is plastic for pure PMMA coating, while the contact is elasto-plastic at the same value of a/R for the composites reinforced with 0.5wt% and 1wt% GO.

Figure 5-14 shows the contact pressure as a function of the a/R. For the samples coated with pure PMMA, the contact pressure increases from 100 to 233 MPa and then seems to take a stable path as the a/R value exceeds 0.35. In the samples coated with composites containing GO the contact pressure increases continuously.

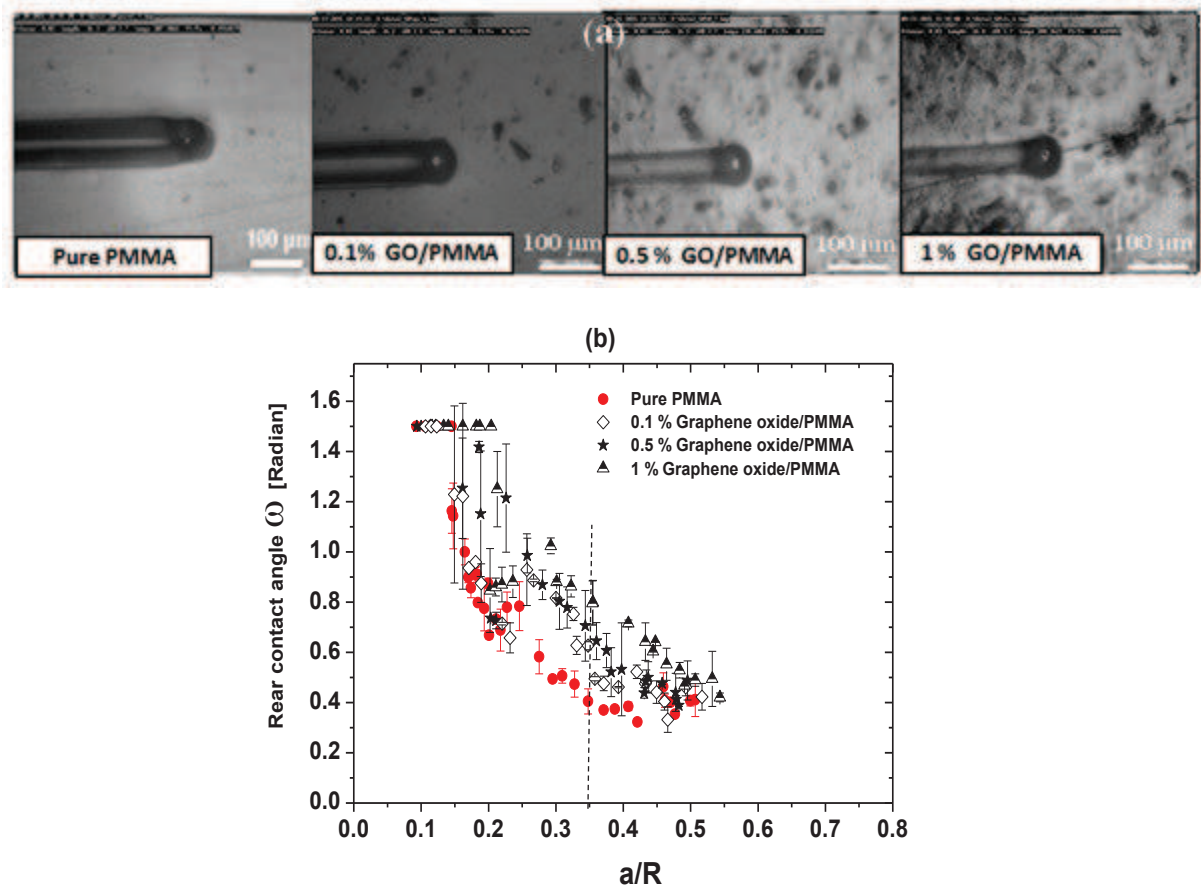


Figure 5-13 a) Selected images at ( $\sim 0.35$ ) contact strain for different percentage of GO. b) Rear contact angle versus contact strain for coated samples with PMMA reinforced with different percentage of GO.

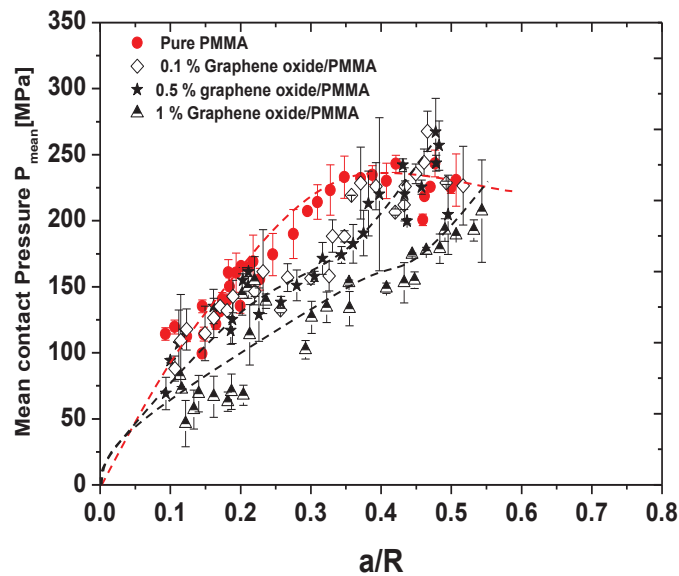


Figure 5-14 Mean contact pressure versus  $a/R$  for coated samples with PMMA reinforced with different percentage of GO.

## 5.5 Comparative study of the effect of different techniques of the coating

Two coatings composites prepared by in situ polymerization and by solution mixing, with the same percentage of filler (0.1% and 0.5 GO). The tests were performed on PMMA substrate coated with PMMA/GO composite. All the experiments were made at room temperature, 4% humidity, scratch/ sliding speed 0.03 mm/s and  $0.05\text{ N} < F_n < 1.5\text{ N}$ , and with two tip radius  $250\text{ }\mu\text{m}$  and  $98\text{ }\mu\text{m}$ .

Photographs in Figure 5-15 show that the solution mixing technique is effective technique to improve the dispersibility of GO in PMMA matrix due to the very dilute medium used during solution mixing process. This maybe can enhance Young's modulus and hardness of the resultant composites.

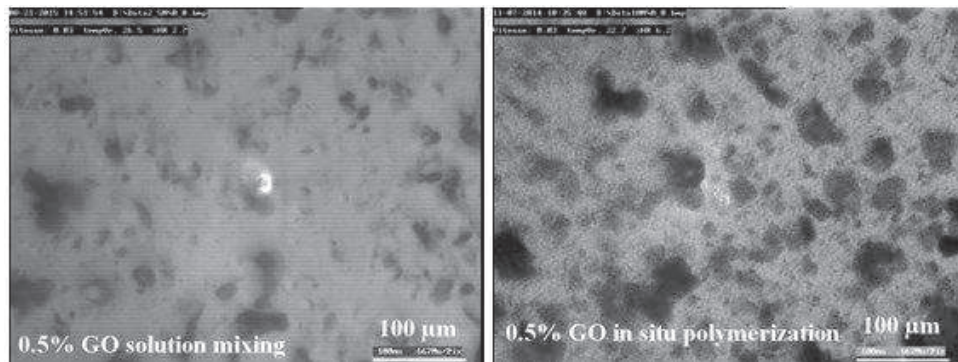


Figure 5-15 Photographs showing the dispersibility of graphene oxide in PMMA nanocomposites prepared by two different techniques.

The experimental results (Figure 5-16) indicate that the nanocomposite prepared by in situ polymerization technique is more effective in reducing the friction coefficient than the composite prepared by solution mixing technique. This is perhaps due to the difference in the roughness (samples coated by solution mixing technique have a higher surface roughness as compared with the samples coated by in situ polymerization technique, as we previously mentioned) and also due to decreased of the number of thick graphene oxide layers which played a key role in reducing the coefficient of friction in the samples coated by in situ polymerization technique.

For the same above reasons, the samples coated by in situ technique showed local friction coefficient less than samples coated by solution mixing technique Figure 5-17.

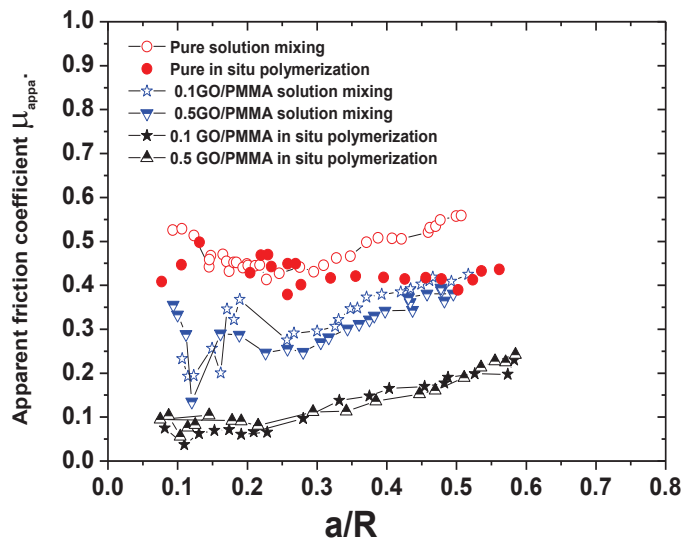


Figure 5-16 Apparent friction coefficient as a function of  $a/R$ , for samples coated by two different techniques with two tips ( $98 \mu\text{m}$  and  $250 \mu\text{m}$  Radius).

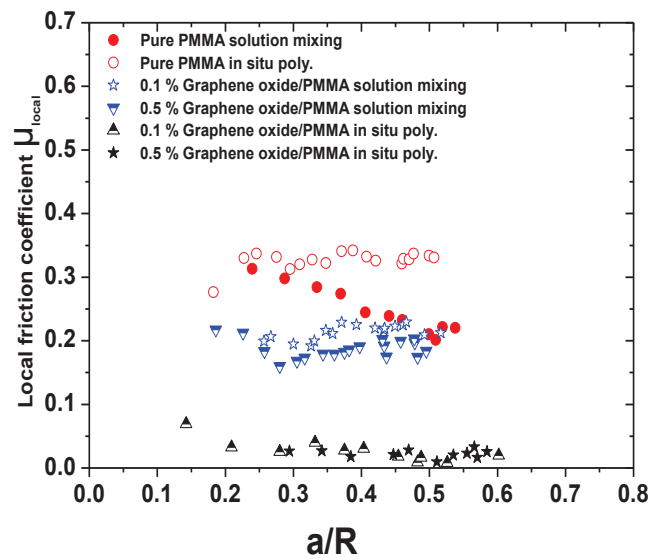


Figure 5-17 Local friction coefficient as a function of  $a/R$ , for the samples coated by two different techniques with tips radius ( $98 \mu\text{m}$ ).

Figure 5-18 shows the evolution of the rear contact angle as a function of the ratio  $a/R$  for samples coated with two different techniques, the results indicated that:

- The elastic domain ends at  $a/R = 0.2$ , for the composite coating by in-situ polymerization, while for the composite coating by solution mixing technique it ends at  $a/R = 0.16$ .
- There are huge changes in elasto-plastic domain.

- There is a shift in the beginning of plastic domain from  $\frac{a}{R} = 0.35$  for composite solution mixing to more than 0.6 for composite coating prepared by in situ polymerization.

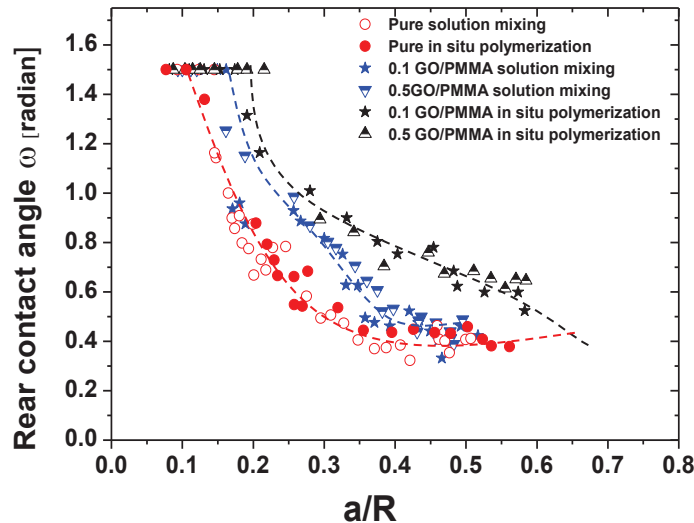


Figure 5-18 Rear contact angle versus contact strain for samples coated by two different techniques with two tips (98  $\mu\text{m}$  and 250 $\mu\text{m}$  Radius).

## 5.6 Conclusions

Graphene oxide (GO) was synthesized from graphite using Hummers method, the FTIR, UV spectra and XPs spectroscopy was used to confirm the success of prepared graphene oxide.

For the samples prepared by in situ polymerization technique:

1. The introduction of graphene oxide can increase Young's modulus and hardness by 9% and 17.5% respectively.
2. The introduction of graphene oxide in PMMA can decrease the coefficient of friction.
3. The introduction of GO can modify the nature of the contact and improves the elasto-plastic of the contact. There is no significant change in the nature of contact shape with increasing the weight percent of GO.

For samples prepared by solution mixing technique:

1. There is a significant effect of adding GO on the elastic modulus and hardness.
2. The introduction of graphene oxide in PMMA can decrease the coefficient of friction and the optimum behavior was observed for PMMA/GO composite coating containing 1wt% of GO.
3. There are clear modification and improvement in the elasto-plastic domain with increasing the concentration of the GO in the composite coatings.
4. A solution mixing technique is an effective technique to improve the dispersibility of GO in PMMA matrix due to the very dilute medium used during the process.
5. In general, the in-situ polymerization technique for coating is more effective than the solution mixing technique in decreasing the coefficient of friction.

## 6 Multi walled carbon nanotube (MWCNT) grafted PMMA

The chemical functionalization of carbon nanotubes (CNTs) could improve their chemical compatibility with polymeric matrix. Multiwall carbon nanotubes grafted poly (methyl methacrylate) (PMMA) are prepared by in situ atom transfer radical polymerization (ATRP) using a “grafting from” approach. The thickness of the polymer layer in the functionalized MWCNTs can be well-controlled by the feed ratio of MMA to MWCNT and also by the volume ratio of the solvent to MMA. The general strategy for grafting polymers from the MWCNTs via in situ ATRP is described in (section 3.1.6.2).

### 6.1 Chemical composition and structure characterization

In the first study, the commercially available MWCNT-OH containing around 4.7% OH groups was modified with PMMA following the protocol described in section 3.1.6.2 (steps iv and v). The chemical composition of unmodified and modified MWCNTs was determined by XPs. It can be seen from the data in (Table 6-1) that the Br content after this modification was only 0.04% in the resulting MWCNT-Br. The reason for the low percentage of Br can be attributed to the low percentage of hydroxyl groups in the commercial MWCNT-OH (only ~5%). Therefore, the functionalization with PMMA was not successful, as highlighted by transmission electron microscopy, Figure 6-1 and in Table 6-2 (CPMMA1<sup>e</sup>, CPMMA2<sup>e</sup> and CPMMA3<sup>e</sup>). Indeed, the functionalization with PMMA was achieved using the MWCNT-Br as initiator of the atom transfer radical polymerization of methyl methacrylate (grafting from approach).

In general, a decrease of the amount of initiator (i.e of Br groups in this case) leads to the increase of PMMA molecular weight.

<i>Product</i>	<i>Synthesis way</i>	<i>O%</i>	<i>C%</i>	<i>Br%</i>
MWCNT- OH	commercial	5	95	0
MWCNT-Br	Lab.	5	94.76	0.04
MWCNT-PMMA	Lab.	4.30	95.7	/
MWCNT-COOH	commercial	4.0	/	/
MWCNT-COOH	Lab.	11	89.0	0
MWCNT-Br-4	Lab.	10.20	87.9	1.9
MWCNT-PMMA4	Lab.	18	82.0	/

Table 6-1 Elemental atomic composition of the modified MWCNT

However, in this study, it seems more likely that the little amount of Br sites and their non-easy accessibility lead to a non-success of the polymerization process even if no Br groups

remained. Indeed, no clear growth on the nanotubes surface was observed after PMMA functionalization, thus proving a non-success of the PMMA functionalization.

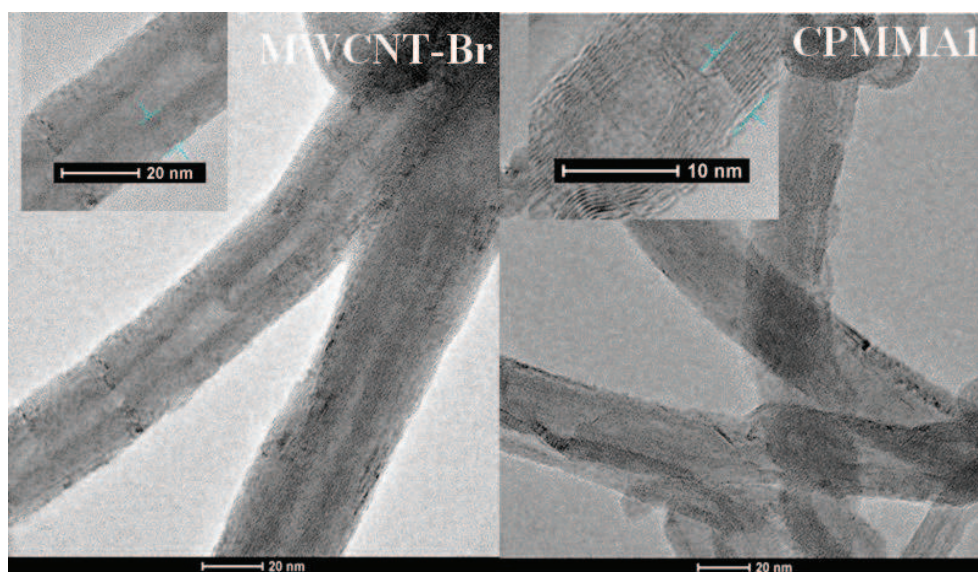


Figure 6-1 Transmission Electron Microscopy of MWCNT-Br and MWCNT-grafted-PMMA (CPMMA1).

Therefore, a second strategy consisting of 5 steps (steps i to v in Chapter three, section 3.1.6.2) was tested in order to increase the hydroxyl content on the MWCNT. It started with a commercially available MWCNT-COOH containing about 4% carboxyl groups. After an acidic treatment, an increase of the carboxyl group's content from 4% to 11% was observed. The use of this new MWCNT-COOH resulted in the formation of MWCNT-Br with higher Br content (1.9% instead of 0.04%), Table 6-1. This result may be attributed to an increase of the density of hydroxyl groups on the MWCNTs surface related to the increase of the carboxyl group's content. ATRP was then conducted on this new MWCNT-Br.

Table 6-2 showed the experimental conditions used in order to functionalize MWCNT with PMMA chains.

<i>Code</i>	<i>f<sup>a</sup></i>	<i>MCN<sup>b</sup></i>	<i>MS<sup>c</sup></i>	<i>Temp.</i> (°C)	<i>Time (h)</i>	<i>L(%)<sup>d</sup></i>
CPMMA1 <sup>e</sup>	10:1	50:1:1	1:10	60	24	/
CPMMA2 <sup>e</sup>	10:1	50:1:1	1:10	60	48	/
CPMMA3 <sup>e</sup>	10:1	50:1:1	1:10	60	72	/
CPMMA4 <sup>f</sup>	10:1	50:1:1	1:5	60	24	49.1
CPMMA6 <sup>f</sup>	10:1	50:1:1	1:1	60	24	65.5
CPMMA8 <sup>f</sup>	20:1	100:1:1	1:1	60	24	71.5

Table 6-2 Experimental conditions used in order to functionalize MWCNT with PMMA chains. <sup>a)</sup> f: monomer: MWCNT-Br (wt.:wt.), <sup>b)</sup> MCN: monomer : CuBr :PMDETA (mol:mol:mol), <sup>c)</sup> MS: monomer: solvent (v:v) <sup>d)</sup> L% the loss weight fraction of polymer calculated from TGA data, <sup>e)</sup> functionalization starting from commercially available MWCNT-OH, <sup>f)</sup> from commercially available MWCNT-COOH.

Moreover, TGA results (Figure 6-2) of the unmodified MWCNT and MWCNT-grafted PMMA (CPMMA4, CPMMA6 and CPMMA8), revealed three main weight-loss zones. The rapid weight decrease in the second region ( $\sim 200\text{--}385\text{ }^{\circ}\text{C}$ , the onset are at  $\sim 300\text{ }^{\circ}\text{C}$ ) may readily be attributed to the decomposition of PMMA polymer. Indeed, this weight loss is not observed for MWCNT-OH and MWCNT-Br. The significant weight reduction in the third region ( $\sim 380\text{--}627\text{ }^{\circ}\text{C}$ , the onset are at  $\sim 540\text{ }^{\circ}\text{C}$ ) is probably due to the decomposition of MWNTs. Moreover, the decomposition temperature of the MWNT core of MWNT-PMMA (onset is  $\sim 540\text{ }^{\circ}\text{C}$ ) is lower by about ( $100\text{--}110\text{ }^{\circ}\text{C}$ ) than that of MWNT-OH (onset  $640\text{ }^{\circ}\text{C}$ ). A possible explanation is that the grafting of PMMA on the surface of MWNT has peeled the individual nanotube from the usual carbon nanotube cords and thus the decomposition temperature of the tubes significantly decreased.

In addition, the loss weight fraction of PMMA in CPMMA6 sample was 65.5%, while it was 71.5% in CPMMA8 sample. These results indicate that the functionalization of MWCNT can be well-controlled by the feed ratio of MMA (Table 6-2). Indeed, the amount of monomer was doubled in CPMMA8, thus leading to longer polymer chains and subsequently a higher PMMA weight loss observed by TGA. Furthermore, an increase of the solvent volume used for the polymerization reaction has also an effect on the density of the grafted polymer. Indeed, the increase of a volume of the solvent five times for CPMMA4 (vs. CPMMA6) leads to the reduction of the weight fraction of polymer from 65.5% (CPMMA6) to 49.1% (CPMMA4). This can be explained by the fact that a decrease of the monomer concentration during the polymerization process causes a decrease of the polymerization kinetic, thus leading to smaller polymer chains and therefore the thickness of the polymer layer on MWCNTs surface is also reduced.

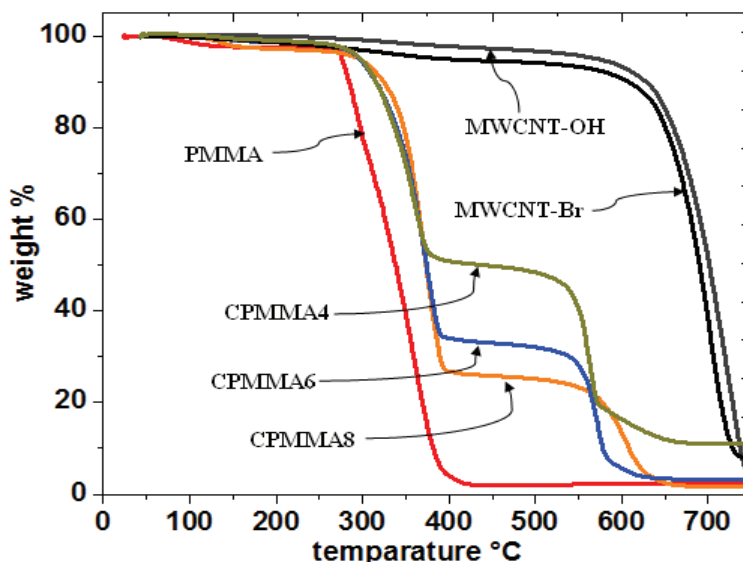


Figure 6-2 Curves of the MWCNT-OH, MWCNT-Br PMMA-functionalized MWNT and linear PMMA.



The structure of the different samples was observed by transmission electron microscopy. MWCNT grafted PMMA (samples CPMMA6 and CPMMA8) were compared to non-functionalized MWCNTs (MWCNT-COOH and MWCNT-Br) the presence of PMMA on

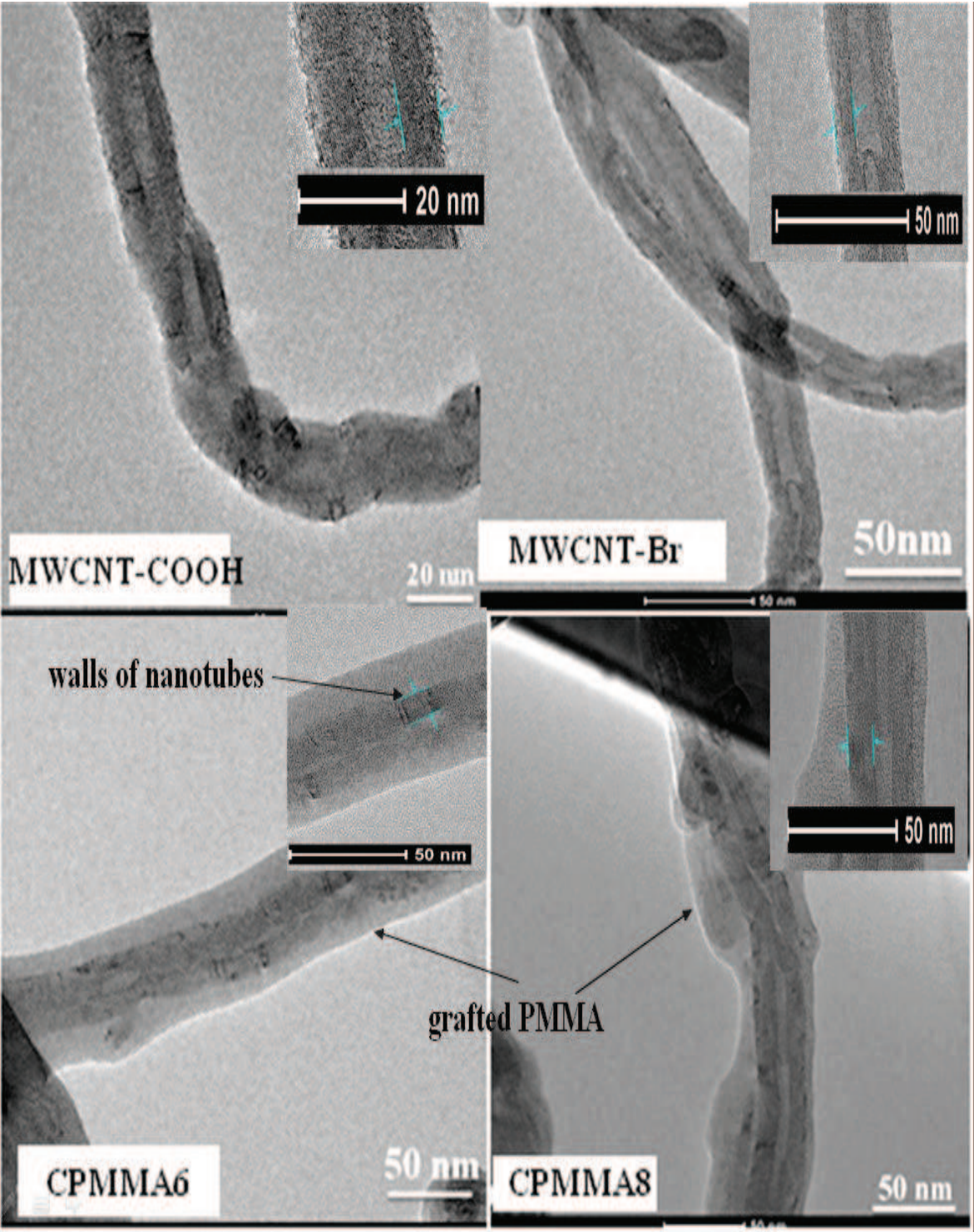


Figure 6-3 Transmission Electron Microscopy of MWCNT-COOH, MWCNT-Br and MWCNT-grafted-PMMA (CPMMA6 and CPMMA8) dispersed in THF.

MWCNT surface can be clearly detected. However, as observed on Figure 6-3, the thickness of the polymer layers was not homogenous, therefore it difficult to calculate precisely their thickness. It seems however that, the polymer layer is less homogenous in thickness in CPMMA8 compared to CPMMA6.

In order to confirm the PMMA grafting, FTIR analyses were carried on MWCNTs. As shown in Figure 6-4, the absorption signal of carbonyl band at around  $1730\text{ cm}^{-1}$  is barely detected for the MWNT-Br and MWCNT-OH samples, while it is strongly visible for MWCNT-PMMA. Moreover, one can notice that the intensity of this pick at  $1730\text{ cm}^{-1}$  increases with the increasing density of the polymer (Table 6-2). Finally, the C=C absorption band change observed around  $1630\text{ cm}^{-1}$  for MWCNT-PMMA samples confirmed the success of the functionalization.

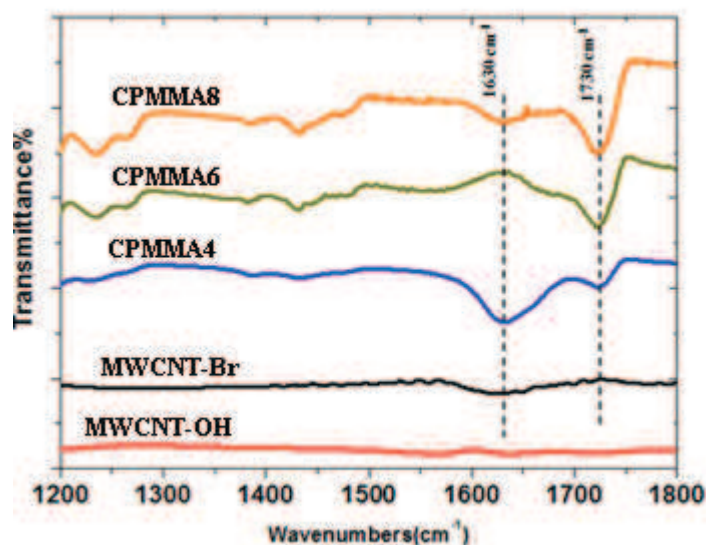


Figure 6-4 FTIR spectra recorded for the MWCNT-OH, MWCNT-Br and PMMA-functionalized MWCNT.

## 6.2 Characterization of PMMA/MWCNT-g-PMMA composites

Two different methods are used for preparing PMMA composites reinforced with a variety weight percent of MWCNT grafted PMMA (CPMMA6), by in-situ polymerization and solution mixing composites (section 3.2.1 and 3.2.3 respectively). We choice CPMMA6, because it contains the moderate amount of grafted PMMA on MWCNTs.

Prior to mechanical studies, the structures of the composites prepared by a solution mixing technique are checked by GPC and DSC (analysis from the ICS polymer characterization platform). The GPC results, Table 6-3, revealed that all composites prepared by solution mixing technique have almost the same molecular weight, which confirms that the quality of the matrix for the all composites is not affected during the synthesis step.

	$M_w$	$M_n$	$MW/M_n$	$T_g$ °C
Pure PMMA Powder (lab.)	$1.262 \cdot 10^5$	$8.918 \cdot 10^4$	1.415	119.78
CPMMA6 0.1%	$1.407 \cdot 10^5$	$1.039 \cdot 10^5$	1.354	109.82
CPMMA6 0.5%	$1.286 \cdot 10^5$	$9.406 \cdot 10^4$	1.368	123.73

Table 6-3 Results of GPC and DSC analysis for PMMAs prepared via solution mixing technique with and without MWCNTs.

### 6.2.1 Surface mechanical properties of in situ polymerization coatings

For mechanical tests, the PMMA samples were coated during the polymerization with a thickness  $\approx 150 \mu\text{m}$ . Young's modulus and hardness were estimated by the nanoindentation technique for sample coated with pure PMMA coating and for samples coated with PMMA composites reinforced with MWCNT grafted PMMA (CPMMA6) 0.05, 0.1 and 0.2 wt%. Figure 6-5 displays the results obtained on the surfaces from nanoindentation experiments. The data were fitted with the Oliver-Pharr model with a Poisson's ratio value of 0.3.

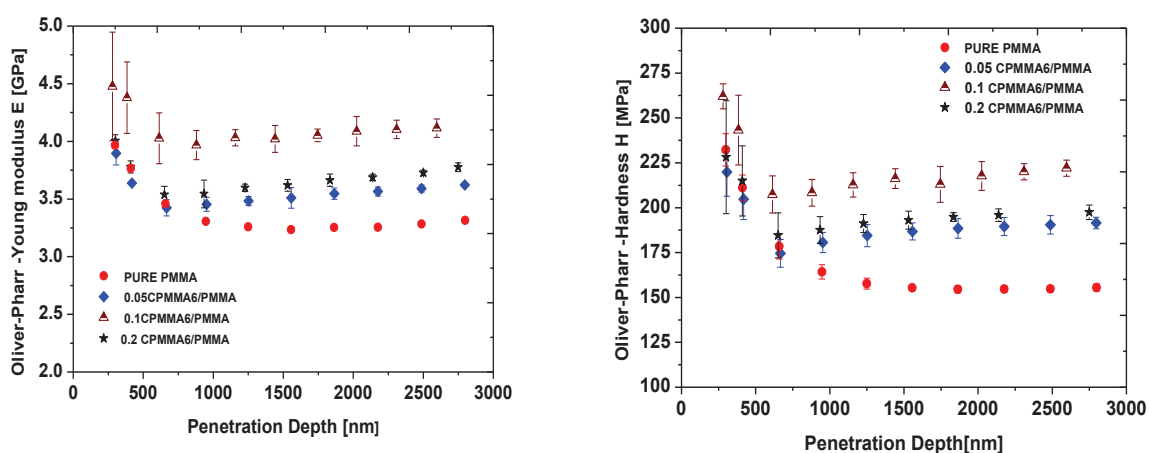


Figure 6-5 Variation of Young's modulus (on the left) and of hardness (on the right) for MWCNT grafted PMMA (CPMMA6) / PMMA composites.

The experimental results show an increase in the Young's modulus and hardness for the composite coatings compared to pure PMMA coating. For example, PMMA composites reinforced with (0, 0.05, 0.1 and 0.2 wt%) MWCNT (CPMMA6) have a Young's modulus of 3.25, 3.51, 4.02 and 3.7 GPa and hardness of 155, 186, 216 and 193 MPa respectively.

The surface response to shear is characterized by friction tests. Figure 6-6 shows the evolution of the apparent friction coefficient  $\mu_{app}$  as a function of the  $a/R$  ratio for two tip radius ( $R = 98$  and  $250 \mu\text{m}$ ) at room temperature, sliding speed  $0.03 \text{ mm/s}$  and normal load from  $0.05 \text{ N}$  to  $3 \text{ N}$ . The experimental results indicate that:

- Composites coating reinforced with 0.1 and 0.2 wt % of CPMMA6 showed decrease in the friction coefficient at low contact strain compared to the pure coating. For example, at a/R ratio of 0.35, the pure coating showed friction coefficient of 0.42 while composites with (0.1 and 0.2 wt %) showed friction coefficient of 0.3 and 0.18 respectively (Figure 6-6).
- At high value of a/R, the friction coefficient for composite containing 0.1% CPMMA6 continuously increases and becomes higher than that of pure coating, while the composite with 0.2% doesn't show increase in friction coefficient.

Figure 6-7 showed the calculated local friction coefficient as a function of the a/R ratio. The experimental results indicate that the local friction coefficient (at a/R ratio) of 0.35 for composite coatings CPMMA6 /PMMA with several percentages (0, 0.1 and 0.2 wt. %) was 0.26, 0.15 and 0.08 respectively.

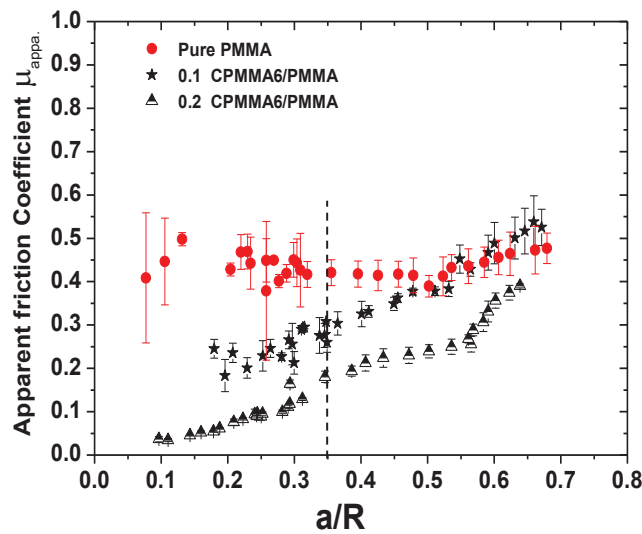


Figure 6-6 Effect of MWCNT-grafted PMMA on the apparent friction coefficient with two tip radius ( $R = 98$  and  $250\mu\text{m}$ ) at room temperature, sliding speed  $0.03\text{mm/s}$  and normal load from  $0.05\text{ N}$  to  $3\text{ N}$ .

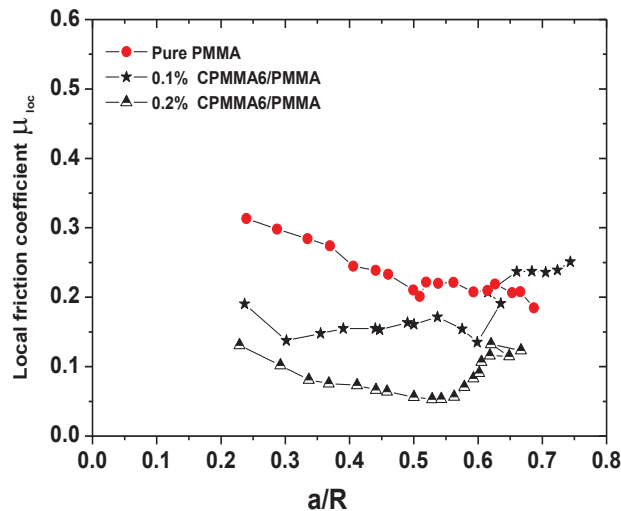


Figure 6-7 Effect of MWCNT-grafted PMMA on the local friction coefficient with tip radius ( $R = 98$ ).

It is apparent from the experimental results that the introduction of MWCNT-g-PMMA (CPMMA6) slightly modified the nature of the contact and improves the elasto-plastic response of the contact (Figure 6-8).

It seems that the elastic domain was expanded, where the elasto-plastic domain for pure coating began at contact strain 0.14, while for CPMMA6/PMMA composite coating it begun at  $a/R$  of 0.2. At the same value of  $a/R$  (0.35), the value of  $\omega$  changes significantly with the introduction of CPMMA6. It is about 0.45 radian for pure PMMA coating having higher value of friction coefficient of 0.42. For the composites 0.1 and 0.2 wt % of the CPMMA6 the value of  $\omega$  increases to about 0.63 radian and 0.84 radian respectively.

The in-situ photographs of the contact at  $a/R$  value of 0.35 explained that the nature of the contact is plastic for pure PMMA coating, while the contact is elasto-plastic at the same value of  $a/R$  for the composites with 0.1 and 0.2wt%.

The beginning of the plastic domain for samples coated with pure PMMA at  $a/R$  of 0.3, whereas for samples coated with composite coating reinforced with 0.1 and 0.2wt% of CPMMA6 at  $a/R$  values 0.44 and 0.6 respectively.

All samples are yield plastically at the same rear contact angle ( $\omega$ ) of  $\sim 0.4$  radian.

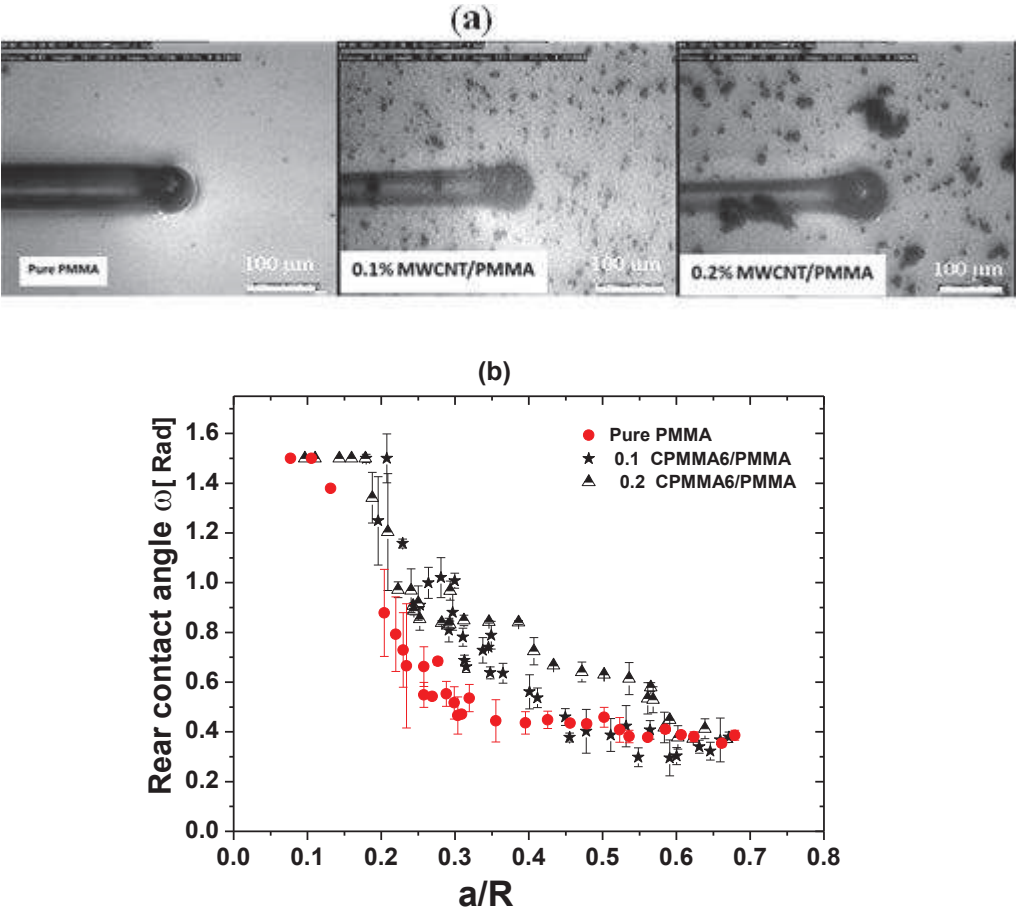


Figure 6-8 a) Selected images at  $a/R \sim 0.35$  b) Rear contact angle versus  $\sim 0.35$  for coated samples with PMMA reinforced with different percentage of MWCNT-grafted-PMMA (CPMMA6).

Figure 6-9 shows the contact pressure as a function of the ratio  $a/R$ . The samples coated with pure PMMA the contact pressure increases from 100 to 250 MPa and then seems to be almost constant as the  $a/R$  ratio exceeds 0.36, whereas in the samples coated with composites coating showed shifting in elasto- plastic domain and the plastic domain has begun at a higher value of the  $a/R$  compare with pure coating.

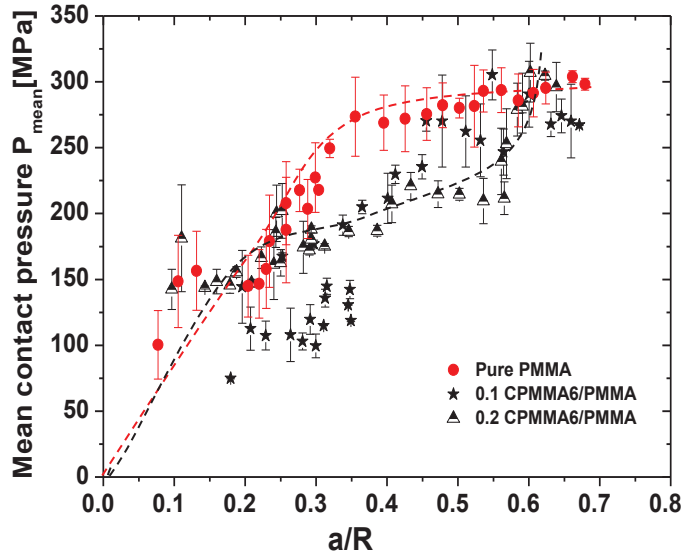


Figure 6-9 Variation of the mean contact pressure with  $a/R$ .

## 6.2.2 Surface mechanical properties of solution mixing coatings

The nano-indentation experiments were carried out on glass slide substrate by pure PMMA coating and CPMMA6/PMMA composite (Figure 6-10). The results that have been adopted were at a penetration depth of  $1\mu\text{m}$  to avoid the effect of the substrate. Young's modulus and hardness were detected by the nano-indenture for sample coated with a pure PMMA coating and for samples coated with composites of PMMA reinforced varied percentage of MWCNTs grafted PMMA(CPMMA6) (0, 0.5, 1 and 2wt%). Composite films were deposited on a clean glass plate. After the last drying step, the coating thicknesses is 12-15  $\mu\text{m}$ , which entails that we can probe the coating up to 1.5  $\mu\text{m}$  to get its own mechanical response.

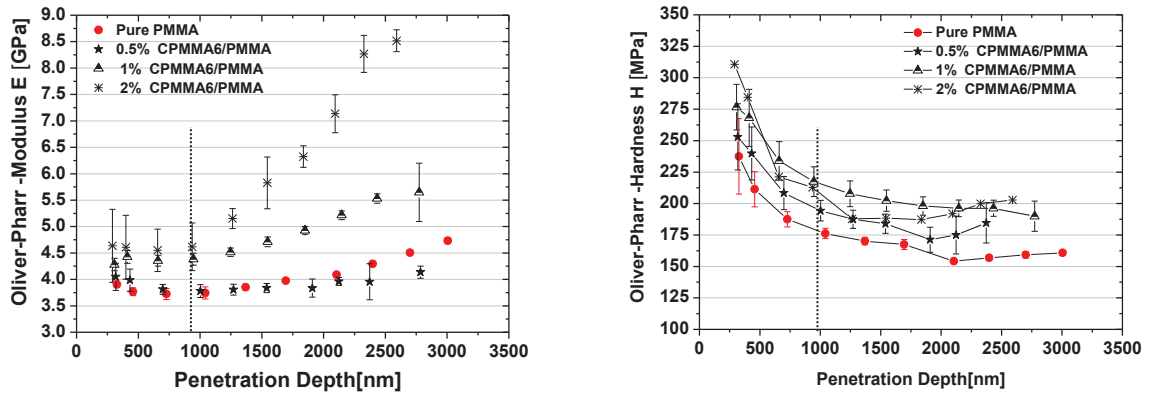


Figure 6-10 Variation of Young's modulus (on the left) and of hardness (on the right) for CPMMA6/PMMA composites.

The experimental results showed that the Young's modulus and hardness increase with the increase of the percentage of CPMMA6 in the composite compared with pure coating.

At the penetration depth of  $1\mu\text{m}$ , the pure PMMA and PMMA / 0.5 wt% CPMMA6 coating have quite the same modulus, 3.8 GPa, while for 1% and 2 wt% of CPMMA6/PMMA composites Young's modulus increased to 4.4 GPa and 4.6 GPa respectively.

With regards to the effect of CPMMA6 percentage on the hardness of the composites, the experimental results showed that the hardness increased from 176 MPa for pure PMMA coating to 194 MPa for 0.5 wt% CPMMA6 and 217 MPa for 1 and 2 wt% of CPMMA6.

Scratch tests were performed at room temperature, 4% humidity, scratch/ sliding speed 0.03 mm/s and  $0.05\text{N} \geq F_n \geq 1.5\text{N}$ . Each point represents the average of the three tests. The solution mixing technique was used to prepare coating composites reinforced with 0.5, 1 and 2% of MWCNT-grafted PMMA (CPMMA6). The substrate is PMMA coated by Doctor Blade technique with coating thickness of ( $\sim 20\mu\text{m}$ ).

Figure 6-11 shows the friction coefficient as a function of the  $a/R$ , with two tip radius  $98\mu\text{m}$  and  $250\mu\text{m}$  for all samples except 2% CPMMA6 with  $98\mu\text{m}$  tip radius. The experimental results for the samples coated with PMMA composite containing 0, 0.5, 1 and 2% of CPMMA6 indicate that the introduction CPMMA6 can decrease the friction coefficient of PMMA composites. For example, at  $a/R$  ratio of 0.35, the apparent friction coefficient decreased from 0.46 for pure coating to 0.3, and 0.16 for composite containing 0.5 and 1wt% CPMMA6, respectively.

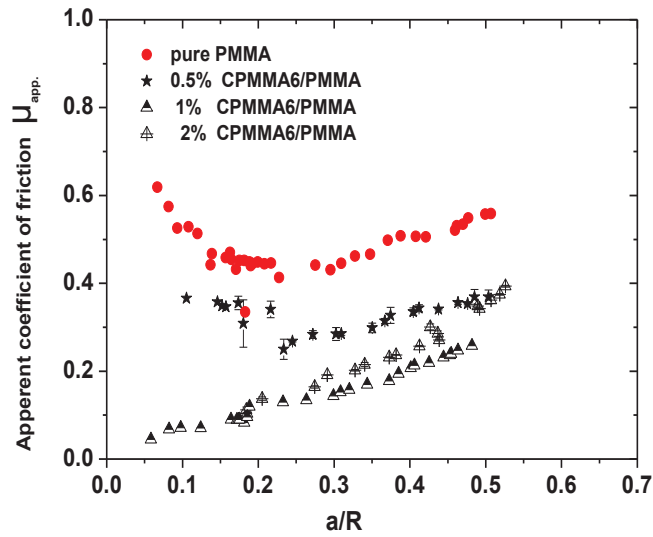


Figure 6-11 Effect of MWCNT-grafted PMMA (CPMMA6) on the apparent friction coefficient with two tip radius ( $R = 98$  and  $250\mu\text{m}$ ).

With a farther increase in the weight percent of the CPMMA6 to 2% a slight increase in the coefficient of friction was observed and this may be due to the increase of agglomerated CPMMA6 with increasing its percentage in the composite.

Figure 6-12 showed the calculated local friction coefficient as a function of the  $a/R$  ratio for the pure and PMMA nanocomposites.

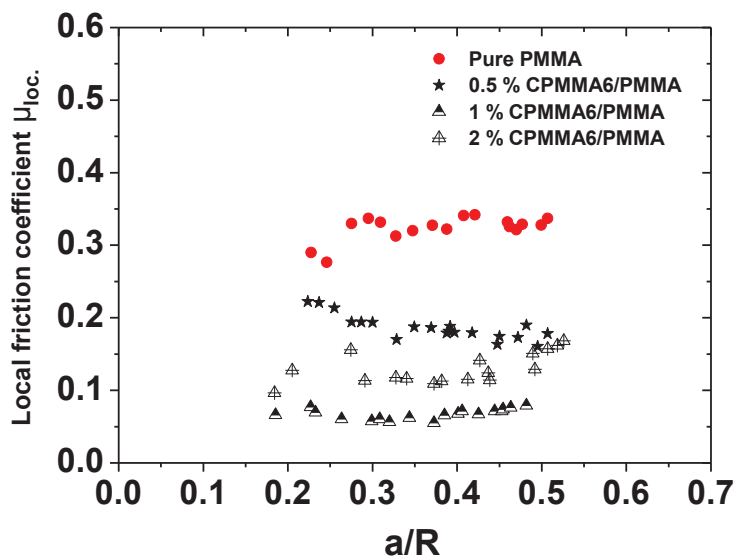


Figure 6-12 Effect of MWCNT-grafted PMMA (CPMMA6) on the local friction coefficient with tip radius ( $R = 98\ \mu\text{m}$ ).

The experimental results indicate that the local friction coefficient for composite coatings CPMMA6/PMMA with different percentages of CPMMA6 (0, 0.5, 1 and 2 wt. %) and at the same value of the  $a/R$  (0.35) was 0.32 and 0.18, 0.06 and 0.11 respectively.



It seems that the local friction coefficient decreases with increasing the percentage of CPMMA6 up to 1%, farther increasing in the percentage of CPMMA6, particularly for 2%, cause the increase in the local friction coefficient and this may be due to increase in the interfacial shear strength.

Figure 6-13 shows the rear contact angle as a function to (a/R). It is apparent from the experimental result that the introduction of MWCNT grafted PMMA (CPMMA6) can modify the nature of the contact and expand the elastic-plastic domain at the contact. The increasing the weight percentage of MWCNTs grafted PMMA have an effect on the shape of the contact during the scratch process.

The elastic domain is shifted from the a/R of 0.14 for pure PMMA coating to 0.27 for 2% CPMMA6/PMMA composite. At the same value of the a/R (0.35), the value of omega changed significantly with the introduction of CPMMA6. It is about 0.4 radian for pure PMMA coating having higher value of friction coefficient 0.42 and increases with increasing the weight percent of CPMMA6 in the composite to about 0.65, 0.83 and 0.92 radian for composite contains 0.5, 1 and 2 wt% of CPMMA6 respectively.

The plastic domain for pure coating begins at a/R of 0.35, while for the composite reinforced with 0.5, 1 and 2% of CPMMA6 the plastic domain begins at a/R ratio 0.43, 0.55 and 0.55 respectively, due to increase the modulus and hardness of the composites.

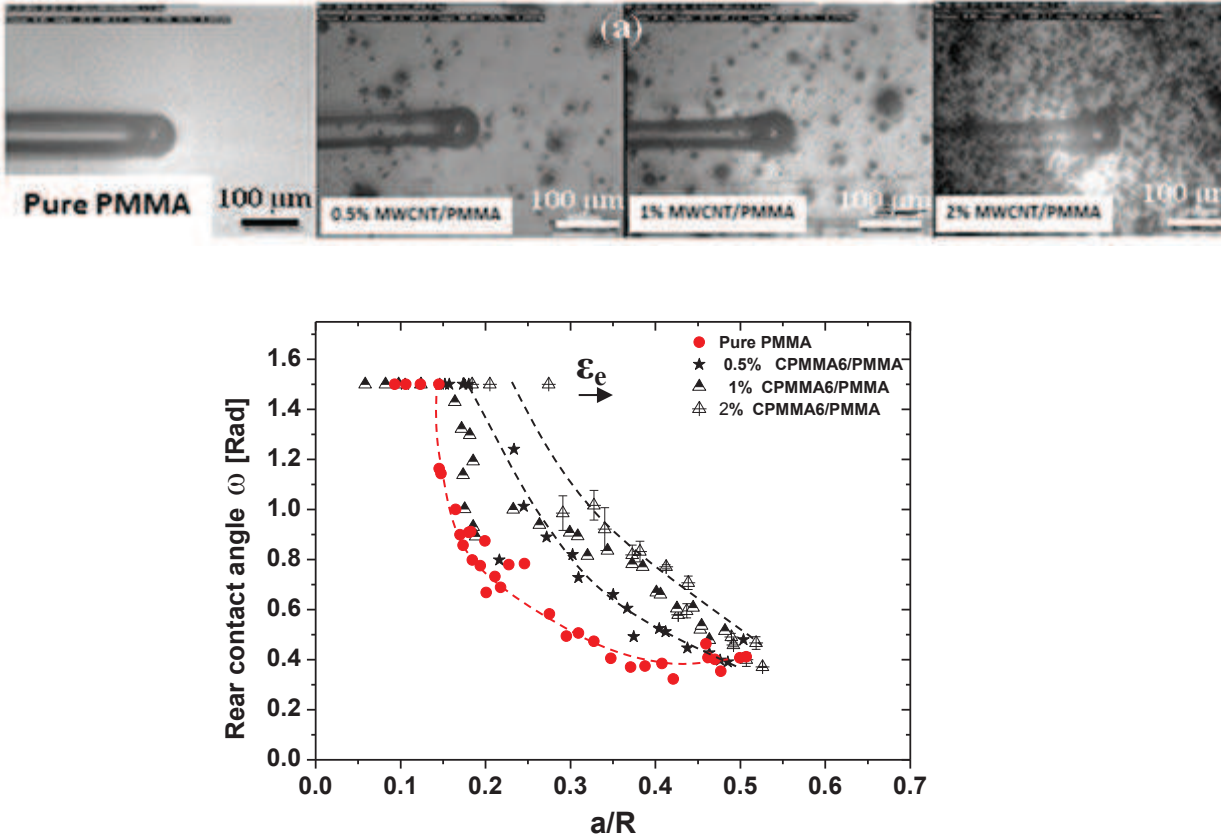


Figure 6-13 a) Selected images at the a/R (~0.33) b) Rear contact angle versus a/R for coated samples with PMMA reinforced with different percentage of MWCNT-grafted PMMA (CPMMA6) prepared by solution mixing process.

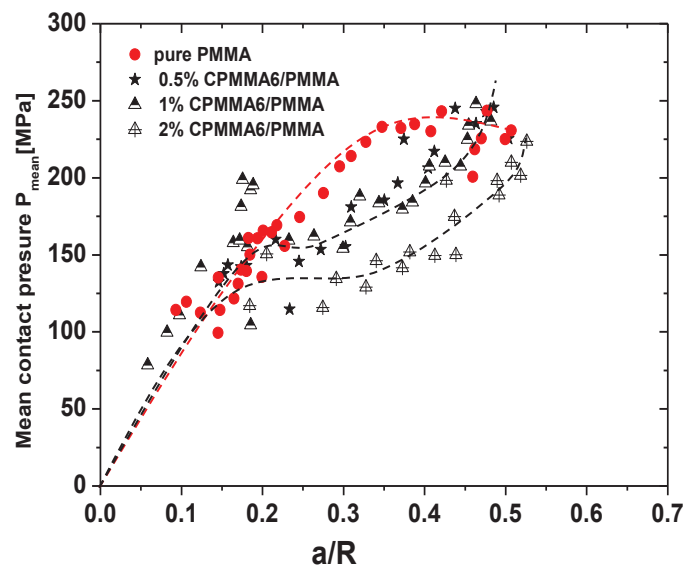


Figure 6-14 Mean contact pressure versus  $a/R$  for coated samples with PMMA reinforced with different percentage of MWCNT-grafted PMMA (CPMMA6) prepared by solution mixing process.

Figure 6-14 shows the mean contact pressure as a function of the mean contact strain. For the samples coated with pure PMMA, the contact pressure increases from 100 to 233 MPa and then seems to take a stable path as the  $a/R$  ratio exceeds 0.35, whereas in the samples coated with composites containing 0.5% and 1% of CPMMA6, the contact pressure increases continuously and intersects with pure PMMA curve at the  $a/R$  value of 0.5 and at 0.55 in the case of 1% and 2wt% of CPMMA6 respectively, in agreement with the evaluation of the rear contact angle.

### 6.3 Comparative study of the effect of different techniques of coating

Two composites coatings were prepared by two techniques, the in-situ polymerization and solution mixing, with the same percentage of filler (0.1% of CPMMA6). Scratch tests were performed on PMMA substrate coated with PMMA/CPMMA6 composite. All the experiments were made at room temperature, 4% humidity, scratch/ sliding speed 0.03 mm/s and  $0.05 \text{ N} < F_n < 1.5 \text{ N}$  and with two tip radius of 250  $\mu\text{m}$  and 98  $\mu\text{m}$ .

Unlike the behavior of the composite coatings that are reinforced with FLG or GO, the experimental results indicate that the nanocomposite prepared by solution mixing technique is more effective in the reduction friction coefficient of friction than the composite prepared by in-situ polymerization technique. The experimental results showed that the samples coated by solution mixing process have lower apparent and local friction coefficient than the samples coated by in situ polymerization technique Figure 6-15.

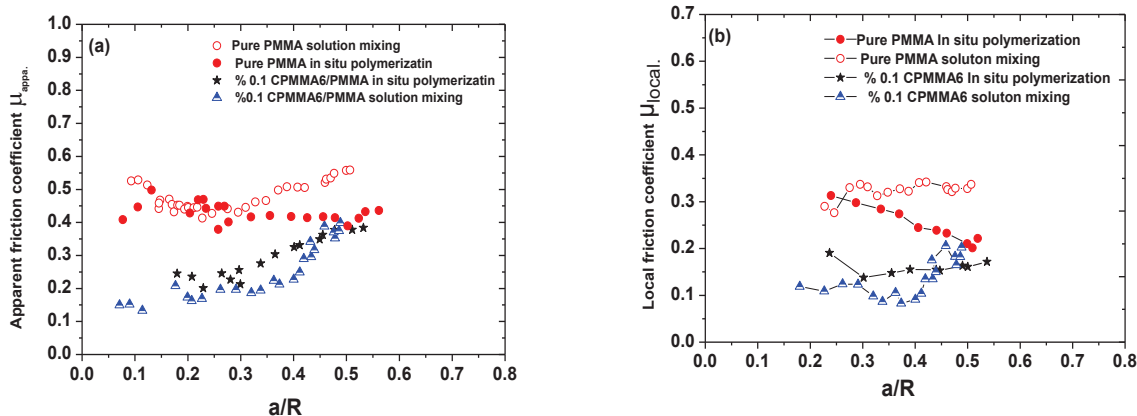


Figure 6-15 a) The apparent friction coefficient as a function of a/R ratio with two tips (98  $\mu\text{m}$  and 250  $\mu\text{m}$  Radius) b) The local friction coefficient as a function of a/R ratio with tip Radius 98  $\mu\text{m}$ , for samples coated by two different techniques.

This reduction in the coefficient of friction may be due to the fact that the solution mixing technique is the most effective way in improving the dispersibility and the compatibility of MWCNT-grafted PMMA in PMMA solution. Figure 6-16 illustrates that the sample which prepared by solution mixing technique has a better dispersion in the PMMA matrix than the sample that prepared by in-situ technique.

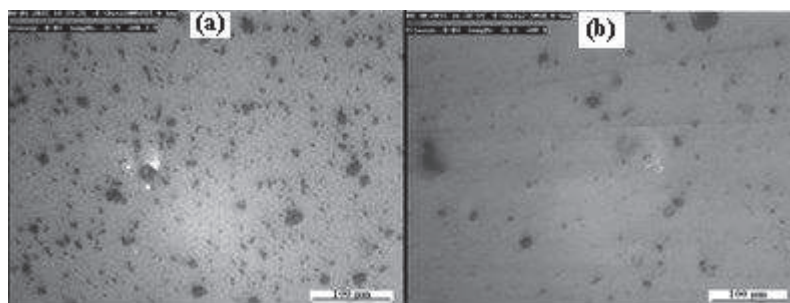


Figure 6-16 a) 0.1% CPMMMA6/PMMA composite coating prepared by in-situ polymerization technique, b) 0.1% CPMMMA6/PMMA composite coating prepared by solution mixing technique.

Figure 6-17 shows the evolution of the rear contact angle as a function of the a/R value for PMMA coated samples with two types of coating. At the same value of a/R (0.35) the composite prepared by in-situ polymerization technique has rear contact angle of 0.7 while for nanocomposite that prepared by the solution mixing technique, it is 0.83.

There is no significant difference in the beginning of plastic domain between the two types of coating composites.

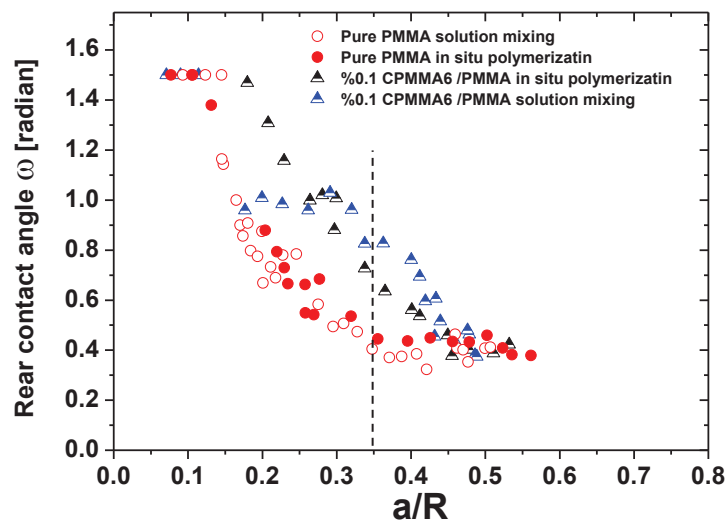


Figure 6-17 The rear contact angle versus  $a/R$  for samples coated by two different techniques with two tips Radius ( $98\ \mu\text{m}$  and  $250\ \mu\text{m}$ ).

## 6.4 PMMA reinforced MWCNT grafted with different thickness layer of PMMA

Tribological and mechanical tests were performed for the samples coated with PMMA reinforced with 2wt% of MWCNTs grafted PMMA chains with variety weights fraction of PMMA layer grafted on the surface of MWCNTs. According to the Table 6-2 the loss weights fraction of grafted PMMA was 49.1%, 65.5% and 71.5% for CPMMA4, CPMMA6 and CPMMA8 respectively. The solution for coating was prepared by solution mixing method. Control sample coated with pure PMMA was prepared by the same method.

### 6.4.1 Surface mechanical properties

The use of MWCNT grafted PMMA can enhance dispersibility of nanotubes in a polymer matrix and permit a more efficient stress transfer from the matrix to MWCNTs due to the increase of the interface area between nanotubes and polymer matrix (Figure 6-18). As a result, the polymer grafted MWCNTs can simultaneously improve the stiffness, strength, ductility and toughness of the polymers compare with MWCNTs before grafting with PMMA chains[114], [115]. The hardness,  $H$ , and elastic modulus,  $E$ , obtained by nanoindentation technique. Figure 6-19 presents Young's modulus and hardness for sample coated with a pure PMMA and for samples coated with composites of PMMA reinforced with 2% MWCNTs grafted with different weight fraction of PMMA (CPMMA4, CPMMA6, and CPMMA8).

The composite films were deposited on a clean glass plate. After the last drying step, the coating thicknesses was 12-15  $\mu\text{m}$  which entails that we can probe the coating up to 1.2  $\mu\text{m}$  to get its own mechanical response.

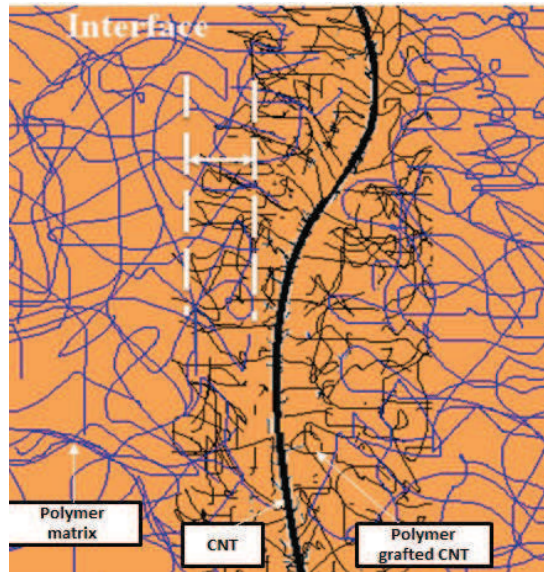


Figure 6-18 The scheme shows the interfacial interaction zone between MWCNT-grafted-PMMA and PMMA matrix.

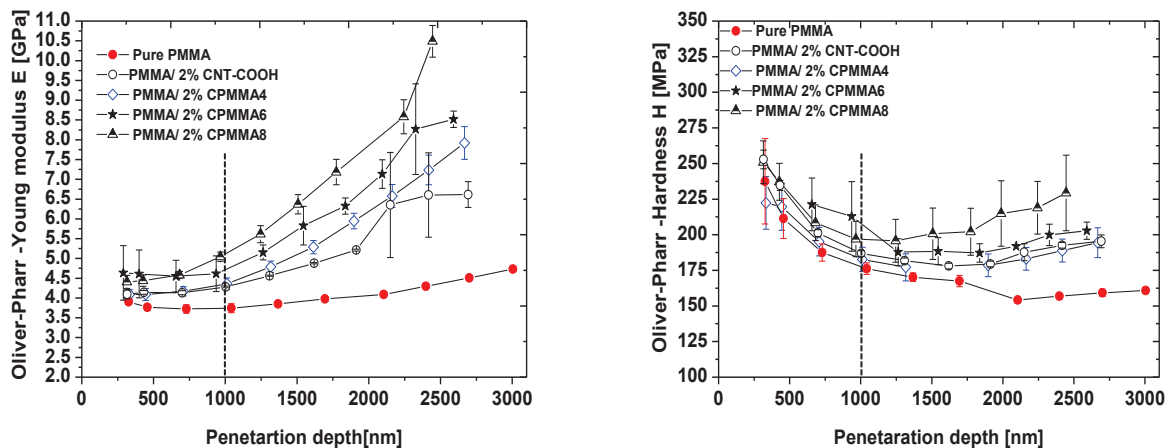


Figure 6-19 Variation of Young's modulus (on the left) and of hardness (on the right) with samples coated by solution mixing process by the nanoindentation.

The experimental results showed a slight increasing in the elastic modulus with increasing the weight fraction of PMMA coated MWCNT. The modulus increased, indeed, from 4.2 GPa for MWCNT-COOH and CPMAA4 to 4.6 GPa for CPMAA6 and 5 GPa for CPMAA8.

Figure 6-20 plots the apparent friction coefficient as a function of the  $a/R$  ratio with tip radius 98  $\mu\text{m}$  at room temperature, slip/scratch speed 0.03mm/s and normal load from 0.05N to 1.5N, the thickness of coating layers  $\approx 20\mu\text{m}$ .

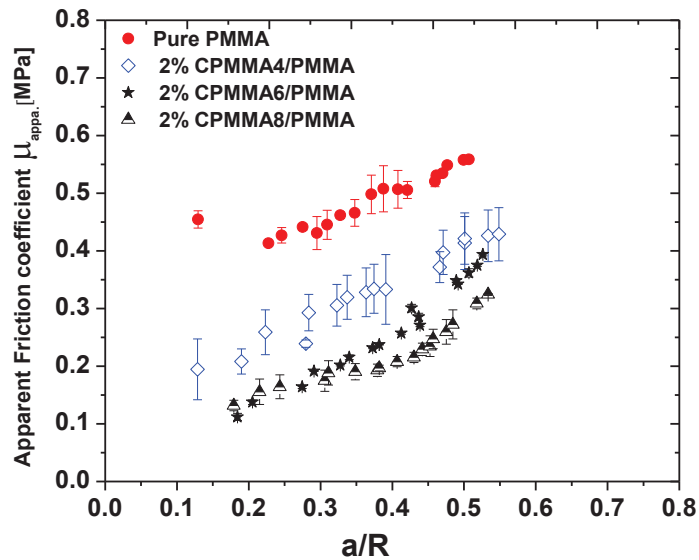


Figure 6-20 Effect of the thickness of PMMA layer grafted on MWCNTs surface on the apparent friction coefficient (Rtip 98 $\mu$ m).

In general, all types of grafted MWCNTs can decrease the apparent friction coefficient regardless the thickness of the PMMA layer on MWCNT walls. On the other hand, at the ratio of  $a/R$  (0.35) the apparent friction coefficient decreased from 0.31 for CPMMA4/PMMA coating to 0.22 for CPMMA6/PMMA and 0.19 for CPMMA8/PMMA. This shows that the coefficient of friction decreases systematically with the increase of the weight fraction of polymer grafted on the surface of MWCNTs.

The increase of Young's modulus of the composites with the increase of the thickness of the polymer layer grafted on the walls of the nanotubes may be the first reason that caused a decrease of the friction coefficient. The second reason for decreasing the coefficient of friction may be attributed to the formation of a thin friction film on the counter face and with increasing the thickness of the PMMA layer that grafted nanotubes surface, this film became more uniform and smoother.

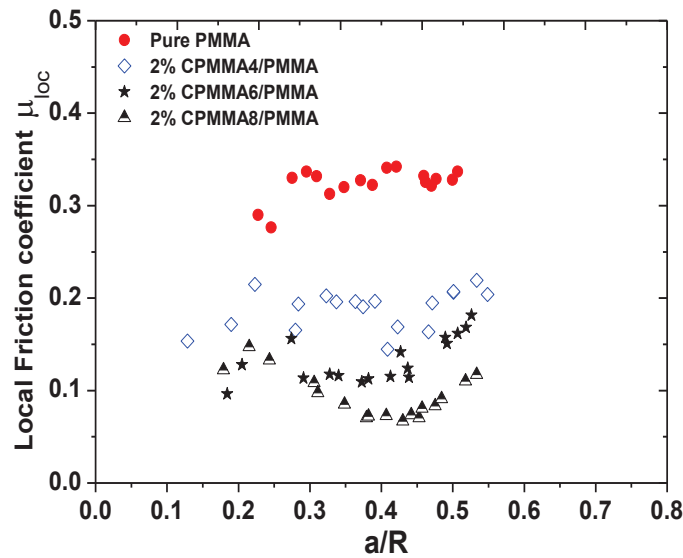


Figure 6-21 Effect of the thickness of PMMA layer grafted on MWCNT surface upon local friction coefficient (Rtip 98 $\mu$ m).

The introducing of MWCNT-g-PMMA in PMMA has also a large impact on local friction coefficient decrease (Figure 6-21). The experimental results showed that the local friction coefficient decreases with the increase in the weight fraction of polymer grafted on the surface of MWCNTs. For example, at the  $a/R$  of 0.35 the local friction coefficient decreases from 0.19 for the CPMMA4/PMMA coating to 0.11 for CPMMA6/PMMA and 0.08 for CPMMA8/PMMA.

It is apparent from the experimental result that the introduction of MWCNT grafted PMMA can modify the nature of the contact and expand the elastic -plastic domain at the contact as shown in Figure 6-22. It is important to mention that the increase of the weight fraction of PMMA grafted on the MWCNTs surface has an impact on the shape of the contact during the scratch process. The plastic domain for pure coating begins at  $a/R$  of 0.35 contact strain, while for the composite CPMMA4/PMMA the plastic domain begins at  $a/R$  of 0.45 and for CPMMA6 and CPMMA8 at 0.5. This perhaps due to increasing the toughness with increasing thickness of the PMMA grafted MWCNTs.

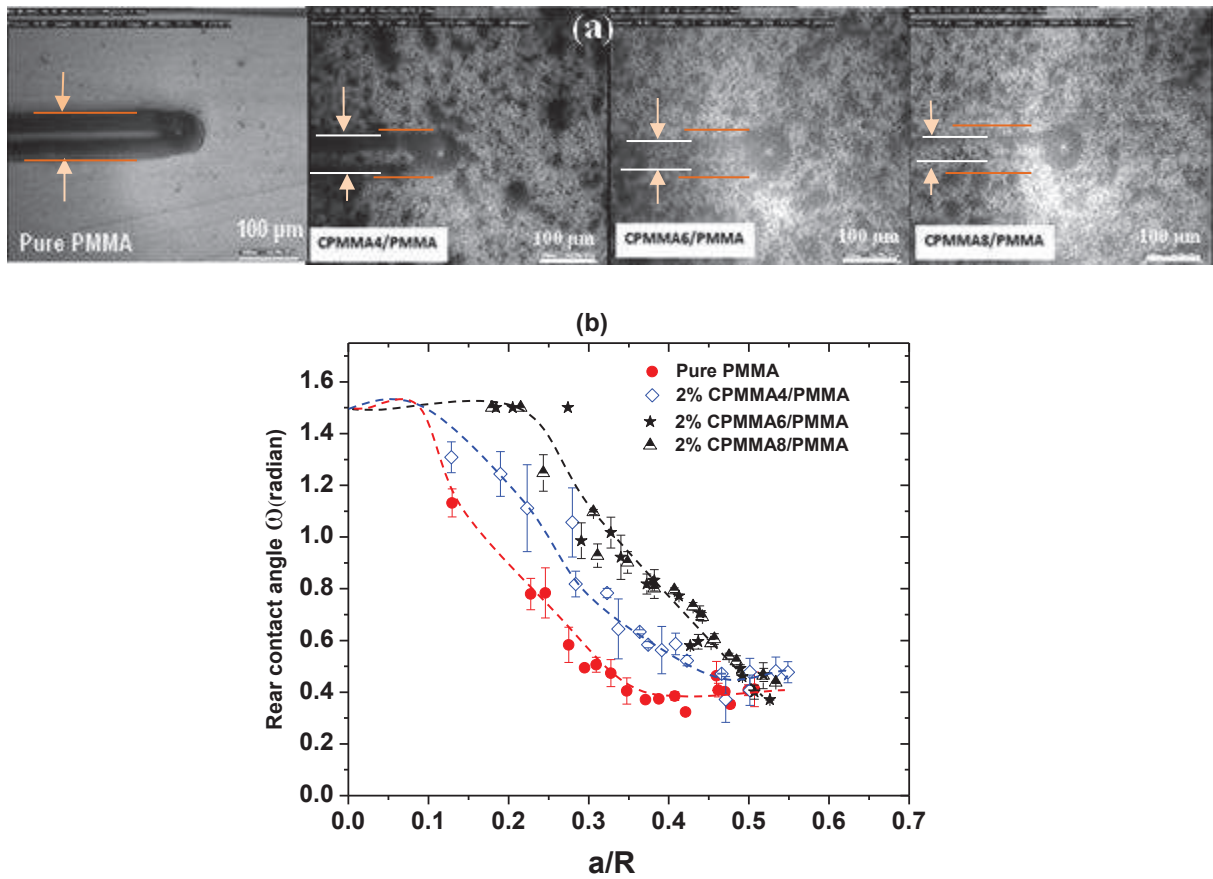


Figure 6-22 a) Selected images at  $a/R$  ( $\sim 0.33$ ) b) Effect of the thickness of PMMA layer grafted on MWCNT surface upon the rear contact angle with tip radius ( $98\mu\text{m}$ ).

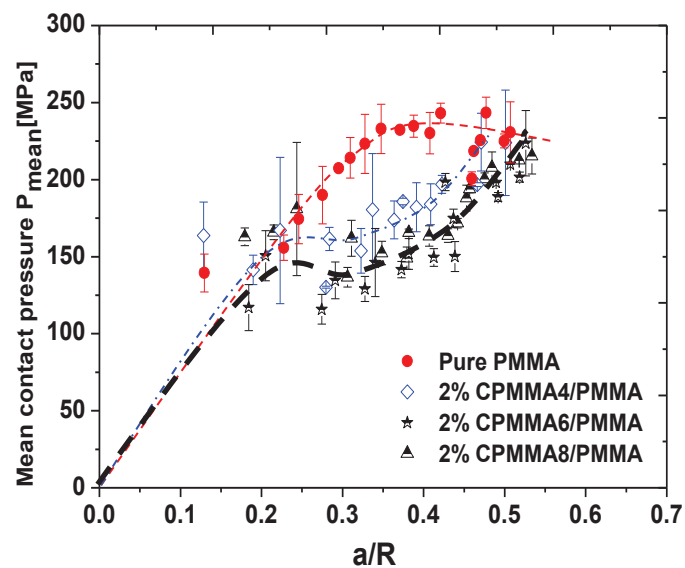


Figure 6-23 Effect of the thickness of PMMA layer grafted on MWCNTs surface upon the mean contact pressure with tip radius ( $98\mu\text{m}$ ).



Figure 6-23 shows the contact pressure as a function of  $a/R$  value. For the samples coated with pure PMMA, the contact pressure increases from 100 to 233 MPa and then it seems to take a stable path as the  $a/R$  ratio exceeds 0.35, whereas on the composite coatings, the contact pressure increases continuously. In view of the evolution of the rear angle, one may assume that the contact behavior of the thickly coated sample is essentially elastic–plastic. In general, the effect of the thickness of PMMA grafted on MWCNT surface upon the mean contact pressure is not clear.

### 6.5 Comparative study of the effect of coating thickness on the surface mechanical properties

In order to study the effect of change the ratio of coating thickness to weight percent of reinforced filler on the surface behavior of the coated samples. Two composites coating were prepared, first have thickness  $150\mu\text{m}$  reinforced with 0.1 CPMMA6/PMMA and the second have thickness  $20\mu\text{m}$  reinforced 1% CPMMA6/PMMA. Young’s modulus and hardness are measured by the nanoindentation technique. The results showed that Young’s modulus and hardness for the composites reinforced with 1% CPMMA6 was 4.4 GPa and 217 MPa respectively. While for composite reinforced with 0.1% of CPMMA6 was 4.1 GPa and 220 MPa respectively.

For scratching tests the experiments were made at room temperature, 4% humidity, sliding speed of  $0.03\text{ mm/s}$ ,  $0.05\text{ N} < F_n < 1.5\text{ N}$  and with two tip radius of  $250\ \mu\text{m}$  and  $98\ \mu\text{m}$ .

Figure 6-24 shows the effect of increasing the percentage of CPMMA6 by 10 times with decreasing the thickness of the coating by 8 times and the experimental results indicate that the composite reinforced with 1% CPMMA6 has a friction coefficient less than the composite reinforced with 0.1% CPMMA6. Figure 6-25 shows the rear contact angle and mean contact pressure as a function to  $a/R$  value, the results showed that both types of coating have quite the same behavior.

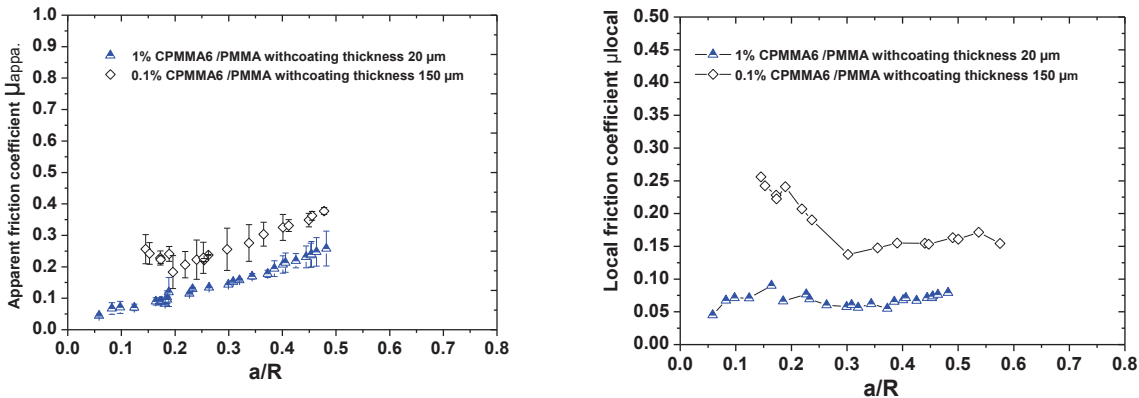


Figure 6-24 The apparent friction coefficient (left) and the local friction coefficient (right) versus  $a/R$  value.

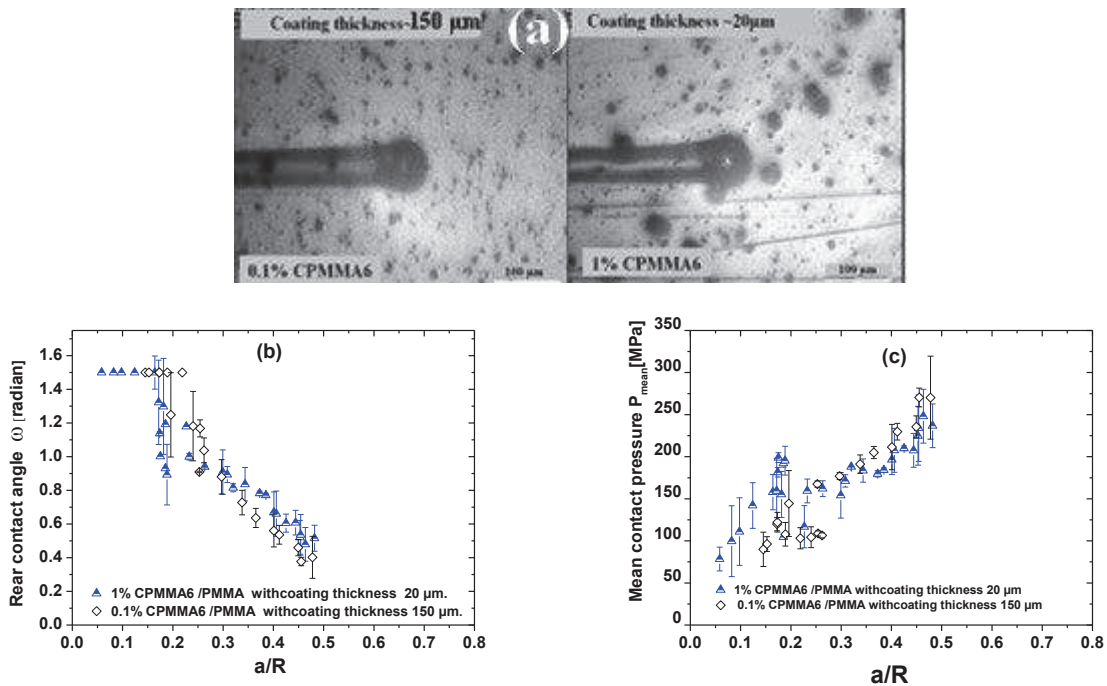


Figure 6-25 a) The selected images at  $a/R$  ( $\sim 0.35$ ), b) Rear contact angle and c) mean contact pressure (right) versus  $a/R$  values.

## 6.6 Conclusions

1. MWCNTs grafted with PMMA Poly (methyl methacrylate) by in situ atom transfer radical polymerization (ATRP) “grafting from” approach, were prepared with different thickness of PMMA grafted layers.
2. PMMA nanocomposites coating reinforced with a variety weight percent of MWCNTs grafted PMMA were prepared by two different methods, in-situ polymerization and solution mixing technique.
3. Young’s modulus and hardness for composites coating prepared by in situ polymerization technique showed increase by 20% and 40% respectively comparing with pure coating. The composite coatings reinforced with 0.2 wt % of MWCNT-g-PMMA showed decrease in the friction coefficient and shift the beginning of plastic domain to higher contact strain.
4. Composites coating prepared by solution mixing technique showed an increase in the Young's modulus and hardness by 24% and 20% respectively compared to pure coating.
5. Unlike the behavior of the composite coatings reinforced with FLG or GO, the solution mixing technique for coating is more effective in decreasing the coefficient of friction than In-situ polymerization technique.
6. The increase of the thickness of PMMA layer grafted on MWCNTs has a slightly effect on the enhancement the modulus and hardness of the resultant composite coating and this matter need more study. On the other hand, the increase the thickness

of PMMA layer has a clear effect on decrease of the coefficient of friction. It also improves the elasto-plastic behavior at the contact.

7. In short, the optimum nanocomposites coating that gave the minimum value of friction coefficient and better mechanical properties are 1% CPMMA6 and 2% CPMMA8.

## 7 Erucamide

The main objective of this part is to prepare the coating solution as a slipping layer and study its surface properties which are supposed to cover the hard layer in a double coating (the main objective of our study).

PMMA substrate coated with PMMA /Erucamide composite as a slipping layer, instead of adding Erucamide to the whole substrate which may have effect on its mechanical properties. The principle mechanism of work the slipping agents is the migration to the surface and the drying step during coating process which includes the heating under vacuum may help to accelerate the migration of Erucamide toward coating surface.

The composites coating was deposited on PMMA substrate by used Doctor Blade equipment with coating thickness  $\approx 20\mu\text{m}$  (section 3.4.2).

### 7.1 Surface mechanical properties of coating

The surface response to shear is characterized by friction tests. Figure 7-1 shows the evolution of the apparent friction coefficient  $\mu_{\text{app}}$  as a function of the  $a/R$  ratio for two tip radius ( $R = 98$  and  $250\mu\text{m}$ ) at room temperature, slip/scratch speed  $0.03\text{mm/s}$  and normal load between  $0.05\text{ N}$  to  $1.5\text{ N}$ . The experimental results indicate that the samples coated with PMMA/ Erucamide composite coating showed reduction of the coefficient of friction. At the ratio  $a/R$  of  $0.35$ , the friction coefficient decreases from  $0.47$  for pure coating to  $0.25$  and  $0.17$  for  $0.1$  and  $0.2\%$  of Erucamide respectively.

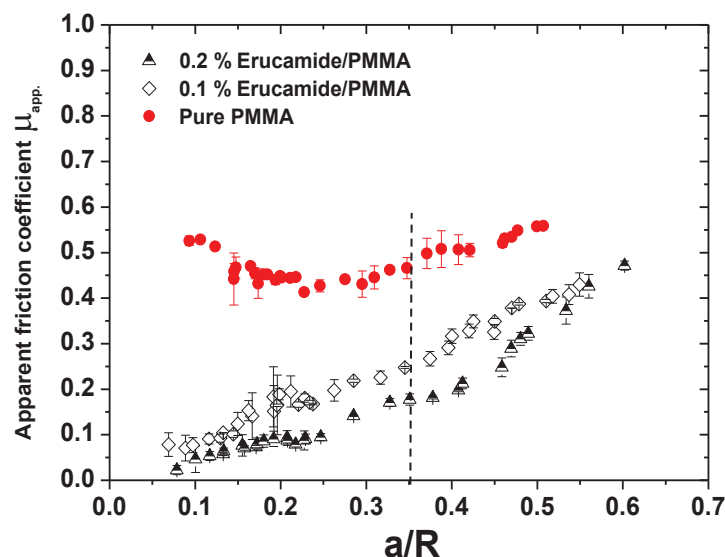


Figure 7-1 Effect of Erucamide on the apparent friction coefficient for two tip radius ( $R = 98$  and  $250\mu\text{m}$ ), the thickness of coating layers  $\approx 20\mu\text{m}$ .

Figure 7-2 showed that the local friction coefficient was decreased with increasing the weight percent of Erucamide, for example, at  $a/R$  (0.35) the local friction coefficient decreased from 0.32 for pure coating to 0.15 and 0.06 for 0.1 and 0.2 wt. % of Erucamide respectively. This reduction in the coefficient of friction is due to formation of a thin film from molecules of Erucamide that migrated from the bulk which causes lowering the interfacial shear stress during the scratch process.

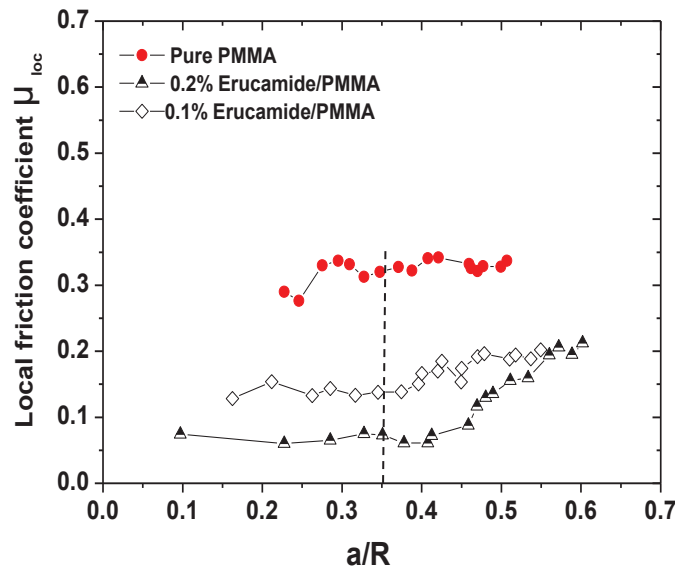


Figure 7-2 Effect of Erucamide on the local friction coefficient for tip radius 98  $\mu\text{m}$  at room temperature, slip/scratch speed 0.03mm/s and normal load from 0.05 N to 1.5 N. The thickness of coating layers  $\approx 20\mu\text{m}$ .

Figure 7-3 shows the evolution of the rear contact angle as a function of the  $a/R$  for PMMA coated samples with 0.1 and 0.2 % of Erucamide. The experimental results indicated that the introduction of Erucamide can modify the nature of the contact and improve the elasto-plastic behavior at the contact. The elastic domain shifts from 0.14 for pure coating to 0.24 for Erucamide composites coating, and also the plastic domain begins at  $a/R$  value 0.35 for pure coating while at 0.45 and 0.52 for 0.1 and 0.2 wt % Erucamide respectively. The value of omega ( $\omega$ ) changed significantly with the introduction of Erucamide compared to pure coating. There is however no significant change in the value of omega ( $\omega$ ) with increasing the percentage of Erucamide, despite that the coefficient of friction decreased (as mentioned above).

The in-situ photographs of the contact at the  $a/R$  of 0.35 explained that the nature of the contact is plastic for pure PMMA coating, while the contact is elasto-plastic at the same value of  $a/R$  for PMMA/Erucamide composites. No significant change in the shape of contact with increasing the weight percent of Erucamide is observed. 0.2 % of Erucamide is considered to be the maximum percentage to be used for reinforced PMMA coating layer, more than this percentage the haze appear in the samples.

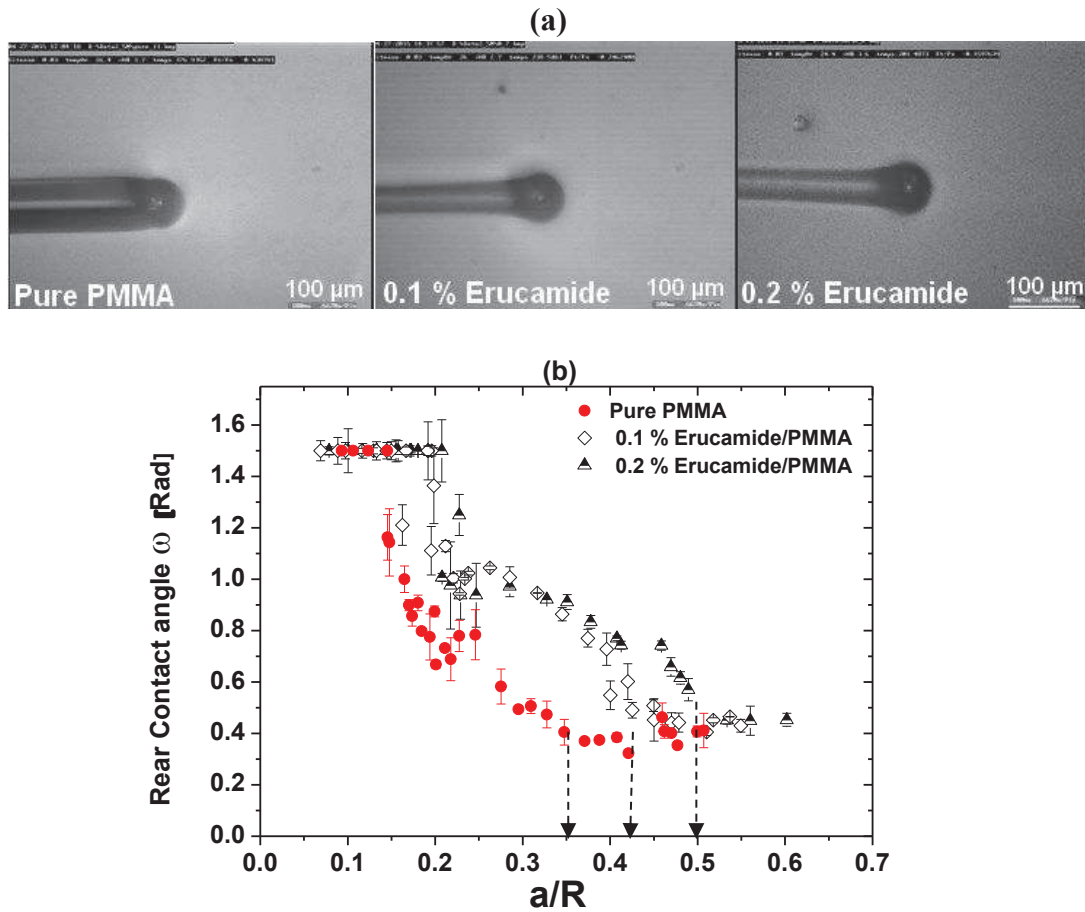


Figure 7-3 a) Selected images concerning to the  $a/R$  value = 0.35 are shown. b) Variation of  $\omega$  with  $a/R$  value for various percentage of Erucamide in PMMA (sliding speed = 0.03 mm/s, tips radius = 98  $\mu\text{m}$  and 250  $\mu\text{m}$ ).

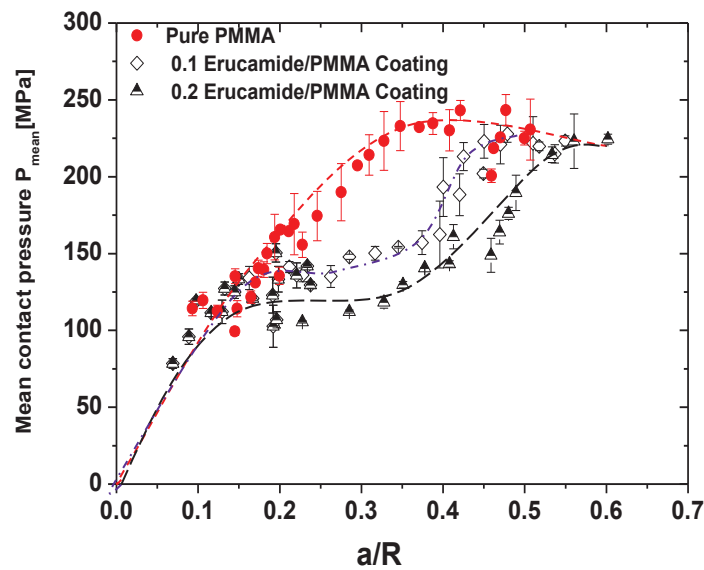


Figure 7-4 variation of mean contact pressure with the  $a/R$  value for various percentage of Erucamide in PMMA at room temperature,  $0.05\text{N} \leq F_n \leq 1.5\text{N}$ , sliding /scratching speed = 0.03 mm/s, tip radius = 98  $\mu\text{m}$  and 250  $\mu\text{m}$ .

Figure 7-4 shows the mean contact pressure as a function of  $a/R$ . For the samples coated with pure PMMA, the contact pressure increases from 100 to 233 MPa and then seems to take a stable path as the ratio  $a/R$  exceeds 0.34, whereas in the samples coated with composites Erucamide, the contact pressure take a stable path at higher contact strain.

### 7.2 Comparative study of the different roles between soft layer and hard layer in decreasing the coefficient of friction

For the purpose of analyzing the different roles for each of the hard coating layer and the soft coating layer in decreasing the friction coefficient, two different coating layers (1% CPMMA6/PMMA as a hard layer and 0.2 % Erucamide as a soft layer) having almost the same local friction coefficient ( $\mu \approx 0.05$ ) and another two layers (2% CPMMA6/PMMA as a hard layer and 0.1% Erucamide as a soft layer) which they have local friction coefficient ( $\mu \approx 0.12$ ) (Figure 7-5).

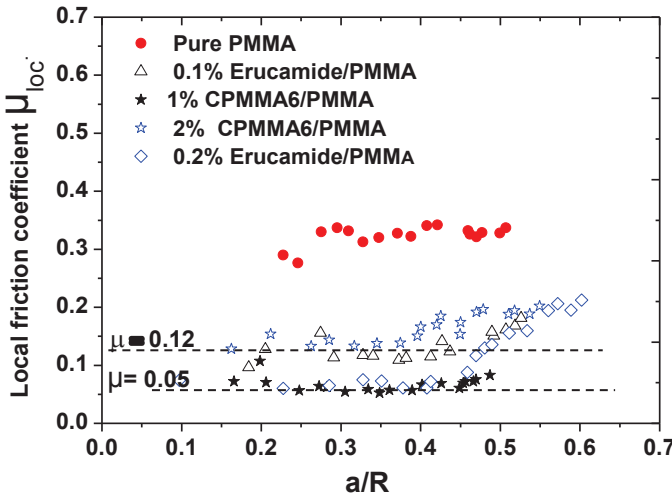


Figure 7-5 Local friction coefficient versus  $a/R$ .

At low local friction coefficient (0.05) the two types of coating (hard and soft layer) have almost the same behavior of rear contact angles versus  $a/R$  values. In contrast, it seems that the hard layer has higher values of mean contact pressure at the same  $a/R$  values. At local friction coefficient (0.12) there is no clear difference in the behavior of rear contact angles and mean contact pressure versus  $a/R$  values (Figure 7-6), (Figure 7-7).

Figure 7-8 shows the increase in the values of the contact diameter ( $2a$ ) with increasing the normal load. In case of low local friction coefficient (0.05) (Figure 7-8a), the hard layer showed low values of contact diameter compare with soft layer, while at relatively high local friction coefficient (0.12) the two types of coating have quite same behavior (Figure 7-8b).

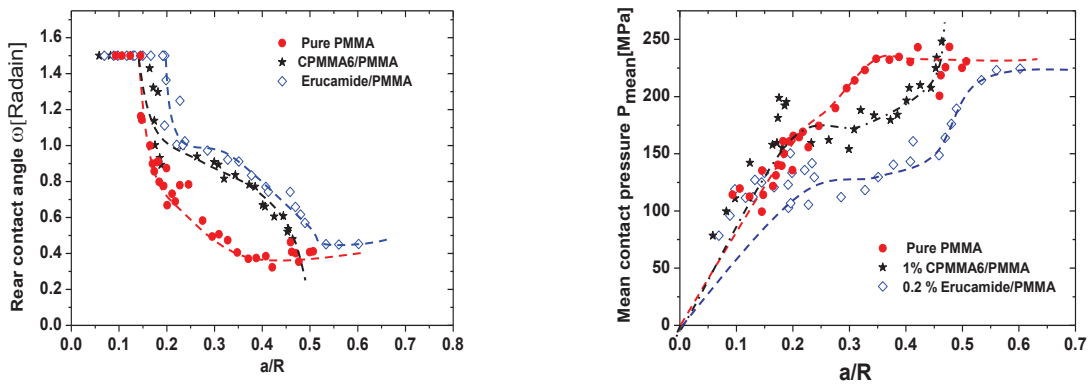


Figure 7-6 Rear contact angle (left), mean contact pressure (reight) versus  $a/R$  for coating layer have 0.05 local friction coefficient.

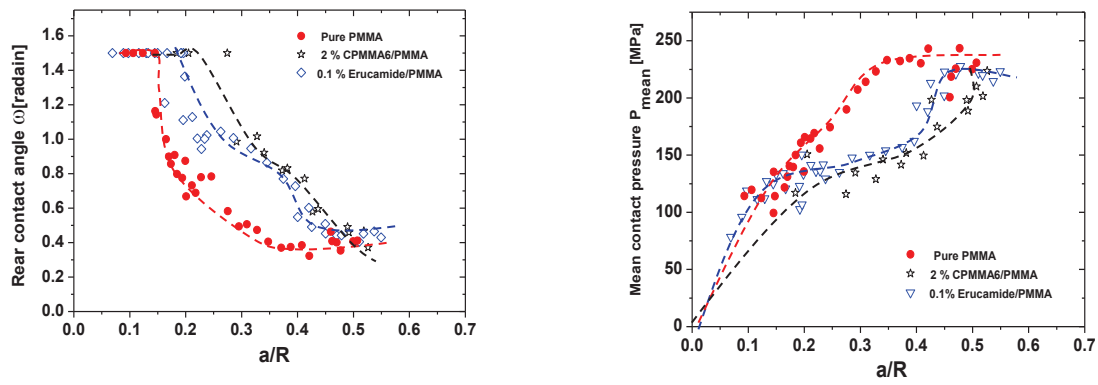


Figure 7-7 Rear contact angle (left), mean contact pressure (reight) versus  $a/R$  for coating layer have 0.12 local friction coefficient.

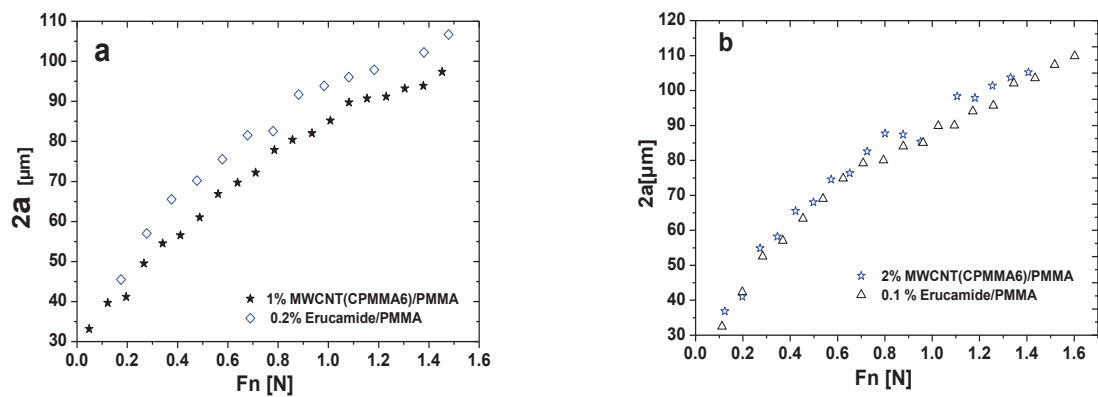


Figure 7-8 Shows the change of contact diameter ( $2a$ ) versus  $a/R$  values.



### 7.3 Conclusions

- 1- PMMA /Erucamide composite coating as a slipping layer were prepared by solution mixing technique.
- 2- Introducing Erucamide in the composite coating can decrease the apparent coefficient of friction with increasing the percentage of Erucamide in the composite.
- 3- Local friction coefficient was decreased with increasing the weight percent of Erucamide.
- 4- The experimental results indicated that the introduction of Erucamide can modify the nature of the contact and improves the elasto-plastic at the contact. The plastic domain has begun at higher contact strain in the case of PMMA/Erucamide coating
- 5- Preliminary results of the behavior of the slipping layer which has average thickness 20  $\mu\text{m}$ , confirms the possibility of using this layer in reducing the interfacial shear stress during scratching.
- 6- The Presence of slipping agents in PMMA matrix may be causing reduced the mechanical properties of the coating layer and may cause increase in friction coefficient due to plowing effect, therefore, it is better to use slipping layer with less thickness to decreasing the plowing during scratch process.

## General conclusions

Coating for tribo-elements is mainly made to protect the surface of the substrate from wear and a material harder than the substrate is generally chosen for the coating. A softer coating material may be chosen to give lubricated surface on a substrate[1].

Current work contains four main approaches:

The Preparation and functionalization a various types of carbon nanofillers: few layers graphene functionalized with Octadecylamine, Graphene oxide and MWCNT-grafted with PMMA chains prepared by in situ atom transfer radical polymerization (ATRP) using a “grafting from” approach. All functionalized filler are characterized by FTIR, TGA, XPS and TEM.

PMMA nanocomposites coating fabricated by two techniques: in situ polymerization and solution mixing process. The effect of various nanocarbon fillers on surface mechanical properties of PMMA nanocomposite coating was studied.

The effect of slipping agent (Erucamide) on surface mechanical properties of PMMA composite coating was studied.

The structures of the composites are checked by GPC and the results showed that the quality of the matrix (PMMA) of composites that prepared by solution mixing method was more controllable than the composites that prepared by in situ polymerization method.

Elastic modulus and hardness of PMMA reinforced with various nanocarbon fillers were studied by used nanoindentation tests, the experimental results showed:

For composites prepared by in situ polymerization process (Table 1), the maximum increasing in the elastic modulus and the hardness was 15% and 36 % respectively compare with pure PMMA coating (Taking into consideration, that the maximum percentage for nanofiller was 0.2%).

<i>Component</i>	<i>E (GPa)</i>	<i>H(MPa)</i>	<i>μ<sub>appa.</sub></i>	<i>μ<sub>local</sub></i>
Pure PMMA	3.23±0.01	150 ± 1	0.42	0.27
0.05 FLG-C18/PMMA	3.1±0.1	166±5	0.45	0.3
0.1 FLG-C18/PMM	3.73±0.02	180 ±0.67	0.25	0.13
0.2 FLG-C18/PMMA	3.68 ±0.04	212 ±7	0.15	0.04
0.05 GO/PMMA	3.2±0.01	152 ±4	0.2	0.06
0.1 GO/PMMA	3.3±0.04	178 ±5	0.14	0.03
0.5 GO/PMMA	3.5±0.01	184±5	0.14	0.03
0.05MWCNT-grafted	3.62±0.03	190 ±1.9	/	/

PMMA(CPMMA6)/PMMA				
0.1MWCNT-grafted	4.1±0.03	220 ±1.7	0.3	0.14
PMMA(CPMMA6)/PMMA				
0.2 MWCNT-grafted	3.8±0.03	195±3.5	0.18	0.07
PMMA(CPMMA6)/PMMA				

Table 1 Surface mechanical properties for PMMA nanocomposites prepared by in-situ polymerization technique.

For composites prepared by solution mixing method (Table 2), the maximum increasing in elastic modulus and hardness was 25% and 28% respectively (Taking into consideration, that the maximum percentage for nanofiller was 1%). This confirms the effectiveness of carbon nanofiller in enhancing the mechanical properties of the composite coatings, due to them high aspect ratio that can enhance the mechanical stability and increases the load bearing capacity of the nanocomposite coatings.

Scratching provides a suitable and trustworthy means to investigate the mechanical properties of organic polymers under various contact conditions. The scratch resistance of transparent nanocomposite films reinforced with different types of nano carbon fillers (FLG, GO and MWCNT-g-PMMA) was characterized by friction test.

It was confirmed that the carbon nanofillers, even at low percentage can reduce the friction coefficient of the PMMA composite coating and it is also confirmed that the friction coefficient of PMMA decreases directly with increase the percentage of the carbon nanofiller in the composite. On the other hand using an excessive amount of carbon nanofiller can affect the transparency of the coating and therefore the coating layer become darker.

Our strategy for coating provided a perfect adhesion between the coating layer and the substrate, no case of separation or delamination in the interface between coating and substrate during scratching tests were recorded. This is due to the fact that polymer used as a matrix for composite coating was the same type of polymer of the substrate.

It was observed that decrease in friction coefficient by introducing nanocarbon fillers associated improved the elastic modulus and hardness of the composite coatings (detected by the nanoindentation experiments), so it may be concluded that the self-lubricating nature of nanocarbon filler has a great effect on modified the surface properties of the composite coating and reduces its friction coefficient and also broadening the fully elastic and elastic - plastic regions during the contact by increasing the yielding strain at the contact.

A significant increasing in the value of rear contact angle  $\omega$  by introduction carbon nanofillers. Moreover, the value of rear contact angle increased with increasing the weight percent of the filler and decreasing the friction coefficient of the composite coating. Thus, it can be concluded that the decrease in friction coefficient is associated with increased value of the rear contact angle.

In short, it was observed that the yielding contact strain and the elasto- plastic domain of the contact are significantly increased for the samples showing lower friction coefficient.

<i>Components</i>	<i>E (GPa)</i>	<i>H(MPa)</i>	$\mu_{appa.}$	$\mu_{local}$
Pure PMMA	3.7±0.06	176 ± 4	0.46	0.32
0.1% FLG-C18/PMMA	3.95±0.1	200±2.5	0.23	0.12
0.5% FLG-C18/PMMA	4.2±0.03	200±3.5	0.2	0.09
1% FLG-C18/PMMA	4.5 ± 0.1	225 ±12	0.17	0.06
0.01% GO/PMMA	/	/	0.34	0.21
0.5% GO/PMMA	3.8±0.05	190 ±7	0.3	0.2
1% GO/PMMA	4.7±0.05	197±4.5	0.16	0.05
0.1% MWCNT-grafted-PMMA(CPMMA6)/PMMA	4.11±0.13	201 ±12	0.19	0.09
0.5% MWCNT-grafted-PMMA(CPMMA6)/PMMA	3.8±0.12	194 ±8	0.32	0.18
1% MWCNT-grafted-PMMA(CPMMA6)/PMMA	4.4±0.03	217±11	0.17	0.05
2% MWCNT-grafted-PMMA(CPMMA6)/PMMA	4.6±0.6	212±12	0.23	0.11

Table 2 Surface mechanical properties for PMMA nanocomposites prepared by solution mixing technique.

Poly methyl methacrylate (PMMA) functionalized multi walled carbon nanotubes are prepared by in situ atom transfer radical polymerization (ATRP) using a “grafting from” approach. The thickness of the polymer layer in the functionalized MWCNT can be well controlled by the feed ratio of MMA to MWCNT and also by the volume ratio of solvent to MMA.

We studied the influence of increasing the thickness of the PMMA layer grafted MWCNT on surface mechanical properties of PMMA grafted MWCNT/PMMA nanocomposite coatings. It was found, that the coefficient of friction relatively decreases with the increase of the

weight fraction of polymer grafted on the surface of MWCNT (Table3). Moreover, the elastic modulus also increased with increasing the weight fraction of PMMA grafted MWCNT.

<i>Components</i>	<i>E (GPa)</i>	<i>H(MPa)</i>	<i>μ<sub>appa.</sub></i>	<i>μ<sub>local</sub></i>
Pure PMMA	3.7±0.06	176 ± 4	0.46	0.32
2%MWCNT-grafted PMMA (CPMMA4)	4.3±0.15	182 ±4.5	0.32	0.2
2%MWCNT-grafted PMMA(CPMMA6)	4.6±0.6	212±12	0.23	0.11
2%MWCNT-grafted PMMA(CPMMA8)	5±0.13	200±12	0.19	0.08

Table3 Surface mechanical properties for PMMA nanocomposites reinforced with MWNT grafted different thickness of PMMA layers.

In short, it can be concluded that the carbon nanofillers enhance the friction resistance of polymer composite coatings by:

- 1- Modifying the strain hardening and shifted elastic plastic and fully plastic to higher contact strains, due to improve the mechanical properties.
- 2- Decreasing the friction coefficient and broadening the fully elastic and elastic plastic regions during the contact due to the self-lubricating nature of nanocarbon filler.

The composites 0.2% FLG-C18/PMMA, 0.5% GO/PMMA and 0.2% MWCNT-graft PMMA that prepared by in-situ polymerization technique and 1% of FLG-C18/PMMA, GO/PMMA and MWCNT grafted PMMA (CPMMA6) and 2% MWCNT grafted PMMA (CPMMA8) that prepared by solution mixing technique have the optimum effect on decreasing the friction coefficient and enhance the mechanical properties and if we take into account the economic cost, FLG-C18/PMMA can be the best among the rest composites due to its low cost.

PMMA /Erucamide composite coating as a slipping layer were prepared based solution mixing technique. Introducing Erucamide in the composite coating can decrease the apparent coefficient of friction with increasing the percentage of Erucamide in the composite. The experimental results indicated that the introduction of Erucamide can also modify the nature of the contact by improves the elasto-plastic behavior at the contact. And also the plastic domain has begun at higher contact strain in the case of PMMA/Erucamide coating compare with pure coating. 0.2 % of Erucamide considered the maximum percentage can be used for reinforced PMMA coating layer, more than this percentage the haze appear in the samples. Preliminary results of the behavior of the slipping layer which has average thickness 20 μm, confirms the possibility of using this layer to reduce the interfacial shear stress during scratching.

## Perspective and future work

The main objective of the present study is to prepare and study the mechanical and surface behavior of PMMA coated solution reinforced with hard filler and PMMA coated solution mixed with slip agent, which represent the basis step to study the surface behavior of double layers coating contain hard thick relatively layer and soft thin layer (slipping layer) Figure1. The role of hard layer is to support load and increase the mean contact pressure while the thin soft layer can play a major role in decreasing the shear stress during scratch process which can decrease the friction coefficient and also the wear rate into contact.

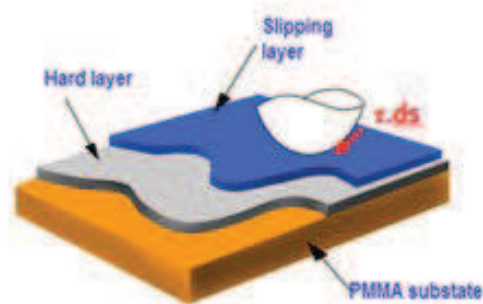


Figure1 Sketch show PMMA substrate coated with double layers

However, more work to do on double coating, One solution may also be the developing a mechanical behavior for coating, is to find a suitable synergetic combination nanocarbon filler with Erucamide to prepare hybrid composites coating, the role of Erucamide as anti-plasticizer to decrease the plasticity effect for nanoparticles.

There is need to study the effect of different structures of nanocarbon fillers on the mode of deformation and on the critical load for nanocomposite coatings.



# **Annex A**

## **Bulk mechanical measurements**



## Sample preparation for bulk mechanical measurements

To prepare PMMA nanocomposites for tensile test the large sheets of pure PMMA and PMMA nanocomposites were prepared on a glass surface (dish of diameter  $\sim 5$  cm). The composites powders prepared by solution mixing (as in § 3.2.3) were dissolved in dry THF (1 g /5 mL) and mechanically sheared (6500 rpm, 30 min) in an ice bath. The concentrated composite solution was poured into a glass dish where the solvent evaporated to leave a film after drying, first at room temperature for 24 h and then under vacuum at 70°C for 48 h (to let its weight reaches an equilibrium value).

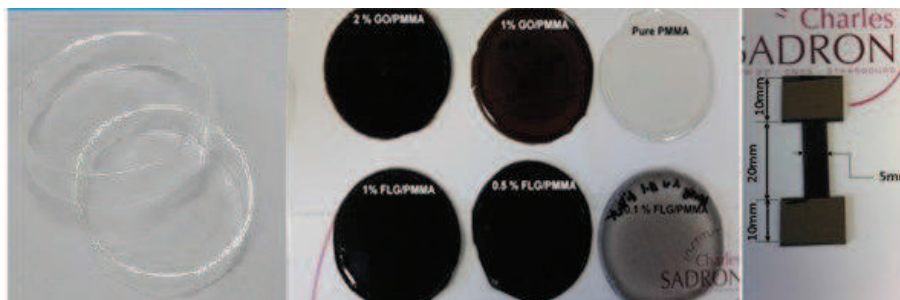


Figure A-1 Samples for tensile test

The films were then peeled from the substrate and cut into strips of 5 mm width  $\times$  40 mm length  $\times$  0.4 mm thickness. A grinding paper with dimensions 1 cm  $\times$  2 cm is affixed at both ends of the sample as in (Figure A-1) to ensure a good grip in the tensile machine. Typically, five samples of every composite were prepared for tensile test.

### The effect of many types of nanocarbon filler on the Stress–strain behavior of PMMA nanocomposites

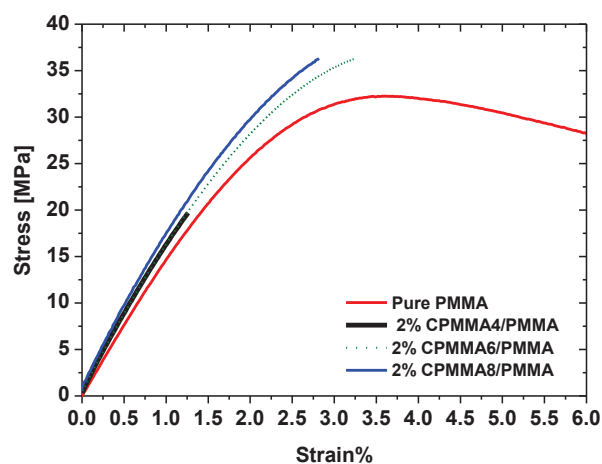


Figure A-2 Effect increasing PMMA thickness grafted MWCNT on the stress-strain relationship

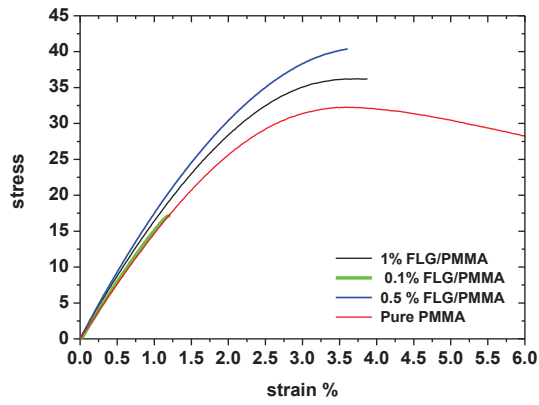
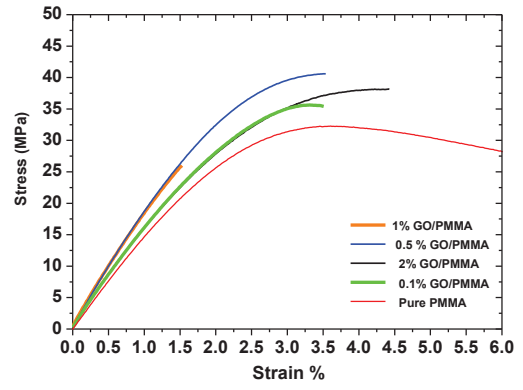
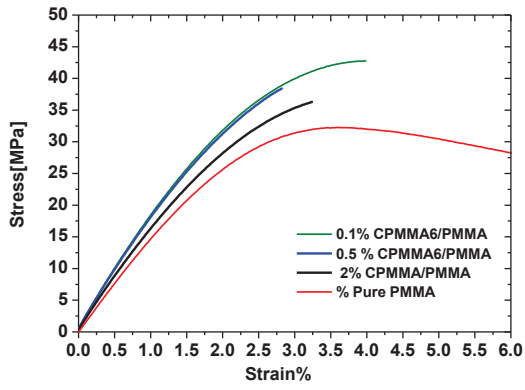


Figure A-3 Effect many types of carbon nanofillers on the stress-strain relationship



## References

- [1] K. Friedrich and A. K. Schlarb, *Tribology of polymeric nanocomposites: friction and wear of bulk materials and coatings*, vol. 55. Elsevier, 2011.
- [2] A. B. Morgan and C. A. Wilkie, *Flame retardant polymer nanocomposites*. John Wiley & Sons, 2007.
- [3] M. Cadek, J. N. Coleman, K. P. Ryan, V. Nicolosi, G. Bister, a. Fonseca, J. B. Nagy, K. Szostak, F. Béguin, and W. J. Blau, “Reinforcement of Polymers with Carbon Nanotubes: The Role of Nanotube Surface Area,” *Nano Lett.*, vol. 4, no. 2, pp. 353–356, 2004.
- [4] E. Beyou, S. Akbar, P. Chaumont, and P. Cassagnau, “Polymer Nanocomposites Containing Functionalised Multiwalled Carbon NanoTubes : a Particular Attention to Polyolefin Based Materials,” 1991.
- [5] S. Iijima, “Helical microtubules of graphitic carbon,” *Nature*, vol. 354, no. 6348, pp. 56–58, 1991.
- [6] P. L. Dickrell, S. B. Sinnott, D. W. Hahn, N. R. Raravikar, L. S. Schadler, P. M. Ajayan, and W. G. Sawyer, “Frictional anisotropy of oriented carbon nanotube surfaces,” *Tribol. Lett.*, vol. 18, no. 1, pp. 59–62, 2005.
- [7] B. Dong, Z. Yang, Y. Huang, H.-L. Li, L. Liu, and F.-Y. Yan, “Preparation and tribological properties of poly(methyl methacrylate)/multi-walled carbon nanotubes composites,” *J. Mater. Sci.*, vol. 40, no. 16, pp. 4379–4382, Aug. 2005.
- [8] G. Schönhense and H. J. Elmers, “PEEM with high time resolution – imaging of transient processes and novel concepts of chromatic and spherical aberration correction,” *Surf. Interface Anal.*, vol. 38, pp. 1578–1587, 2006.
- [9] J. Kim, H. Im, and M. H. Cho, “Tribological performance of fluorinated polyimide-based nanocomposite coatings reinforced with PMMA-grafted-MWCNT,” *Wear*, vol. 271, no. 7–8, pp. 1029–1038, Jul. 2011.
- [10] K. S. K. S. Novoselov, A. K. a. K. Geim, S. V. S. V Morozov, D. Jiang, Y. Zhang, S. V. V Dubonos, I. V. V Grigorieva, and a. a. a Firsov, “Electric field effect in atomically thin carbon films.,” *Science (80-. )*, vol. 306, pp. 666–669, 2004.
- [11] J. Song, J. Zhang, and C. Lin, “Influence of Graphene Oxide on the Tribological and Electrical Properties of PMMA Composites,” *J. Nanomater.*, vol. 2013, pp. 1–5, 2013.
- [12] B. Das, K. Eswar Prasad, U. Ramamurty, and C. N. R. Rao, “Nano-indentation studies on polymer matrix composites reinforced by few-layer graphene,” *Nanotechnology*, vol. 20, no. 12, p. 125705, Mar. 2009.
- [13] D. Berman, A. Erdemir, and A. V. Sumant, “Reduced wear and friction enabled by graphene layers on sliding steel surfaces in dry nitrogen,” *Carbon N. Y.*, vol. 59, pp. 167–175, 2013.
- [14] A. Senatore, V. D. Agostino, V. Petrone, P. Ciambelli, and M. Sarno, “Graphene Oxide Nanosheets as Effective Friction Modifier for Oil Lubricant : Materials , Methods , and Tribological Results,” *ISRN Tribol.*, vol. 2013, pp. 1–9, 2013.

- [15] S. C. Tjong and Y.-W. Mai, *Physical properties and applications of polymer nanocomposites*. Elsevier, 2010.
- [16] B. Pan, S. Zhang, W. Li, J. Zhao, J. Liu, Y. Zhang, and Y. Zhang, "Tribological and mechanical investigation of MC nylon reinforced by modified graphene oxide," *Wear*, vol. 294–295, pp. 395–401, Jul. 2012.
- [17] J. R. Potts, S. H. Lee, T. M. Alam, J. An, M. D. Stoller, R. D. Piner, and R. S. Ruoff, "Thermomechanical properties of chemically modified graphene/poly(methyl methacrylate) composites made by in situ polymerization," *Carbon N. Y.*, vol. 49, no. 8, pp. 2615–2623, 2011.
- [18] J. Markarian, "Slip and antiblock additives: surface medication for film and sheet," *Plast. Addit. Compd.*, vol. 9, no. 6, pp. 32–35, 2007.
- [19] C. a Bishop, U. Kingdom, G. Tullo, and S. E. Associates, "How Items Such as Dust , Oligomers & Slip Agents Can Affect the Polymer Film Surface Quality and be Potential Problems in High-tech Roll-to-roll Vacuum Deposition Applications," *Vacuum*, pp. 1–6, 2006.
- [20] M. X. Ramírez, D. E. Hirt, and L. L. Wright, "AFM Characterization of Surface Segregated Erucamide and Behenamide in Linear Low Density Polyethylene Film," *Nano Lett.*, vol. 2, no. 1, pp. 9–12, 2002.
- [21] G. Wypych, *Handbook of antiblocking, release, and slip additives*. ChemTec Publishing, 2005.
- [22] Y. Bautista, J. Gonzalez, J. Gilabert, M. J. Ibañez, and V. Sanz, "Correlation between the wear resistance, and the scratch resistance, for nanocomposite coatings," *Prog. Org. Coatings*, vol. 70, no. 4, pp. 178–185, 2011.
- [23] C. Gauthier, a.-L. Durier, C. Fond, and R. Schirrer, "Scratching of a coated polymer and mechanical analysis of a scratch resistance solution," *Tribol. Int.*, vol. 39, no. 2, pp. 88–98, Feb. 2006.
- [24] S. Anandhan and S. Bandyopadhyay, "Polymer Nanocomposites : From Synthesis to Applications," 2003.
- [25] F. C. Krebs, "Fabrication and processing of polymer solar cells: A review of printing and coating techniques," *Sol. Energy Mater. Sol. Cells*, vol. 93, no. 4, pp. 394–412, 2009.
- [26] J. Voevodin, AA and Muratore, C and Zabinski, "Chameleon or Smart Solid Lubricating Coatings," *Encycl. Tribol.*, pp. 347–354, 2013.
- [27] W. P. Limited, *Physical properties and applications of polymer nanocomposites Related titles* : 2010.
- [28] J.-H. Du, "The present status and key problems of carbon nanotube based polymer composites," *eXPRESS Polym. Lett.*, vol. 1, no. 5, pp. 253–273, May 2007.
- [29] T. Ramanathan, H. Liu, and L. C. Brinson, "Functionalized SWNT/polymer nanocomposites for dramatic property improvement," *J. Polym. Sci. Part B Polym. Phys.*, vol. 43, no. 17, pp. 2269–2279, 2005.
- [30] X. L. Xie, Y. W. Mai, and X. P. Zhou, "Dispersion and alignment of carbon nanotubes in polymer matrix: A review," *Mater. Sci. Eng. R Reports*, vol. 49, no. 4, pp. 89–112, 2005.

- [31] R. J. Young, I. a. Kinloch, L. Gong, and K. S. Novoselov, "The mechanics of graphene nanocomposites: A review," *Compos. Sci. Technol.*, vol. 72, no. 12, pp. 1459–1476, 2012.
- [32] V. Georgakilas, M. Otyepka, A. B. Bourlinos, V. Chandra, N. Kim, K. C. Kemp, P. Hobza, R. Zboril, and K. S. Kim, "Functionalization of graphene: Covalent and non-covalent approaches, derivatives and applications," *Chem. Rev.*, vol. 112, no. 11, pp. 6156–6214, 2012.
- [33] V. T. Le, C. L. Ngo, Q. T. Le, T. T. Ngo, D. N. Nguyen, and M. T. Vu, "Surface modification and functionalization of carbon nanotube with some organic compounds," *Adv. Nat. Sci. Nanosci. Nanotechnol.*, vol. 4, no. 3, p. 035017, 2013.
- [34] P. Liu, "Modifications of carbon nanotubes with polymers," *Eur. Polym. J.*, vol. 41, no. 11, pp. 2693–2703, 2005.
- [35] M. Salami-Kalajahi, V. Haddadi-Asl, F. Behboodi-Sadabad, S. Rahimi-Razin, and H. Roghani-Mamaqani, "Properties of PMMA-carbon nanotubes nanocomposites prepared by (grafting through) method," *Polym. Compos.*, vol. 33, no. 2, pp. 215–224, 2012.
- [36] P. M. Ajayan and J. M. Tour, "Q & A Nanotube composites," *Nature*, vol. 447, no. June, p. 1066, 2007.
- [37] P. Bilalis, D. Katsigiannopoulos, A. Avgeropoulos, and G. Sakellariou, "Non-covalent functionalization of carbon nanotubes with polymers," *RSC Adv.*, vol. 4, no. 6, p. 2911, 2014.
- [38] G. Gonçalves, P. a. a. P. Marques, A. Barros-Timmons, I. Bdkin, M. K. Singh, N. Emami, and J. Grácio, "Graphene oxide modified with PMMA via ATRP as a reinforcement filler," *J. Mater. Chem.*, vol. 20, no. 44, p. 9927, 2010.
- [39] F. Mammeri, J. Teyssandier, C. Darche-Dugaret, S. Debacker, E. Le Bourhis, and M. M. Chehimi, "Carbon nanotube–poly(methyl methacrylate) hybrid films: Preparation using diazonium salt chemistry and mechanical properties," *J. Colloid Interface Sci.*, vol. 433, pp. 115–122, 2014.
- [40] J. Cuppoletti, "Nanocomposites and polymers with analytical methods," *INTECH Open Access, Rijeka*, vol. 82, 2011.
- [41] Z. Spitalsky, D. Tasis, K. Papagelis, and C. Galiotis, "Carbon nanotube–polymer composites: Chemistry, processing, mechanical and electrical properties," *Prog. Polym. Sci.*, vol. 35, no. 3, pp. 357–401, Mar. 2010.
- [42] N. G. Sahoo, S. Rana, J. W. Cho, L. Li, and S. H. Chan, "Polymer nanocomposites based on functionalized carbon nanotubes," *Prog. Polym. Sci.*, vol. 35, no. 7, pp. 837–867, Jul. 2010.
- [43] J. N. Coleman, U. Khan, W. J. Blau, and Y. K. Gun'ko, "Small but strong: A review of the mechanical properties of carbon nanotube–polymer composites," *Carbon N. Y.*, vol. 44, no. 9, pp. 1624–1652, Aug. 2006.
- [44] V. Mittal, *Optimization of polymer nanocomposite properties*. John Wiley & Sons, 2009.
- [45] J. N. Coleman, U. Khan, W. J. Blau, and Y. K. Gun'ko, "Small but strong: A review of the mechanical properties of carbon nanotube-polymer composites," *Carbon N. Y.*, vol. 44, no. 9, pp. 1624–1652, 2006.

- [46] C. Velasco-santos, A. L. Martí, F. T. Fisher, R. Ruoff, and V. M. Castan, "Improvement of Thermal and Mechanical Properties of Carbon Nanotube Composites through Chemical Functionalization," no. 15, pp. 4470–4475, 2003.
- [47] Z. Jia, Z. Wang, C. Xu, J. Liang, B. Wei, D. Wu, and S. Zhu, "Study on poly(methyl methacrylate)/carbon nanotube composites," *Mater. Sci. Eng. A*, vol. 271, no. 1–2, pp. 395–400, 1999.
- [48] M. a. Pantoja-Castro, J. F. Pérez-Robles, H. González-Rodríguez, Y. Vorobiev-Vasilievitch, H. V. Martínez-Tejada, and C. Velasco-Santos, "Synthesis and investigation of PMMA films with homogeneously dispersed multiwalled carbon nanotubes," *Mater. Chem. Phys.*, vol. 140, no. 2–3, pp. 458–464, 2013.
- [49] S. J. Park, M. S. Cho, S. T. Lim, H. J. Choi, and M. S. Jhon, "Synthesis and Dispersion Characteristics of Multi-Walled Carbon Nanotube Composites with Poly(methyl methacrylate) Prepared by In-Situ Bulk Polymerization," *Macromol. Rapid Commun.*, vol. 24, no. 18, pp. 1070–1073, 2003.
- [50] K. W. Putz, C. A. Mitchell, R. Krishnamoorti, and P. F. Green, "Elastic modulus of single-walled carbon nanotube/poly (methyl methacrylate) nanocomposites," *J. Polym. Sci. Part B Polym. Phys.*, vol. 42, no. 12, pp. 2286–2293, 2004.
- [51] S. Anandhan and S. Bandyopadhyay, *Polymer nanocomposites: from synthesis to applications*. INTECH Open Access Publisher, 2011.
- [52] K. Holmberg and A. Matthews, "23.1 Introduction," no. Cvd, 2001.
- [53] K. Holmberg, A. Matthews, and H. Ronkainen, "Coatings tribology—contact mechanisms and surface design," *Tribol. Int.*, vol. 31, no. 1–3, pp. 107–120, 1998.
- [54] P. B. Bowden, "The elastic modulus of an amorphous glassy polymer," *Polymer (Guildf.)*, vol. 9, pp. 449–454, 1968.
- [55] J. Richeton, G. Schlatter, K. S. Vecchio, Y. Rémond, and S. Ahzi, "A unified model for stiffness modulus of amorphous polymers across transition temperatures and strain rates," *Polymer (Guildf.)*, vol. 46, no. 19, pp. 8194–8201, Sep. 2005.
- [56] G. Mittal, V. Dhand, K. Y. Rhee, S.-J. Park, and W. R. Lee, "A review on carbon nanotubes and graphene as fillers in reinforced polymer nanocomposites," *J. Ind. Eng. Chem.*, vol. 21, pp. 11–25, 2014.
- [57] W. Wang, P. Ciselli, E. Kuznetsov, T. Peijs, and a H. Barber, "Effective reinforcement in carbon nanotube-polymer composites.," *Philos. Trans. A. Math. Phys. Eng. Sci.*, vol. 366, no. 1870, pp. 1613–1626, 2008.
- [58] A. Kelly and amd W. R. Tyson, "Tensile properties of fibre-reinforced metals: copper/tungsten and copper/molybdenum," *J. Mech. Phys. Solids*, vol. 13, no. 6, pp. 329–350, 1965.
- [59] M. K. Singh, T. Shokuhfar, J. J. de Almeida Gracio, A. C. de Sousa, J. M. Da Fonte Ferreira, H. Garmestani, and S. Ahzi, "Hydroxyapatite modified with carbon nanotube-reinforced Poly (methyl methacrylate): a novel nanocomposite material for biomedical applications," *Adv Funct Mater*, vol. 9999, pp. 1–7, 2008.
- [60] S.-Y. Fu, X.-Q. Feng, B. Lauke, and Y.-W. Mai, "Effects of particle size, particle/matrix interface adhesion and particle loading on mechanical properties of

- particulate–polymer composites,” *Compos. Part B Eng.*, vol. 39, no. 6, pp. 933–961, Sep. 2008.
- [61] Y.-W. Mai and Z.-Z. Yu, *Polymer nanocomposites*. Woodhead publishing, 2006.
- [62] Q. Wang, Q. Xue, H. Liu, W. Shen, and J. Xu, “The effect of particle size of nanometer ZrO<sub>2</sub> on the tribological behaviour of PEEK,” *Wear*, vol. 198, no. 1–2, pp. 216–219, 1996.
- [63] X. S. Xing and R. K. Y. Li, “Wear behavior of epoxy matrix composites filled with uniform sized sub-micron spherical silica particles,” *Wear*, vol. 256, no. 1, pp. 21–26, 2004.
- [64] D. Tabor, “The hardness of solids,” *Rev. Phys. Technol.*, vol. 1, no. 3, p. 145, 1970.
- [65] G. M. Swallowe, *Mechanical Properties and Testing of Polymers: an A–Z reference*, vol. 3. Springer Science & Business Media, 2013.
- [66] W. C. Oliver and G. M. Pharr, “Measurement of hardness and elastic modulus by instrumented indentation: Advances in understanding and refinements to methodology,” *J. Mater. Res.*, vol. 19, no. 01, pp. 3–20, 2004.
- [67] B. J. Briscoe, P. D. Evans, S. K. Biswas, and S. K. Sinha, “The hardnesses of poly(methylmethacrylate),” *Tribol. Int.*, vol. 29, no. 2, pp. 93–104, 1996.
- [68] J. Malzbender, J. M. J. den Toonder, a. R. Balkenende, and G. de With, “Measuring mechanical properties of coatings: a methodology applied to nano-particle-filled sol–gel coatings on glass,” *Mater. Sci. Eng. R Reports*, vol. 36, no. 2–3, pp. 47–103, 2002.
- [69] M. S. Alam and K. K. Verma, “Investigation of thermal and hardness properties of MWCNTs filled PMMA polymer nanocomposites,” vol. 2, no. 2, pp. 31–34, 2014.
- [70] K. Friedrich, H. J. Sue, P. Liu, and a. a. Almajid, “Scratch resistance of high performance polymers,” *Tribol. Int.*, vol. 44, no. 9, pp. 1032–1046, 2011.
- [71] H. Pelletier, C. Gauthier, and R. Schirrer, “Friction effect on contact pressure during indentation and scratch into amorphous polymers,” *Mater. Lett.*, vol. 63, no. 20, pp. 1671–1673, 2009.
- [72] B. Briscoe, a Delfino, and E. Pelillo, “Single-pass pendulum scratching of poly (styrene) and poly (methylmethacrylate),” *Wear*, pp. 319–328, 1999.
- [73] G. Subhash and W. Zhang, “Investigation of the overall friction coefficient in single-pass scratch test,” *Wear*, vol. 252, no. 1–2, pp. 123–134, 2002.
- [74] B. J. Briscoe and S. K. Sinha, “Scratch resistance and localised damage characteristics of polymer surfaces--a review,” *Materwiss. Werksttech.*, vol. 34, no. 10–11, pp. 989–1002, 2003.
- [75] W. Boentoro, a. Pflug, and B. Szyszka, “Scratch resistance analysis of coatings on glass and polycarbonate,” *Thin Solid Films*, vol. 517, no. 10, pp. 3121–3125, 2009.
- [76] G. Malucelli and F. Marino, “Abrasion Resistance of Polymer Nanocomposites – A Review,” pp. 1–19, 2009.
- [77] K. Miyoshi and K. W. Street, “Novel carbons in tribology,” *Tribol. Int.*, vol. 37, no. 11–12, pp. 865–868, 2004.
- [78] B. Dong, Z. Yang, Y. Huang, and H. L. Li, “Study on tribological properties of multi-walled carbon nanotubes/epoxy resin nanocomposites,” *Tribol. Lett.*, vol. 20, no. 3–4, pp. 251–254, 2005.



- [79] D. Lahiri, F. Hec, M. Thiesse, A. Durygin, C. Zhang, and A. Agarwal, "Nanotribological behavior of graphene nanoplatelet reinforced ultra high molecular weight polyethylene composites," *Tribol. Int.*, vol. 70, pp. 165–169, 2014.
- [80] S. Sathyanarayana and C. Hübner, *Structural Nanocomposites*. 2013.
- [81] J. Wang, Z. Shi, Y. Ge, Y. Wang, J. Fan, and J. Yin, "Solvent exfoliated graphene for reinforcement of PMMA composites prepared by in situ polymerization," *Mater. Chem. Phys.*, vol. 136, no. 1, pp. 43–50, Sep. 2012.
- [82] M. Wang, K. P. Pramoda, and S. H. Goh, "Enhancement of the mechanical properties of poly(styrene-co-acrylonitrile) with poly(methyl methacrylate)-grafted multiwalled carbon nanotubes," *Polymer (Guildf.)*, vol. 46, no. 25, pp. 11510–11516, Nov. 2005.
- [83] X. Y. Yuan, "Improved properties of chemically modified graphene/poly(methyl methacrylate) nanocomposites via a facile in-situ bulk polymerization," *Express Polym. Lett.*, vol. 6, no. 10, pp. 847–858, Aug. 2012.
- [84] J. Yang, J. Hu, C. Wang, Y. Qin, and Z. Guo, "Fabrication and Characterization of Soluble Multi-Walled Carbon Nanotubes Reinforced P(MMA-co-EMA) Composites," *Macromol. Mater. Eng.*, vol. 289, no. 9, pp. 828–832, Sep. 2004.
- [85] M. Mansha, C. Gauthier, P. Gerard, and R. Schirrer, "The effect of plasticization by fatty acid amides on the scratch resistance of PMMA," *Wear*, vol. 271, no. 5–6, pp. 671–679, 2011.
- [86] K. Holmberg, H. Ronkainen, A. Laukkanen, and K. Wallin, "Friction and wear of coated surfaces - scales, modelling and simulation of tribomechanisms," *Surf. Coatings Technol.*, vol. 202, no. 4–7, pp. 1034–1049, 2007.
- [87] S. Lafaye, C. Gauthier, and R. Schirrer, "Analysis of the apparent friction of polymeric surfaces," *J. Mater. Sci.*, vol. 41, no. 19, pp. 6441–6452, Sep. 2006.
- [88] S. Lafaye, C. Gauthier, and R. Schirrer, "A surface flow line model of a scratching tip: Apparent and true local friction coefficients," *Tribol. Int.*, vol. 38, no. 2, pp. 113–127, 2005.
- [89] B. Bhushan, *Modern Tribology Handbook, Two Volume Set*. Crc Press, 2000.
- [90] S. Lafaye, C. Gauthier, and R. Schirrer, "Analyzing friction and scratch tests without in situ observation," *Wear*, vol. 265, no. 5–6, pp. 664–673, Aug. 2008.
- [91] E. Charrault, C. Gauthier, P. Marie, and R. Schirrer, "Structural recovery (physical ageing) of the friction coefficient of polymers," *J. Polym. Sci. Part B Polym. Phys.*, vol. 46, no. 13, pp. 1337–1347, 2008.
- [92] a. Rubin, N. Rébutin, P. Gérard, and C. Gauthier, "Mechanical properties of a rubber-reinforced block copolymer PMMA: Effect of the nanostructuring on tribological performances," *Mater. Lett.*, vol. 135, pp. 184–187, 2014.
- [93] C. Gauthier, S. Lafaye, and R. Schirrer, "Elastic recovery of a scratch in a polymeric surface: experiments and analysis," *Tribol. Int.*, vol. 34, no. 7, pp. 469–479, Jul. 2001.
- [94] C. Gauthier and R. Schirrer, "Time and temperature dependence of the scratch properties of poly(methylmethacrylate) surfaces," *J. Mater. Sci.*, vol. 35, no. 9, pp. 2121–2130, 2000.

- [95] B. J. Briscoe, E. Pelillo, F. Ragazzi, and S. K. Sinha, "Scratch deformation of methanol plasticized poly (methylmethacrylate) surfaces," *Polymer (Guildf)*, vol. 39, no. 11, pp. 2161–2168, 1998.
- [96] H. Pelletier, A.-L. Durier, C. Gauthier, and R. Schirrer, "Viscoelastic and elastic–plastic behaviors of amorphous polymeric surfaces during scratch," *Tribol. Int.*, vol. 41, no. 11, pp. 975–984, Nov. 2008.
- [97] J. L. Bucaille, C. Gauthier, E. Felder, and R. Schirrer, "The influence of strain hardening of polymers on the piling-up phenomenon in scratch tests: Experiments and numerical modelling," *Wear*, vol. 260, no. 7–8, pp. 803–814, 2006.
- [98] T. S. Kenneth Holmberg and Allan Matthews, "coatings Tribology: Properties, Techniques and Applications in Surface Engineering," *Vacuum*, vol. 1, 1995.
- [99] E. W. Roberts, "Ultralow friction films of MoS<sub>2</sub> for space applications," *Thin Solid Films*, vol. 181, no. 1, pp. 461–473, 1989.
- [100] B. J. Briscoe, P. D. Evans, S. K. Biswas, and S. K. Sinha, "The hardnesses of poly (methylmethacrylate)," *Tribol. Int.*, vol. 29, no. 2, pp. 93–104, 1996.
- [101] S. K. Sinha, T. Song, X. Wan, and Y. Tong, "Scratch and normal hardness characteristics of polyamide 6/nano-clay composite," *Wear*, vol. 266, no. 7–8, pp. 814–821, 2009.
- [102] S. K. Sinha and D. B. J. Lim, "Effects of normal load on single-pass scratching of polymer surfaces," *Wear*, vol. 260, no. 7–8, pp. 751–765, 2006.
- [103] C. Xiang, H.-J. Sue, J. Chu, and B. Coleman, "Scratch behavior and material property relationship in polymers," *J. Polym. Sci. Part B Polym. Phys.*, vol. 39, no. 1, pp. 47–59, Jan. 2001.
- [104] *Tribology\_of\_Polymeric\_Nanocomposites\_Vol55\_2008* ([www.isotextile.blogspot.com](http://www.isotextile.blogspot.com)).pdf. .
- [105] B. J. Briscoe and S. K. Sinha, *1.1 introduction*. 2013.
- [106] I. Janowska, T. Romero, P. Bernhardt, F. Vigneron, D. Begin, O. Ersen, M. J. Ledoux, and P. H. Coung, "Few-layer graphene synthesis by mechanical ablation of graphite material," *Carbon NY*, vol. 50, pp. 3092–3116, 2012.
- [107] J. Li, X. Zeng, T. Ren, and E. van der Heide, "The Preparation of Graphene Oxide and Its Derivatives and Their Application in Bio-Tribological Systems," *Lubricants*, vol. 2, no. 3, pp. 137–161, 2014.
- [108] J. William S. Hummers and R. E. Offeman, "Preparation of Graphitic Oxide," *J. Am. Chem. Soc.*, vol. 80, no. 1937, p. 1339, 1958.
- [109] H. Kong, H. Kong, C. Gao, C. Gao, D. Yan, and D. Yan, "Controlled Functionalization of Multiwalled Carbon Nanotubes by in Situ Atom Transfer Radical Polymerization," *J. Am. Chem. Soc.*, pp. 412–413, 2004.
- [110] L. Qiu, Y. Chen, Y. Yang, L. Xu, and X. Liu, "A Study of Surface Modifications of Carbon Nanotubes on the Properties of Polyamide 66/Multiwalled Carbon Nanotube Composites," *J. Nanomater.*, vol. 2013, pp. 1–8, 2013.
- [111] H. Pelletier, C. Mendibide, and A. Riche, "Mechanical characterization of polymeric films using depth-sensing instrument: Correlation between viscoelastic-plastic

- properties and scratch resistance,” *Prog. Org. Coatings*, vol. 62, no. 2, pp. 162–178, 2008.
- [112] M. a Salam and R. Burk, “Synthesis and characterization of multi-walled carbon nanotubes modified with octadecylamine and polyethylene glycol,” *Arab. J. Chem.*, 2013.
- [113] J. R. Potts, S. H. Lee, T. M. Alam, J. An, M. D. Stoller, R. D. Piner, and R. S. Ruoff, “Thermomechanical properties of chemically modified graphene/poly(methyl methacrylate) composites made by in situ polymerization,” *Carbon N. Y.*, vol. 49, no. 8, pp. 2615–2623, Jul. 2011.
- [114] D. Blond, V. Barron, M. Ruether, K. P. Ryan, V. Nicolosi, W. J. Blau, and J. N. Coleman, “Enhancement of Modulus, Strength, and Toughness in Poly(methyl methacrylate)-Based Composites by the Incorporation of Poly(methyl methacrylate)-Functionalized Nanotubes,” *Adv. Funct. Mater.*, vol. 16, no. 12, pp. 1608–1614, Aug. 2006.
- [115] G. L. Hwang, Y.-T. Shieh, and K. C. Hwang, “Efficient Load Transfer to Polymer-Grafted Multiwalled Carbon Nanotubes in Polymer Composites,” *Adv. Funct. Mater.*, vol. 14, no. 5, pp. 487–491, May 2004.
- [116] K. Zhang, J. Y. Lim, and H. J. Choi, “Amino functionalization and characteristics of multi-walled carbon nanotube/poly(methyl methacrylate) nanocomposite,” *Diam. Relat. Mater.*, vol. 18, no. 2–3, pp. 316–318, Feb. 2009.



# Development and rheological analysis of a surface polymer nanocomposite anti-friction

## Résumé

L'objectif de cette thèse est l'identification de couplages (nanoparticules / matrice de poly(méthyl-méthacrylate) PMMA) qui renforcent la rigidité de surface du PMMA tout en conservant le maximum de transparence. Le choix s'est porté sur trois types de nanoparticules carbonées : du graphène multicouches (FLG), de l'oxyde de graphène (GO) et des nanotubes de carbones (MWCNT). Une première décrit la préparation et la fonctionnalisation de ces trois types de nanoparticules pour assurer une meilleure dispersion dans la matrice. Deux méthodes ont été retenues pour réaliser ces matériaux composites : la polymérisation en masse et le mélange en solution. Une seconde partie présente la caractérisation des propriétés mécaniques de ces revêtements en trois étapes : en volume, en surface et sous forme de revêtement en couches minces (15-20 $\mu$ m). Les résultats majeurs montrent que les nano-composites réalisés retardent l'apparition de la plasticité comparé à un PMMA pur, même à faible pourcentage, et permettent ainsi de limiter les effets de rayures de surfaces. Le faible pourcentage de renfort permet de conserver la transparence et plus l'épaisseur diminue plus on peut augmenter ce taux de renfort sans dégrader les propriétés mécaniques du revêtement. Les nanoparticules choisies comme agents de renfort de la matrice polymère s'avèrent être également de très bons candidats pour la diminution du frottement comparée à un plastifiant type Erucamide

**Mots clés:** Polymère; nanoparticules de carbone; revêtement nanocomposite; coefficient de frottement; mécanique de contact; tribologie.

## Résumé en anglais

The goal of this thesis is the identification of couplings (nanoparticles / matrix poly (methyl methacrylate) PMMA) which ensure PMMA surface rigidity while maintaining maximum transparency. The choice fell on three types of carbonaceous nanoparticles: Few layer graphene (FLG), graphene oxide (GO) and carbon nanotubes (MWCNT). A first part describes the preparation and functionalization of these three types of nanoparticles to provide a better dispersion in the matrix. Two methods were used to prepare nanocomposite materials: bulk polymerization and solution blending. A second part presents the characterization of the mechanical properties of these coatings in three stages: volume, surface and thin layer coating (15-20 $\mu$ m). The main results show that nanocomposites made delay the onset of plasticity compared with pure PMMA, even at a low percentage and help to limit the effects of surface scratches. The small percentage of reinforcement keeps the transparency and the more the thickness decreases the more the rate of reinforcement can increase without degrading the mechanical properties of the coating. Moreover, nanoparticles chosen as the polymer matrix of reinforcing agents prove to be very good candidates for reduction in friction compared to a plasticizer such Erucamide.

**Keywords:** Polymer; carbon nanoparticles; nanocomposite coating; coefficient of friction; mechanical contact; tribology.